Control of Macrophage Metabolism by Oxidized Phospholipids

Implications in Obesity-Associated Adipose Tissue Inflammation

Vlad Serbulea

M.S. Biological & Physical Sciences, University of Virginia, 2014

B.S. Chemistry & Biochemistry, University of California, Santa Barbara, 2012

A Dissertation Presented to the Graduate Faculty of the University of Virginia in Candidacy for the Degree of Doctor of Philosophy

Department of Pharmacology

University of Virginia

March 2018

Norbert Leitinger, PhD

Michelle Bland, PhD

Bimal N. Desai, PhD

Thurl E. Harris, PhD

Ku-lung (Ken) Hsu, PhD

Kevin R. Lynch, PhD

ABSTRACT

Oxidative stress is a phenomenon that has been associated with nearly every disease known to man (1). The regulation of reduction and oxidation (redox) reactions is crucial to the survival of every organism. As such, many organisms have evolved numerous systems for sensing redox balance and maintaining homeostasis. Metabolic and inflammatory diseases such as diabetes, obesity, and atherosclerosis involve a causal redox imbalance. It is unclear whether the perceived redox imbalance associated with diseases causes or merely correlates with inflammation.

This dissertation attempts to address this question by studying redox regulation in adipose tissue macrophages during the development of obesity. The overarching hypothesis of this work is that lipid oxidation products, formed in adipose tissue during obesity, reprogram macrophages for inflammation. The focus of this research lies in interrogating the changes in macrophage metabolism and function brought on by oxidized phospholipids. This work attempts to summarize and explain the various nuances of macrophage redox balance at the cellular and molecular level.

Using a combination of mass spectrometry, flow cytometry, and extracellular flux analysis, this study uncovers new viewpoints in a controversial field. We obtained unexpected results, which redefine previous notions regarding adipose tissue macrophage polarization. In brief, this work provides evidence that a majority of resident adipose tissue macrophages are of the *Mox* macrophage polarization phenotype emphasizing antioxidant production. Furthermore, this work adds to a growing body of literature that macrophage metabolism can directly influence and determine macrophage function, paving the way for novel therapeutics targeting macrophage bioenergetics.

ACKNOWLEDGEMENTS

I find it hard to believe that this is the end. This journey was arduous and challenging, but alas, it is the end. In this section, I acknowledge those who carried me over the finish line, all of whom deserve endless praise.

To my loving and dedicated fiancée, Annie: thank you for your love, compassion, strength, and sacrifice. You have been there for me through the worst of it. It is no exaggeration to say that I could not have done this without you. Throughout the last 5 years, you have been my greatest supporter and champion. Every single publication, honor, and award I have received was made possible by you. You have made me into a better person. Thank you for enduring my sarcasm. Thank you for laughing at my jokes; few have such a refined and distinguished sense of humor as you. I dedicate this dissertation to you. To my supportive parents, Laura and Gabe: thank you for encouragement and backing. Were it not for your high expectations, I would not have had the motivation to pursue a doctoral degree (if only to win more arguments). Thank you for always challenging me and pushing me to do better. Thank you, Mom, for always loving me, despite my irritating and controversial points of view. Thank you, Dad, for always having my back. I am eternally grateful to you both. I hope I do you proud. To my brother, Radu: thank you for your patience. I have always been hard on you, and mean at times, but you stuck with me and for that I am grateful. Although you are still in college, I know that you will change the world in an unprecedented way. I'm always on your side, even when I'm challenging you down.

To my advisor and mentor, Dr. Norbert Leitinger: thank you for taking a chance on me. Thank you for letting a chemist learn biology in your lab. Thank you for always guiding me in the right direction, for pushing me to be independent, and for allowing me to assemble my own team to pursue research. Thank you for constantly pushing me to improve professionally, for sending me to more conferences than I thought I wanted to go to, and for encouraging me to be results-oriented. Without your constant input, I would have worked hard to no avail. You taught me how to minimize the effort and maximize the output for each experiment, which is the reason my graduate career was so successful. I will always be in your debt.

To my students, now colleagues, Paxton Voigt and Dory DeWeese: thank you for your dedication. Training the two of you was the most rewarding part of this graduate experience. I have learned and gained so much from working with you. It is safe to say you taught me more than I have you. I will never be able to repay your efforts and constant help. I was lucky to have you on my team. The two of you are the most promising of your generation. Paxton, your incredible attention to detail and unrivaled perseverance will make you one of the best doctors the world has ever seen. Dory, your unmatched curiosity and infectious enthusiasm will make you a better investigator than I will ever be. Going forward, the two of you can always count on my support. In the future, I should be so lucky to work with people of half as talented. To my friends and successors, Clint Upchurch and Katelyn Ahern: thank you for your patience and understanding. Working with me has not been easy. Thank you for persevering through my frustrating, irritating, and annoying antics. Clint, you have more than proven yourself a capable scientist; I have no doubt your successes will be self-evident. Thank you for all

the scientific, moral, and philosophical debates, and for always questioning me. Katelyn, thank you for being a good friend and constant skeptic. Thanks for the fatty acids, I owe you one. To my friends and colleagues Michael Schappe, Leon DeLalio, and Kelley McQueeney: thank you for commiserating with me. Thank you for all the discussions that you entertained. Thank you for giving me perspective when things seemed at their worst, and sharing in the glory, when things were at their best. I always had excellent company during this graduate study. I hope we can work together in the future.

To Dr. Kyle Hoehn: thank you for your constant help and support. From teaching me about extracellular flux analysis to stimulating my interest in metabolism, you have helped me become into the scientist I am now. Cheers mate. To my thesis committee, Drs. Michelle Bland, Ku-Lung Hsu, Kevin Lynch, Thurl Harris, and Bimal Desai: thank you for your help and guidance. Thank you for your criticism, it only made my work stronger and more meaningful. Thank you for your encouragement and praise, I am humbled to have worked with renowned investigators such as yourselves. Thank you to all my collaborators, which are too many to list here. One of the greatest joys of working in this field getting to experience new and exciting research each week. Thank you for allowing me to share in the ground-breaking studies, and for allowing me to use your projects to perfect many of my techniques. To Dr. Sean Davies from Vanderbilt University: thank you for teaching me all about lipid mass spectrometry. In one short week, you gave me a technical skill which I proved to be essential to my body of scientific work. Thank you to the SFRBM, NIH, and AHA for funding this work.

Finally, a special thank you to the Department of Pharmacology, including Jolene, Deborah, Antoinette, and Tammy. Your constant hard work made all of this possible.

TABLE OF CONTENTS

Abstract i
Acknowledgements ii
Table of Contents vi
Summary of Tables viii
Summary of Figures ix
1 Chapter 1: General Introduction 1
1.1 Origins of Oxidative Stress 1
1.2 Cellular Targets and Products of Oxidation 2
1.2.1 Nucleic Acids 2
1.2.2 Lipids 3
1.3 Cellular Redox-Regulatory Systems 9
1.3.1 Glutathione and Glutaredoxin 9
1.3.2 Thioredoxin and Thioredoxin Reductase 10
1.4 Structure and Biological Functions of Oxidized Phospholipids 11
1.5 How are OxPLs Recognized by Cells? 13
1.5.1 OxPLs modify proteins at the cell membrane and in the cytosol 16
1.5.2 OxPLs are DAMPs recognized by PRR 16
1.5.3 OxPLs bind to soluble, membrane-bound, and intracellular receptors 18
1.6 Adipose Tissue Experiences Obesity-Associated Oxidative Stress and Inflammation 23
1.7 Macrophage's Metabolism Supports its Function 24
1.8 Major Questions and Unknowns About Obesity-Associated Oxidative Stress 26
2 Chapter 2: Experimental Methods 29
2.1 Mice 29
2.2 Air Oxidation of Phospholipids 29
2.2.1 Chemical Reagents 29
2.2.2 Classification 30
2.3 Bone marrow isolation and culture 31
2.4 Metabolomics 31
2.5 Ceramide Measurement by LC-MS 32
2.6 Mitochondrial and Glycolytic Stress Tests 32
2.7 Separation of oxidized phospholipid classes 34
2.8 Oxidized phospholipid measurement by LC-MS/MS 34
2.9 Isolation of stromal vascular fraction from adipose tissue 37
2.10 Flow cytometry analysis of adipose tissue macrophages 37
2.11 Statistical Analysis 38
2.12 Quantitative Real Time-PCR 38
3 Chapter 3: Macrophages sensing oxidized DAMPs reprogram their metabolism to support redox homeostasis and inflammation through a TLR2-Syk-ceramide dependent mechanism 41
3.1 Abstract 41
3.2 Introduction 42
3.3 Results 43
3.3.1 OxPLs induce a metabolic shift to glutathione (GSH) synthesis in macrophages 43
3.3.2 OxPL-treated macrophages induce the pentose phosphate pathway while relying on glucose metabolism for antioxidant gene expression 49
3.3.3 The macrophage metabolic adaptation to OxPLs involves transient suppression of aerobic glycolysis accompanied by Hif1α-dependent and independent gene expression 53
3.3.4 OxPLs redirect TCA metabolism and inhibit macrophage respiratory capacity 59
3.3.5 Mitochondrial inhibition by OxPLs requires TLR2-dependent ceramide accumulation 66

3.3.6 Spleen tyrosine kinase (Syk) is a key mediator of OxPL-induced inflammatory gene expression, ceramide accumulation, and mitochondrial inhibition 72
3.4 Conclusion & discussion 75
4 Chapter 4: Macrophage Phenotype and Bioenergetics are Controlled by Oxidized Phospholipids Identified in Lean and Obese Adipose Tissue 79
4.1 Abstract 79
4.2 Introduction 80
4.3 Results 81
4.3.1 Adipose tissue macrophages from lean mice are metabolically inhibited while those from obese mice are highly energetic 81
4.3.2 A population of CX3CR1^{-} / F4/80^{lo} cells is predominant in lean adipose, while obesity induces accumulation of CX3CR1^{+} / F4/80^{hi} cells in adipose tissue. 86
4.3.3 The majority of resident ATMs are positive for *Mox* markers and are out-populated by *M1*/*M2* ATMs during obesity 91
4.3.4 Analysis of full-length and truncated OxPAPC species in blood from lean and obese mice 94
4.3.5 HFD-feeding leads to a disproportional increase of full-length compared to truncated OxPAPC species in adipose SVF 104
4.3.6 Truncated OxPAPC species inhibit macrophage mitochondrial function and promote antioxidant gene expression while full-length species promote inflammatory gene expression 108
4.4 Conclusion & discussion 112
5 Chapter 5: Oxidized phosphatidylethanolamines selectively induce aerobic glycolysis in macrophages, while promoting antioxidant gene expression 117
5.1 Introduction 117
5.2 Results 119
5.2.1 Full-length OxPE species increase in adipose SVF after high-fat diet feeding. 119
5.2.2 OxPEs abrogate LTA-induced inflammatory gene expression while concurrently promoting weak pro-inflammatory gene expression 127
5.2.3 OxPE induce aerobic glycolysis in macrophages, independent of IL1β 128
6 Chapter 6: Summary, Conclusions, Discussion, and Future Directions 138
6.1 Summary and Conclusions 138
6.2 Discussion 141
6.2.1 Is oxidation so bad? 141
6.2.2 The hormetic response of macrophages to oxidative stress 142
6.2.3 Oxidized lipids are a nuanced system for cellular communication 144
6.2.4 Metabolism determines cellular function 145
6.3 Future Directions 146
7 Publications 148
7.1 Publications Resulting from this Work 148
7.2 Additional Publications 148
8 References 150

SUMMARY OF TABLES

Table 1-1: Catalog of oxidized phospholipids by epitope, based on experimental evidence 7
Table 1-2: Evidence for oxidized phospholipid recognition, sorted by head group 15
Table 2-1: LC-MS parameters for identification and quantification of OxPL..... 36
Table 2-2: Primer Sequences for qRT-PCR..... 39
Table 3-1: Analysis of Acyl-carnitine levels in polarized macrophages 65

SUMMARY OF FIGURES

Figure 3-1: OxPLs induce a metabolic shift to glutathione (GSH) synthesis in macrophages 45
Figure 3-2: Supplement to Figure 3-1 and Figure 3-3 47
Figure 3-3: OxPL-treated macrophages induce the pentose phosphate pathway while relying on glucose metabolism for antioxidant gene expression 51
Figure 3-4: The macrophage metabolic adaptation to OxPLs involves transient suppression of aerobic glycolysis and Hif1α-dependent and independent gene expression 54
Figure 3-5: Supplement to Figure 3-4 56
Figure 3-6: OxPLs redirect TCA metabolism and inhibit macrophage respiratory capacity 61
Figure 3-7: Supplement to Figure 3-6 63
Figure 3-8: Mitochondrial inhibition by OxPLs requires TLR2-dependent ceramide accumulation 68
Figure 3-9: Supplement to Figure 3-8 70
Figure 3-10: Spleen tyrosine kinase (Syk) is a key mediator of OxPL-induced inflammatory gene expression, ceramide accumulation, and mitochondrial inhibition 73
Figure 4-1: Adipose tissue macrophages from lean mice are metabolically inhibited compared to those from obese mice which are highly energetic 84
Figure 4-2: Supplement to Figure 4-3 and Figure 4-4 87
Figure 4-3: Resident CX3CR1^{-} and F4/80^{lo} ATMs are replaced by CX3CR1^{+} and F4/80^{hi} ATMs during obesity 89
Figure 4-4: The majority of resident ATMs are positive for Mox markers and are out-populated by M1/M2 ATMs during obesity 92
Figure 4-5: LC-MS/MS approach for quantifying full-length and truncated OxPAPC species 96
Figure 4-6: Supplement to Figure 4-5 98
Figure 4-7: Supplement to Figure 4-8 and Figure 4-9 100
Figure 4-8: Increase in full-length at the expense of truncated OxPAPC species in blood of mice fed high-fat diet 102
Figure 4-9: High-fat diet feeding leads to a greater increase of full-length compared to truncated OxPAPC species in adipose stromal vascular fraction 106
Figure 4-10: Truncated OxPAPC species promote a quiescent metabolism and antioxidant gene expression while full-length stimulate metabolism and pro-inflammatory gene expression 110
Figure 5-1: Oxidation of PAPE yields many detectable oxidized phospholipids 121
Figure 5-2: Phosphatidylethanolamines increase in adipose SVF, with a preference towards full-length OxPE 123
Figure 5-3: Supplement to Figure 5-2. Levels of OxPE in whole blood. 125
Figure 5-4: OxPE induces weak inflammatory gene expression in macrophages relative to LTA 129
Figure 5-5: Macrophages sensing OxPE shift their metabolism to aerobic glycolysis 131
Figure 5-6: Ferrostatin inhibits OxPAPE-induced *Il1β* gene expression 133
Figure 5-7: OxPAPE-induced aerobic glycolysis is independent of IL1β production 135

1 CHAPTER 1: GENERAL INTRODUCTION

1.1 ORIGINS OF OXIDATIVE STRESS

The ground state of molecular oxygen, referred to as triplet oxygen ($^3O_2$), constitutes the oxygen with which all biological matter on earth interacts. As early as 1929, Lennard-Jones applied molecular orbital theory to predict triplet oxygen to be a di-radical species (2), a notion proven experimentally, helping to explain the paramagnetic property of atmospheric oxygen (2, 3). The di-radical nature of oxygen is an inescapable requirement of mammalian life, driving numerous metabolic processes. Simply put, oxygen is thermodynamically favored to obtain two electrons to pair its two ½ filled orbitals. In eukaryotic cells, oxygen accepts free electrons from the mitochondrial electron transport chain (forming superoxide and peroxide ions), providing a pH gradient within the mitochondria and allowing for ATP production (4). Within this system, antioxidant enzymes, such as superoxide dismutase, manipulate superoxide and peroxide ions to molecular oxygen or hydrogen peroxide, the latter of which catalase reduces to water. Indeed, oxidation reactions are essential for life as we know it, but are also the essence of molecular damage. Paired with oxidation, reduction reactions are equally crucial components of all biological systems, and required to maintain a proper homeostatic equilibrium.

Oxidative stress is an imbalance in the system of reduction and oxidation (redox), favoring oxidation reactions. A common example of oxidative stress is the production of reactive oxygen species by the mitochondria. For example, disruption of the regular flux of the electron transport chain, through inhibition of complex I by rotenone, generates a quantifiable level of superoxide (5), which is detrimental to regular cellular function. Additionally, enzymes like NADPH oxidases (NOX family) (6) and nitric oxide synthases (NOS family) (7) generate reactive oxygen and nitrogen species, respectively. Each of these systems has defined beneficial functions for the cell in addition to perceived detrimental consequences when dysregulated. Within a eukaryotic

cell, numerous components ranging from DNA to proteins to lipids are susceptible to molecular modification by oxidation, leading to a plethora of diseases when left unchecked.

1.2 Cellular Targets and Products of Oxidation

1.2.1 Nucleic Acids

Considered the blueprints for life, nucleic acids like deoxyribonucleic acid (DNA) and ribonucleic acid (RNA), are not only subject to oxidation but also formed through redox-regulated mechanisms. DNA requires the actions of ribonucleotide reductase which, through a free-radical mechanism, removes the hydroxyl group from a ribonucleotide to form the deoxyribonucleotide (8). Oxidation is also a crucial step in the mechanism by which DNA and RNA are demethylated (9).

In the event of redox imbalance, reactive oxygen or nitrogen species oxidize the double bonds present on both DNA and RNA (10). Over 20 species of oxidized nucleic acids can be readily formed through uncontrolled oxidation, and have been measured in various diseases, including but not limited to Alzheimer's disease, colorectal cancer, cardiovascular disease and multiple sclerosis (10, 11). Cells are equipped with a vast contingent of DNA-repair enzymes to correct or excise oxidatively damaged base pairs, yet this is evidently not enough to prevent numerous pathologies. Severe oxidative DNA damage is a highly undesirable endpoint, because the result is, at best, apoptosis and necrosis of the target cell or, at worst, carcinogenesis and uncontrolled cellular proliferation. Before such extensive DNA damage occurs, uncontrolled oxidation often hits the products that DNA and RNA encode for: peptides and proteins.

1.2.1.1 Amino Acids, Peptides, and Proteins

Uncontrolled oxidation of proteins because of redox imbalance often leads to regulated cell death. First, the two most readily oxidized amino acid side chains are the thiol-containing cysteine and

methionine groups. A cysteine residue can form a disulfide bond with another cysteine on the same protein, resulting in tertiary or quaternary protein structural changes, often aiding stability. Considering that structure determines a protein's function, disulfide bond formation must be highly regulated, and, on intracellular proteins, often occurs near the hydrophobic core, protected from the highly reductive intracellular environment (covered in Section 1.3). Many cell-surface proteins (e.g. toll-like receptors) require external disulfide bonds for their appropriate conformation. Reactive oxygen species form erratic disulfide bonds between cysteines on different proteins, resulting in unwanted cross-linking and cellular damage. It is important to note that uncontrolled reductive stress is similarly detrimental, especially regarding the function of extra-cellular and cell-surface proteins. Products of lipid oxidation (covered in **Section 1.2.2**) also modify proteins.

Histidine and lysine are similarly susceptible to oxidation by reactive oxygen species and modification by lipid oxidation products (12, 13). Excess free radicals oxidize the connecting carbon backbone of a peptide, leading to aberrant peptide conformations. Depending on the peptide makeup, cleavage or fragmentation may occur. Each of the aforementioned mechanisms of amino acid oxidation leads to abnormally or erratically folded proteins, triggering the cellular unfolded protein response and endoplasmic reticulum stress (14).

1.2.2 Lipids

1.2.2.1 Fatty Acids

Fatty acids are carboxylic acids with a saturated or unsaturated n-acyl chain. Poly-unsaturated fatty acids (PUFAs) are prime targets of oxidative stress. The double bonds (and, less commonly, triple bonds) are subject to abstraction of a proton by molecular oxygen to form a peroxyl radical group. The peroxyl group, or another oxygen, can modify the newly formed fatty acid radical to form a peroxide group. Oxidation of linoleic acid (LA; octadecaenoic acid; 18:2) and arachidonic

acid (AA; eicosatetraenoic acid; 20:4), which form hydroperoxy-octadecaenoic acid (HPODE) and hydroperoxy-eicosatetraenoic acid (HPETE), respectively, are classic examples of this phenomenon. Further oxidation of HPODE and HPETE species generates hydroxy-octadecaenoic acid (HODE) and hydroxy-eicosatetraenoic acid (HETE), both compounds with well-characterized biological activities. The identified products of fatty acid oxidation number in the thousands when considering the wide variety of PUFAs and oxidized moieties that may form.

Oxidized lipids are more polar and electronegative compared to un-oxidized lipids, which are non-polar. The group resulting from the oxidation, whether it is an aldehyde, carboxylic acid, ketone, epoxide, hydroxide, or peroxide group, significantly increases the polarity, and thus the aqueous solubility of the compound. As a free fatty acid, AA is poorly soluble in water and requires chaperones in cytoplasm or blood, two aqueous media. Reactive oxygen species and cyclooxygenases oxidize AA to highly soluble prostaglandins, molecules with well-studied biological activities (15). Even among already oxidized compounds, further oxidation changes the biological activity. For example, oxidation of glutaric acid, a dicarboxylic acid and product of AA oxidation, leads to addition of a ketone group, creating 2-oxoglutarate (16). This compound, more commonly known as α-ketoglutarate, has several well-defined biological activities and is an integral part of the tricarboxylic acid cycle. Indeed, when one carefully examines the metabolome, one can find numerous structural similarities, if not congruencies, between lipid oxidation products and heavily studied metabolites in well-described biochemical pathways. The oxidized fatty acid forms the structural basis for other oxidized lipids, such as triglycerides and phospholipids.

1.2.2.2 Phospholipids

Phospholipids contain two non-polar fatty acids linked with a glycerol backbone and a polar phosphate head group (except for sphingomyelins, which contain a single fatty acid attached to a sphingosine backbone and phosphocholine head group), and are among the most crucial of

molecules for living organisms. To appreciate the breadth of biological activity by phospholipid oxidation products, one must first understand the role non-oxidized phospholipids play within a cell.

One of the first identified (and, one might argue, the most important) functions of phospholipids is their ability to form a bilayer. The phospholipid bilayer separates the controlled, internal, largely aqueous, cellular environment from the chaotic, external, mostly aqueous, world. There are seven classes of phospholipids distinguished by their head groups: phosphatidylcholines (PC), phosphatidylethanolamines (PE), phosphatidylserines (PS), phosphatidic acid (PA), phosphatidylglycerol (PG), phosphatidylinositol (PI), and sphingomyelin (SM; contains a phosphocholine head group). These phospholipid classes are heterogeneously distributed in subcellular compartments (17). For example, in mammalian cells, the plasma membrane is made up of predominantly PC, PE, and PS. Taking human erythrocytes as an example, the outer leaflet (facing externally) is populated by PC (44.8%) and SM (42.1%), with very little PE (11.1%) (18). On the other hand, PE (43.9%) and PS (29.6%), with a small amount of PC (14.0%) and SM (9.1%) form the inner leaflet (facing the cytoplasm). The inner leaflet also has trace amounts of PI (1.2%) and PA (2.2%). PC and SM share the phosphocholine head group, which has no charge at pH 7. The head groups of PS, PA, and PI have net negative charges while the phosphoethanolamine head group has no charge. Instead, the PE head group contains a highly reactive primary amine. Cells employ many enzymes to maintain an asymmetric plasma membrane phospholipid composition. One can argue that the phosphocholine-containing phospholipids (PC and SM) face externally because they are more resistant to stresses. Similarly, the more charged or reactive phospholipids (PE, PS, PI, and PA) face internally because they produce intracellular signaling molecules, like inositol triphosphate (IP3). This idea is crucial for rationalizing why phospholipid oxidation products are produced, where they originate, and what biological activities they may possess.

Reactive oxygen or nitrogen species readily oxidize PUFA-containing phospholipids. The sheer variety of phospholipid oxidation products is combinatorially immense, considering that oxidized fatty acids can exist in both the *sn*-1 and *sn*-2 locations, and one of seven phospholipid head groups can be present in the *sn*-3 position (see **Table 1-1** for examples of oxidized fatty acid moieties). Regardless of what the oxidative modification is, the oxidized phospholipid (OxPL) becomes markedly more polar than the native phospholipid. In other words, the hydrophobic fatty acid group becomes more hydrophilic when oxidized; thus, the conformation of the phospholipid, especially within a bilayer like the plasma membrane, changes dramatically. This has led to the idea of the "lipid-whisker" model, which proposes that OxPL formed in the plasma membrane disrupt the regular arrangement and protrude outward, presenting the oxidized fatty acid moiety to the exterior of either the outer or inner leaflet (19). This model describes certain cell–cell signaling phenomena. For example, the Hazen group found that cells undergoing apoptosis present oxidized PS (OxPS) on the surface of the cell membrane, facilitating phagocytosis by macrophages (20–22). The Witztum group has used a germ-line encoded antibody to show the presence of oxidized PC (OxPC) on the surface of apoptotic cells (23). There is a thorough review of OxPL biological activity later in **Section 1.4**.

Table 1-1: Catalog of oxidized phospholipids by epitope, based on experimental evidence

General phospholipid structure	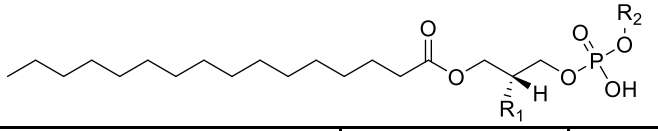		
***sn*-2 Moiety**	**Structure (R_1)**	**Abbreviation (hexadecanoate in *sn*-1)**	**Associated head group (R_2)**
Arachidonoyl	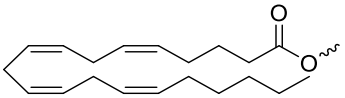	PA-	PC, PE, PS, PA, PG, PI
Oxygenation			
Hydroxy-arachidonoyl	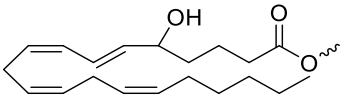	PA(R_2)-OH or HETE-(R_2)	PC (24–27), PE (24–26), PS
Hydroperoxy-arachidonoyl	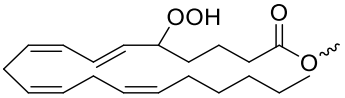	PA(R_2)-OOH or HPETE-(R_2)	PC (27), PE, PS
5,6-Epoxy-isoprostane E2	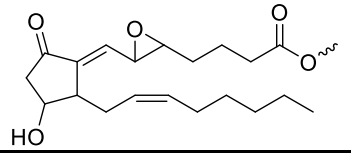	PEI-(R_2)	PC (27–30)
5,6-Epoxy-cyclopentanone	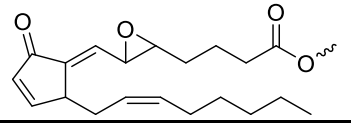	PEC-(R_2)	PC (31, 32)
15-deoxy-Δ12,14-Prostaglandin J2	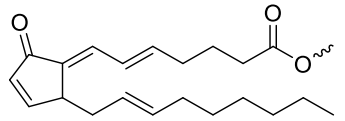	15d-PGJ2-(R_2)	PC (31)
F2-Isoprostane	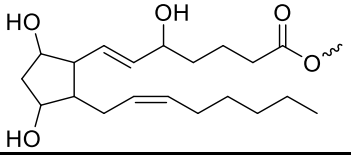	F2-IP-(R_2)	PC (15)
H2-Endoperoxide Isoprostane	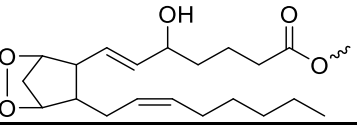	H2-IP-(R_2)	N/A
E2-Isoprostane	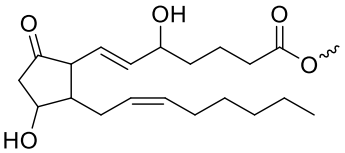	E2-IP-(R_2)	N/A
D2-Isoprostane	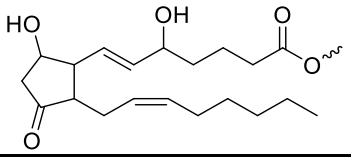	D2-IP-(R_2)	N/A

E2-Isolevuglandin	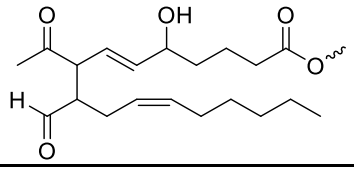	E2-IL-(R_2)	PC (33, 34)
Chain Fragmentation			
Glutaroyl	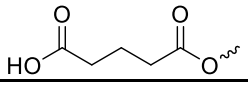	PG-(R_2)	PC (27, 28, 35–37), PE, PS
Azelaoyl	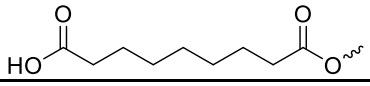	PAze-(R_2) or PAz-(R_2)	PC (27, 38, 39), PE, PS
5-Oxovaleroyl	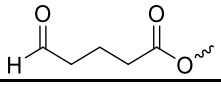	POV-(R_2)	PC (27, 28, 36, 37), PE, PS
9-Oxononanoyl	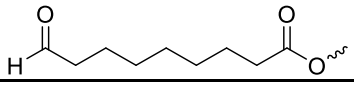	PON-(R_2)	PC (37, 23), PE, PS
5-Hydroxy-8-oxo-6-octenoyl	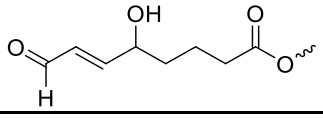	HOOA-(R_2)	PC (20, 21), PS (22)
9-Hydroxy-12-oxo-10-dodecenoyl	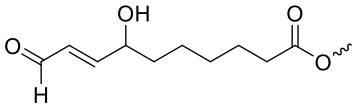	HODA-(R_2)	PC (20, 21), PS (22)
5-Hydroxy-8-oxo-6-octendioyl	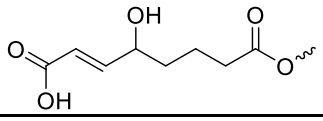	HOdiA-(R_2)	PC (20, 21), PS (22)
9-Hydroxy-10-dodecenedioyl	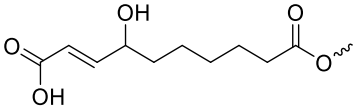	HDdiA-(R_2)	PC (20, 21), PS (22)
5-Keto-8-oxo-6-octenoyl	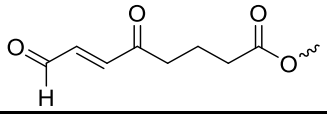	KOOA-(R_2)	PC (20, 21), PS (22)
9-Keto-12-oxo-10-dodecenyl	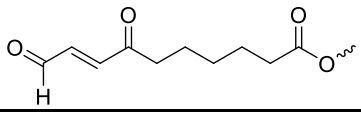	KODA-(R_2)	PC (20, 21), PS (22)
5-Keto-6-octendioyl	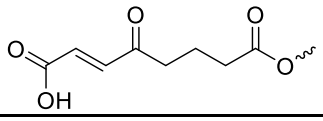	KOdiA-(R_2)	PC (20, 21), PS (22)
9-Keto-10-dodecenedioyl	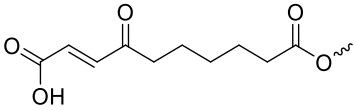	KDdiA-(R_2)	PC (20, 21), PS (22)

1.3 CELLULAR REDOX-REGULATORY SYSTEMS

The redox balance within a cell would be disrupted without both reductive and antioxidant systems in place. Organisms evolved complex enzymatic systems to deal with the pro-oxidant nature of not only the extracellular environment, but also of the intracellular milieu. The key to balancing the oxygen-driven oxidative stress are the elements sulfur and selenium. These two elements are essential to the function of cysteine and selenocysteine, providing these amino acids with excellent reductive potentials.

Many, if not all, of the genetically encoded antioxidant defense systems are subject to transcriptional regulation by the Nrf2-Keap1 system. Keap1 is a cysteine rich protein that is constantly bound to Nrf2, a transcription factor in the cytosol. Oxidative, or electrophilic, stress modifies the cysteines on Keap1 and allows Nrf2 to freely translocate to the nucleus and promote transcription of antioxidant enzymes (40–42). Some of these enzymes include the superoxide dismutases, which convert superoxide to hydrogen peroxide and catalase, which breaks down hydrogen peroxide to water. Among the most basic, yet most effective, antioxidant systems is that centered on the molecule glutathione.

1.3.1 Glutathione and Glutaredoxin

Glutathione is a tripeptide composed of glutamate, cysteine, and glycine (43). Reduced glutathione (GSH) is present in most every discovered organism, and is a powerful reducer of disulfide bonds, giving rise to the oxidized molecule, glutathione disulfide (GSSG). The hydrogen-donating properties of GSH's cysteine residue are key to its reducing capabilities, making it an excellent target for reactive oxygen and nitrogen species. Intracellular glutathione concentration of most biological systems ranges from 10–15mM (44, 45), higher even than free ATP, which is typically present at 1–10mM. Glutathione is predominantly present in the cytosol, but maintains a sizeable reservoir in the mitochondria (44). Attempts to deplete intracellular

glutathione are met with numerous detrimental effects for the cell, often resulting in uncontrolled protein or DNA oxidation and cell death (45, 46). Synthesis of GSH is a two-step process, catalyzed by the rate-limiting glutamate-cysteine ligase and glutathione synthase, both requiring the Nrf2 transcription factor for expression. GSH plays an important role in cancer as well, considering that most cancerous cells harbor significantly higher concentrations of GSH (47, 48). Glutaredoxins are small proteins (~100–130 amino acids; ~12kDa in size) that contain two highly conserved cysteine residues at their core. These cysteines form a disulfide bond in exchange for reducing either protein or small molecule disulfide bonds, creating the "oxidized glutaredoxin" (49). GSH non-enzymatically reduces oxidized glutaredoxins, restoring the reduced glutaredoxin and generating GSSG. An important identified function of this glutathione-glutaredoxin interaction has been in the reduction of disulfides formed by the redox-sensitive enzyme ribonucleotide reductase during the formation of deoxyribonucleotides (dNTPs) (50). The enzyme glutathione reductase reduces GSSG back to GSH, consuming the reductive cofactor NADPH in the process. It is worth mentioning that a prime source of cellular NADPH generation is the pentose phosphate pathway, a metabolic pathway parallel to glycolysis.

1.3.2 Thioredoxin and Thioredoxin Reductase

Similar to the glutaredoxins are the thioredoxins (~12kDa in size), which also contain an intra-protein disulfide bond. Only thioredoxin reductases, which are unique enzymes in their own right, can reduce thioredoxins (51). Thioredoxin reductase is structurally similar to glutathione reductase, but has the added feature of substituting a selenocysteine in place of a regular cysteine. Having a selenol group (selenocysteine) in place of a thiol (cysteine) reportedly generates a greater reductive potential for the protein, resulting in a hundredfold higher catalytic rate (51). The incorporation of selenocysteine occurs by way of a unique co-translational mechanism, in which the presence of a selenocysteine insertion sequence allows for the UGA codon to be interpreted as selenocysteine instead of as a stop codon (52). Although the thioredoxin system is

more effective than the glutathione system at reducing protein disulfide bonds, it is limited by the availability of selenium (51). Another key selenoenzyme (selenocysteine containing enzyme) is glutathione peroxidase (GPX), which has risen to prominence recently due to its involvement in ferroptosis, a novel cell-death pathway (53). GPX takes lipid peroxides as substrates and transfers the peroxide groups onto glutathione (54).

1.4 Structure and Biological Functions of Oxidized Phospholipids

Free radical-induced enzymatic and non-enzymatic mechanisms mediate oxidative modification of lipids. Enzymes such as NADPH oxidase and myeloperoxidase are a key source of intra- and extra-cellular reactive oxygen species. Thus, at sites of inflammation, where neutrophils, macrophages, and other cells generate an environment of high oxidative stress, lipid oxidation products accumulate and exert a variety of biological activities. Polyunsaturated fatty acids and especially arachidonic acid are highly susceptible to lipid peroxidation, leading to the generation of lipid hydroperoxides, which then undergo carbon-carbon bond cleavage giving rise to the formation of truncated, non-esterified aldehydes, and aldehydes still esterified to the parent lipid, termed core-aldehydes. It has been shown that activation of the NADPH oxidase during apoptosis leads to oxidation of the membrane phosphatidylserine (PS), but also phosphatidylcholine (PC), and phosphatidylethanolamine (PE) (55). The presence of oxidized PC (OxPC) on the surface of apoptotic cells has been demonstrated using the monoclonal antibody E06, which exclusively binds to OxPC (23, 56, 57). Furthermore, enzymatic oxidation of phospholipids involving 12/15 lipoxygenase produces biologically active mediators (58, 59). The cholesteryl esters found within LDL are also subject to oxidative modification, which may contribute to endothelial activation (60). Miller et al. found that oxidized cholesteryl esters (OxCE) use TLR4 and Syk to induce a pro-inflammatory response in macrophages (61–64).

Initially, three biologically active phospholipids present in minimally modified low-density lipoprotein (mm-LDL), which were derived from oxidation of 1-palmitoyl-2-arachidonoyl-*sn*-glycero-3-phosphorylcholine (PAPC), were structurally identified: 1-palmitoyl-2-oxovaleroyl-*sn*-glycero-3-phosphorylcholine (POVPC), 1-palmitoyl-2-glutaroyl-*sn*-glycero-3-phosphorylcholine (PGPC), and 1-palmitoyl-2-(5,6-epoxyisoprostane)-PC (PEIPC) (28, 29). These lipids were shown to activate endothelial cells in a structure-specific manner (36, 65). Furthermore, Podrez et al. described a group of CD36-activating truncated OxPLs. These species include an *sn-2* acyl group that requires a γ-hydroxy-α,β-unsaturated carbonyl or a γ-oxo-α,β-unsaturated carbonyl, and were found to be generated during LDL oxidation (20). These lipids, collectively referred to as $oxPC_{CD36}$, were found to directly contribute to the development of foam cell formation in macrophages (21). In this study the authors describe that even trace amounts of $oxPC_{CD36}$ are enough to induce CD36-dependent binding and uptake of LDL (21). Accumulating evidence suggests that biologically active OxPL that are present in atherogenic lipoproteins, in atherosclerotic lesions, and in membrane vesicles released from activated and apoptotic cells, play an essential role in the development of atherosclerosis (66–68). Indeed, OxPL affect a variety of vascular cell types, including endothelial (69–74) and smooth muscle cells (75–77). Furthermore, OxPL have potent effects on immune cells. Studies performed by the Leitinger lab have shown that phospholipid oxidation products of PAPC (OxPAPC) inhibit basic steps of the classical DC maturation process (78). Inhibitory effects on DC, anergic effects on T-cells, as well as on the formation on Treg cells have been reported (78, 79), and one report demonstrates an important role for OxPL on epigenetic modulation of DC activation (80).

Levuglandins and ketoaldehydes are derived from oxidation of arachidonic acid and contain highly reactive aldehydes, which readily form lysyl adducts with proteins, as described by the Salomon lab (81). Macrophages recognize LDL that has been modified with levuglandins (82), free levuglandins, as well as protein-adducts that have been demonstrated at sites of

inflammation and oxidative stress, including atherosclerotic lesions and kidneys of patients with end-stage renal disease (83, 84). However, the exact role of levuglandins and ketoaldehydes in contribution to disease progression remains unclear. Given the ability of levuglandins and ketoaldehydes to react with primary amines, it was postulated that levuglandins might also react with phosphatidylethanolamines. Indeed, it was shown that γ-ketoaldehydes are able to react with ethanolamine at a much faster rate than with lysine (85, 86) to produce compounds that induce inflammatory reactions in macrophages (87). The γ-ketoaldehyde/levuglandin modification of phosphatidylethanolamines produces a highly cytotoxic phosphatidylethanolamine (88), and using mouse models of hypertension, it was shown that scavenging γ-ketoaldehydes prevented immune-mediated hypertension and associated comorbidities (89). Another modification of phosphatidylethanolamines has been described by Sean Davies's group to results in the formation N-acyl-phosphatidylethanolamines (NAPEs), which are precursors to N-acyl-ethanolamides (NAEs), thought to be highly potent satiety signals generated in the intestines (90). Recently, a derivative of carboxyalkylpyrrole(CAP)-phosphatidylethanolamine (CAP-PE) has been identified in the plasma of ApoE-/- mice (91). These CAP-PE derivatives directly bind and activate TLR2/1 to induce platelet activation (91). Similarly to the phosphatidylethanolamine adducts, the CAP-protein derivatives, such as those formed by ω-(2-carboxyethyl)-pyrrole (CEP), have also been shown to induce platelet activation, but even more startlingly, they induce VEGF receptor-independent angiogenesis through TLR2 activation (92). Moreover, the CEPs have been extensively described for their role as a driving force for inflammation in age-related macular degeneration (93).

1.5 How are OxPLs Recognized by Cells?

Phospholipid oxidation products are among several recently characterized danger signals that accumulate under conditions of increased oxidative stress and cell death. They serve as indicators

of inflammation-induced tissue damage and were shown to act as endogenous regulators of the innate immune response (94). For instance, diet-induced oxidative stress is a major cause for vascular, liver and adipose tissue damage, hallmarks of atherosclerosis, fatty liver disease and insulin resistance and diabetes (95). Disturbed redox balance due to chronic inflammation in neurological disorders may contribute to formation and accumulation of OxPLs in the brain (11). Nevertheless, how the recognition of an altered tissue microenvironment by immune cells and the mechanism by which oxidative damage translates into an inflammatory reaction is not clear.

Based on the current literature, OxPLs bind to and initiate a response through soluble acceptors in the blood plasma, by membrane-bound receptors, or by intracellular sensor proteins. Depending on their functional reactive groups, they can either covalently modify these receptor proteins, or bind and interact in a reversible manner. In inflammation, the role of individual OxPLs can either be to act as pro- or anti-inflammatory species. So far, most OxPLs whose biological functions have been investigated have dual pro- and anti-inflammatory effects. OxPLs directly bind to extracellular or cell-surface receptors including LPS binding protein (LBP), CD14, MD-2, and CD36, which may lead to activation or inhibition of TLR4 or TLR2 signaling. OxPLs also bind to intracellular proteins including caspase 11 and Keap1/Nrf2. Here we summarize the evidence for the various systems that recognize or otherwise respond to OxPL. It is important to keep in mind that many studies used OxPL mixtures, which contain many diverse oxidized moieties, making it difficult to conclude which oxidized moieties contribute to which downstream consequences. Nonetheless, **Table 1-1** includes the studies that used enriched, purified, or synthetic OxPL species. **Table 1-2** catalogs the evidence for OxPL effects as distinguished by phospholipid class (i.e. PC, PE, PS, PG, PA, and PI), primarily using mixtures.

Table 1-2: Evidence for oxidized phospholipid recognition, sorted by head group

OxPL	Head group	Structure (R_1)	Activation	Inhibition
OxPC	Choline	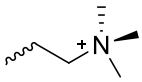	CD36 (96), Nrf2 (27, 97), Cas11/NLRP3 (30), TLR2 (98)	TLR2 (99),TLR4 (100, 101), CD14/MD2 (100), LBP (102)
OxPE	Ethanolamine	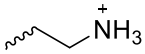	CD36 (27, 19), Nrf2 (27)	TLR2 (99),TLR4 (99, 103), CD14 (102), LBP (102)
OxPS	Serine	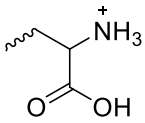	CD36 (22, 27), Nrf2 (27)	CD14 (102), LBP (102)
OxPA	Phosphatidic Acid		Nrf2 (27)	LBP (102)
OxPG	Glycerol	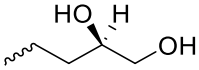	Nrf2 (27)	N/A
OxPI	Inositol	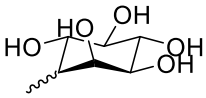	N/A	N/A

1.5.1 OxPLs modify proteins at the cell membrane and in the cytosol

Using cultured RAW 264.7 cells, a commonly-utilized murine macrophage cell line, and fluorescently labeled POVPC (contains an aldehyde) or PGPC (contains a carboxylic acid) Hermetter's group identified primary protein targets of OxPLs by proteomic mass spectrometry (104). They showed that POVPC bind to proteins in the cell membrane by covalently reacting with amino groups. Interestingly, regular POVPC was exchangeable from lipoproteins to cells, where labeled-POVPC modified only a selective group of proteins. PGPC on the other hand, freely travelled through the cell membrane into the cytosol (104). Berliner's group took a different approach to identify the proteome that is modified by OxPLs in endothelial cells, using biotin as affinity tag at the polar head group of the phospholipids (105). They then showed that the interaction of OxPLs with proteins involves modification of cysteines (106).

1.5.2 OxPLs are DAMPs recognized by PRR

After oxidative modification, phospholipids structurally resemble danger-associated molecular patterns (DAMPs) that are recognized by pattern recognition receptors (PRRs) (107). Sensing of these endogenously formed danger or "altered-self" molecules by the innate immune system is mediated by immune-modulating and scavenger receptors such as CD36, TLRs, CD14, LPS-binding protein, and C-reactive protein (108, 109). The fact that the oxidation process renders phospholipids 'visible' to the innate immune system indicates a crucial role for phospholipid oxidation products in the pathogenesis of both chronic-inflammatory and autoimmune diseases (94).

The first indications that OxPLs bear similarities with compounds that can be recognized by TLRs came from the Leitinger lab study showing that these lipids potently inhibit bacterial ligand-induced TLR4 activation (110). The Leitinger lab was first to show that OxPAPC inhibited LPS-induced NF-κB-mediated inflammatory gene expression in human umbilical-vein endothelial cells (HUVEC) and in LPS-injected mice protecting mice from lethal endotoxin shock

(110). They further demonstrated that OxPAPC bound to LPS-binding protein (LBP) and CD14, which blocked the interaction of LPS with both proteins *in vitro* (110). These results were supported by others (100–102, 111), showing that OxPAPC can bind to CD14 and MD2 to interfere with LPS-TLR4/MD2 activation. Moreover, OxPAPC inhibited N-palmitoyl-S-dipalmitoylglyceryl-Cys-Scr-$(lys)_4$ (Pam_3CSK_4)-induced TLR2 activation. High concentrations of serum and supplementation of soluble CD14 in the medium partially restore ligand-induced TLR2 activation in the presence of OxPAPC, suggesting that CD14 is one of the prime targets of OxPAPC. Therefore, the inflammatory response induced by exogenous pathogen associated molecular patterns (PAMPs) such as LPS and endogenous danger signals such as OxPAPC can fundamentally differ, although they share common PRRs.

The protective role of phospholipid oxidation products during acute LPS-induced inflammation may represent an important feedback mechanism whereby accumulating OxPLs limit further tissue-damage by blocking the innate immune response (112). The humoral part of the adaptive immune system recognizes the patterns generated during phospholipid oxidation. Both IgG and IgM antibodies directed against oxidized low-density lipoprotein (OxLDL) are present in the plasma of humans and animals and their titers have been shown to correlate with atherosclerosis progression and measures of lipid peroxidation (113, 114), as well as in several autoimmune disorders such as systemic lupus erythematosus and rheumatoid arthritis (115). Detailed studies in ApoE-deficient mice, which show increased levels of OxLDL, led to the cloning of a set of abundant monoclonal IgM antibodies directed against OxLDL, which includes the prototypic E06 antibody that specifically binds to OxPLs on the surface of OxLDL and apoptotic cells (23, 116, 117). Phospholipid oxidation leads to conformational changes exposing the PC head group, allowing for recognition by the antibody. IgMs recognizing oxidation specific epitopes are thought to exert protective effects by binding to OxPC species (23, 117).

1.5.3 OxPLs bind to soluble, membrane-bound, and intracellular receptors

1.5.3.1 CD14

CD14 is a known co-receptor for both TLR2 and TLR4 that exists in both a membrane-bound and solubilized form. Soluble CD14 is predominantly manufactured and secreted by the liver (118, 119). CD14 enhances the sensitivity of TLR2 activation to Pam_3CSK_4, and is essential for LPS activation of TLR4 (99). Miller et al. have shown that minimally modified-LDL, which contains OxPLs, binds to CD14 (120). As shown by Erridge et al, OxPAPC, in particular the components PGPC and POVPC, are able to strongly inhibit Pam_3CSK_4 activation of TLR2, in a HEK cell model with TLR2-overexpression (99). The authors concluded that this inhibition was likely due to the binding of OxPLs to CD14, due to the rescue of the inhibition after supplementation with soluble CD14 (99). Furthermore, it was found that OxPL mixtures with the head groups PE, PS, and PA were able to induce a mobility shift in soluble CD14, indicating a direct binding interaction of these phospholipids to CD14 (102). Similar OxPL species that bind CD14 also inhibit TLR2-dependent signaling. While it is difficult to elucidate the potential structural requirements for the inhibition of CD14 by OxPLs, there is experimental evidence for PECPC, PEIPC, OxPAPE, OxPAPC, and OxPAPS inhibiting CD14 (31, 100, 102). Walton et al. ruled out an involvement of CD14 in transmitting pro-inflammatory effects of OxPAPC on endothelial cells, instead identifying another GPI-anchored protein recognizing OxPLs (96).

1.5.3.2 LPS binding protein

OxPAPC, and a number of purified components of OxPAPC, directly bind to LPS-binding protein (LBP) and inhibit LPS-driven signaling (102). Unlike for CD14, it was found that OxPLs with any head group (PC, PE, PS, and PA) were able to inhibit the binding of LPS to LBP (102). LPB interacted with 18 total OxPL species, out of the 24 tested. This implies that there is little chemical specificity in the interaction, and that oxidation of the phospholipid is the only

prerequisite for inhibitory interaction with LBP. The head-group does not seem to play a role in the ability of OxPLs to bind to LBP (102). It is unknown whether OxPL-induced inflammation requires LBP.

1.5.3.3 MD2

Another study found that the OxPL KOdiA-PC is able to directly inhibit the binding of LPS to MD2, providing yet another mechanism by which OxPLs inhibit LPS action (121). This was supported by other studies using both binding experiments and functional assays to demonstrate that OxPAPC can compete with LPS to bind MD2 (99, 111). The structural requirements needed to activate or inhibit MD2-driven signaling remain unknown, though one can speculate what the structural requirements are from the crystal structure of MD2 and TLR4 bound with (122) or without LPS (123). The binding of LPS to MD-2 appears to have the hydroxylated fatty acyl chains pointing inward to the structure, allowing the bulky head group to favorably interact with the main TLR4 structure. Taken together, these findings indicate that OxPLs can compete with serum-soluble factors to inhibit LPS and other bacterial or viral components capable of inducing systemic inflammation. This mechanism of scavenging accessory proteins by OxPAPC, or by inhibiting TLR-signaling may represent a negative feedback during inflammation to blunt innate immune responses and provide protection from overshooting inflammatory reactions. This hypothesis was tested by Bochkov and Leitinger, who showed that OxPAPC protects mice against lethal endotoxin shock (110).

1.5.3.4 CD36

CD36 is a membrane protein known to have properties of fatty acid binding and uptake, and is expressed macrophages, dendritic cells, and a variety of non-immune cells including adipocytes. There also exists a soluble form of CD36 whose levels have been correlated with increased risk for type 2 diabetes (124, 125). Podrez et al. classified a series of truncated OxPCs which potently

activate CD36 (20). Podrez et al. found that adding their newly classified OxPLs to cholesterol-containing liposomes led to their CD36-mediated uptake, providing a proof of concept that the OxPL component of oxidized LDL is responsible for its uptake in macrophages (21). The Hazen group further identified OxPS on apoptotic cells as an essential component for CD36-mediated macrophage phagocytosis of apoptotic cells (22). Within this same study, it was shown that loading cells with oxidized phosphatidylserines, but not non-oxidized phosphatidylserines, facilitated their uptake by macrophages (22). There is evidence for CD36 activation by the following species of OxPLs: OxPAPC (20), LysoPC (126), PGPC (127), POVPC (127), HOOA-PC (128), KOOA-PC (128), HOdiA-PC (128), and KOdiA-PC (128) (See **Table 1-2**). As mentioned previously, it was also found that the equivalent OxPS species (the same oxidized fatty acid on PS) bind CD36 (22). CD36 seems to recognize OxPLs containing a truncated acyl-chain, however, due to the difficulty of synthesizing full-length OxPL species, it remains to be shown whether CD36 also binds full-length OxPL.

1.5.3.5 TLR2

Our lab has shown that OxPAPC induces pro-inflammatory gene expression in macrophages via a mechanism that involves TLR2 (98). TLR2 dimerizes with other TLRs, namely TLR1 and TLR6, to recognize distinct sets of ligands (129). TLR2 heterodimers interact with CD36 or CD14, so it is possible that OxPLs induce TLR2-dependent signaling via binding to these accessory receptors. The crystal structure of TLR2 with TLR1 and ligand Pam3CSK4 was elucidated in 2007 and with it, a better understanding of the TLR2 binding pocket (130). Compared to conventional TLR2 agonists, such as lipoteichoic acid (LTA) or Pam3CSK4, OxPLs function as weak agonists for TLR2, with agonistic activity mainly residing in the long-chain fraction of OxPAPC (98). In addition, purified LysoPC (131) and LysoPS (132) are thought to genuinely activate TLR2 while PGPC, POVPC, PECPC, PEIPC, KOdia-PC, OxPAPC and OxPAPE are thought to inhibit TLR2 (31, 99, 103, 132, 133). TLR2-deficiency in mice was shown to be

protective in various settings of non-infectious inflammatory disease models including atherosclerosis, reperfusion injury, and diabetes (134–136). Oxidative tissue damage is a prominent feature in the diseases under the purview of these studies, and as such, TLR2 recognition of oxidatively modified molecules was proposed (134). However, further studies are necessary to fully understand the structural requirements of OxPLs for either activation or inhibition of TLR2.

1.5.3.6 TLR4 and TLR9

Toll-like receptors were initially classified as pathogen-recognition receptors (PRRs) for their ability to recognize bacterial and viral components (137). LPS is the ligand for TLR4, and was shown to strongly induce inflammatory signaling in many cells, with the aid of serum soluble factors LBP, MD2, and CD14. While there are many reports demonstrating that OxPLs inhibit TLR4-mediated effects (99, 102, 121), there is mixed evidence supporting a role for TLR4 in OxPL-induced inflammation. While some studies imply TLR4 in mediating effects of OxPLs (138) or LysoPC (131), many more studies have ruled out an involvement of TLR4 in OxPL-mediated pro-inflammatory effects (99, 101, 102, 139). A key study by Bochkov et al. showed that OxPAPC treatment improved survival of LPS-injected mice supporting a role for OxPLs as inhibitors of TLR4 (110). OxPL species that inhibit LPS-induced TLR4 activation include PGPC, POVPC, PECPC, PEIPC, OxPAPC and OxPAPE (**Table 1-1**)Table 1-2. A recent report showed TLR9 to be activated by CEP in platelets, thereby increasing platelet reactivity (140). These findings further imply an important role for lipid oxidation in the control of thrombosis (128, 141), and increase the spectrum of immune receptors recognizing endogenously formed oxidation products.

1.5.3.7 Keap1 and Nrf2

Nrf2 is a cytosolic transcription factor bound by Keap1, a chaperone protein sensitive to redox balance that promotes the degradation of Nrf2. After oxidative or electrophilic stress, Keap1 is thought to undergo a conformational change, disrupting its ability to bind Nrf2, allowing Nrf2 to translocate to the nucleus and promote transcription of antioxidant response systems (142–144). Human macrophages treated with OxLDL upregulate thioredoxin reductase expression, providing evidence that OxPLs can activate Nrf2 (145). Macrophages expressing Nrf2-dependent antioxidant enzymes, termed Mox, are a significant portion of all macrophages in atherosclerotic plaques and are thought to play a role in advancing atherosclerotic plaque formation (146, 147). It is unclear whether all OxPLs activate Nrf2-dependent gene expression, or just a specific subgroup, such as the cyclopentenone containing OxPLs (148). Additionally, OxPLs are implicated in protein kinase C-dependent signaling (149), which, in turn, has been shown to phosphorylate Nrf2 on a serine residue (150, 151).

1.5.3.8 Caspase-11 and NLRP3

Johnathan Kagan's group showed for the first time that OxPAPC activates caspase-11 and subsequently the NLRP3 inflammasome in dendritic cells (30). This study supports the notion that PRRs have multiple states of activation, dependent on the ligand. The extent of the inflammatory response, as exerted by OxPLs, is less potent than that of classic pro-inflammatory stimuli such as LPS or LTA. Another study has since shown that OxPLs activate the NLRP3 inflammasome in macrophages (152), further supporting the notion that OxPLs are inducers of inflammation in sterile settings. A recent study shows that components of OxPAPC directly bind both caspase-11 and caspase 4, inhibiting activation of the non-canonical inflammasome by LPS, effectively preventing LPS-driven pyroptosis (153).

1.6 Adipose Tissue Experiences Obesity-Associated Oxidative Stress and Inflammation

In the United States of America, obesity affects greater than 30% of the population, including children (154). Obese patients are at greater risk of adverse cardiac events. A hallmark of obesity is the expanded adipose tissue, accompanied by increased local and systemic insulin resistance. During obesity, adipose tissue experiences a marked increase in oxidative stress, as measured by common assays, including quantification of thiobarbituric acid reactive substances (TBARS) and hydrogen peroxide (155). Both insulin sensitivity and obesity-associated insulin resistance are affected by tissue redox homeostasis and oxidative stress (155–157). Two sources are thought to produce the majority reactive oxygen species in adipose tissue during obesity: NADPH oxidase enzymes and the dysfunctional mitochondria. Immune cells like macrophages, but also adipocytes, express NADPH oxidase (NOX) enzymes. The ablation of NOX4 in adipocytes has been shown to delay the onset of insulin resistance during high-fat diet feeding, while concurrently inhibiting adipose tissue inflammation (158). Mitochondrial dysfunction has long been associated with not only obesity, but also aging and cardiovascular disease. Mitochondrial dysfunction in adipose tissue is thought to arise by a number of mechanisms, all leading to an increased level of reactive oxygen species, which in turn, modify proteins, lipids, RNA, and DNA (159). Although there are several reviews purporting that adipocyte and macrophage mitochondrial dysfunction lead to insulin resistance, there is not much evidence to support this. Instead, some studies indicate that ablating regular mitochondrial function in adipocytes, through ablation of mitochondrial transcription factor A (TFAM), inhibited adipose tissue inflammation as well as cellular and whole body insulin resistance (160, 161). Not all oxidative stress experienced by adipose tissue carries the same outcome. Considering how lipid-rich adipose is, it could be that various sources of oxidation (cytosolic or mitochondrial) result in different lipid oxidation products promoting a wide range of outcomes.

Macrophage-driven adipose tissue inflammation is a key factor causing insulin resistance during obesity. Macrophages are myeloid-derived phagocytic immune cells. The best studied role of macrophages is their ability to phagocytose foreign agents, such as bacteria and viruses. Monocytes, macrophage precursors originating from bone marrow are present in blood. During infection, monocytes migrate to tissues and differentiate to macrophages, which are responsible for inducing and resolving inflammation. Pro-inflammatory M1 macrophages secrete pro-inflammatory cytokines such as tumor necrosis factor-α (TNFα) and interleukin-1-β (IL1β). Anti-inflammatory macrophages M2 secrete anti-inflammatory cytokines and tissue repair factors, such as interleukin-10 (IL10) and transforming growth factor-β (TGFβ). A landmark study by Lumeng et al. established the paradigm of adipose tissue macrophage (ATM) phenotypic switching during obesity (162). This study claimed that ATMs from lean mice are anti-inflammatory, M2 (using CD206 as a marker), but switch to pro-inflammatory, M1 (using CD11c as a marker), during obesity. Indeed, ablation of the CD11c-positive macrophages restores insulin sensitivity in high-fat diet fed mice (163). Recent studies using both murine and human samples call this M2 to M1 switch during obesity into question, implying that there is a hybrid M1/M2 population and functional plasticity of macrophages that arises during obesity (164, 165). On the cellular level, pro-inflammatory cytokines, like IL1β released from macrophages, can directly inhibit insulin-stimulated glucose uptake by adipocytes (166). An increasing body of evidence supports a role for adipose tissue macrophages in regulating glucose homeostasis and systemic inflammation (167–171).

1.7 MACROPHAGE'S METABOLISM SUPPORTS ITS FUNCTION

The functional plasticity of macrophages has been tied to changes in their cellular metabolism (172–174). Clasically activated, or M1-polarized, macrophages, compared to an untreated macrophage (M0) shift their metabolism towards aerobic glycolysis (the use of glucose to

produce lactate, even in normoxia), at the cost of mitochondrial ATP generation, to support pro-inflammatory cytokine production (175). Additionally, M1 macrophages rely on succinate-driven Hif1α-dependent glycolytic gene expression, which is necessary for bacterial ligand-induced pro-inflammatory cytokine production. They produce more lactate, as measured *in vitro* using extracellular flux analysis. This phenomenon coincides with an upregulation of inducible nitric oxide synthase (iNOS), resulting in generation of bactericidal nitric oxide from arginine. Alternatively activated, or M2, macrophages, on the other hand, reinforce their mitochondrial ATP production pathway and instead use arginine to produce ornithine via the enzyme arginase (Arg1) (176). M2 macrophages rely on oxidative phosphorylation (OXPHOS) and consume more oxygen using their mitochondria, also measured *in vitro* using extracellular flux analysis (176, 177). Every tissue contains a specific macrophage subtype, ranging from ATMs in the fat pads, to Kupffer cells in the liver, and microglia in the brain. These are referred to as "tissue resident macrophages" and have been described as maintaining tissue homeostasis (178). Recent studies using extensive lineage tracing show that original tissue resident macrophages do not stem from bone-marrow derived monocytes and are, instead yolk-sac derived (179). Furthermore, circulating monocytes are capable of replenishing tissue resident macrophage numbers, should they be diminished (180), implying that a loss of resident ATMs is an unlikely cause of obesity-associated inflammation. The role of resident ATMs is unclear, but we hypothesize they may contribute to tissue redox homeostasis. Metabolic activation of macrophages in obesity has been implied based on *in vitro* stimulation and was demonstrated to be distinct from classical M1 macrophage metabolism (181). However, the bioenergetic profile of murine ATMs remains enigmatic since data from isolated, live ATMs are not available. Furthermore, the endogenously produced DAMPs responsible for promoting metabolic changes and inflammation in adipose tissue have not been identified.

1.8 Major Questions and Unknowns About Obesity-Associated Oxidative Stress

Even though we have learned much about oxidative stress and redox imbalance in the last 20 years, there is still much to be understood. In this study, we investigate the role of OxPLs in the context of adipose tissue inflammation and obesity, though some of the findings may be applicable in multiple tissues with various pathologies. Considering that the immunological environment dictates macrophage phenotypic polarization, and that oxidative stress is a hallmark of both healthy and chronically inflamed tissue, we hypothesize that the formation of oxidized DAMPs may be an important signal for macrophage metabolic and phenotypic adaptation to obesity-associated oxidative tissue damage. The Leitinger lab previously identified phenotypically polarized macrophages in atherosclerotic lesions, coined Mox, that respond to OxPLs by upregulating Nrf2-dependent antioxidant enzymes. However, the metabolic adaptation of macrophages to oxidized DAMPS remains obscure, and the presence of Mox macrophages in metabolically active tissues such as adipose tissue is undetermined. To investigate the role of OxPLs in ATM metabolism, we took the following approach. First, we asked whether OxPLs constitute a source of oxidative stress. In Chapter 3, we show that treatment of macrophages with OxPAPC results in an acute drop in reduced glutathione levels. These levels eventually recover, as we show, due to reprograming of the macrophage glucose metabolism to support glutathione synthesis. Next, we asked how OxPLs affect macrophage cellular metabolism and whether individual OxPL species act differently. In Chapter 3, we show that OxPAPC inhibits macrophage glycolytic and mitochondrial function to a quiescent state through a TLR2-Syk-ceramide driven mechanism. We also show in Chapter 4 that the truncated OxPAPC species promote a quiescent metabolism in macrophages while the full-length species promote an energetic metabolism, supporting inflammatory gene expression. Finally, in Chapter 5, we show that OxPAPE shifts macrophage metabolism towards aerobic glycolysis. Although we found

OxPLs instigated metabolic changes on macrophages, we wanted to identify the OxPL species present in adipose tissue and whether the metabolic reprogramming by OxPLs could be observed in ATMs. In Chapter 4, we designed a liquid chromatography-mass spectrometry method to show that adipose tissue SVF experiences a disproportional gain in full-length OxPAPC species, compared to truncated species. Next, we used extracellular flux analysis and flow cytometry to show that ATMs from lean mice are metabolically quiescent and present markers associated with the Mox macrophage phenotype. Additionally, we found that ATMs from obese mice are metabolically energetic and display markers associated with M1 and M2 macrophages. This data implies that a shift in the oxidized lipid environment during obesity controls the ATM and metabolic polarization state. We conclude that the lipid redox environment of adipose tissue changes with obesity, promoting the formation of inflammatory OxPLs that shift macrophage metabolism to an energetic state. We speculate that this phenomenon occurs during the development of fatty liver disease.

Disclaimer

Portions of this chapter (text and figures) were written as in Serbulea V, DeWeese D, Leitinger N. The effect of oxidized phospholipids on phenotypic polarization and function of macrophages. *Free Radic Biol Med*. 2017 Feb 21. pii: S0891-5849(17)30107-7. doi: 10.1016/j.freeradbiomed.2017.02.035.

2 CHAPTER 2: EXPERIMENTAL METHODS

2.1 MICE

C57BL/6, B6.129-*Tlr2*^{tm1Kir}/J (TLR2 deficient), FVB.129S4(B6)-*Hif1a*^{tm1Jhu}/CkaMmjax (Hif-1α deficient), and B6.129X1-*Nfe2l2*^{tm1Ywk}/J (Nrf2 deficient), B6.129P2-*Syk*$^{tm1.2Tara}$/J (Syk-flox), and B6J.B6N(Cg)-*Cx3cr1*$^{tm1/1(cre)Jung}$/J (CX3CR1-Cre) mice were obtained from Jackson Laboratories and housed in the Pinn vivarium, at the University of Virginia, according to standard animal care and use practices dictated by the University of Virginia's Institutional Animal Care and Use Committee (IACUC). Syk-flox and CX3CR1-Cre mice were bred together to create myeloid-specific Syk-deficient mice (Syk-KO). Diet-induced obesity (DIO; C57BL/6J background) mice and controls were purchased from Jackson Laboratories after 8 to 17 weeks of high-fat diet (HFD) feeding, depending on the experiment.

2.2 AIR OXIDATION OF PHOSPHOLIPIDS

2.2.1 Chemical Reagents

1-palmitoyl-2-arachidonoyl-3-glycero-phosphatidylcholine (PAPC), 1-palmitoyl-2-arachidonoyl-3-glycero-phosphatidylcholine (PLPC), and 1-palmitoyl-2-arachidonoyl-3-glycero-phosphatidylethanolamine (PAPE) were obtained from Avanti Polar Lipids, Inc. As previously described, PAPC (1mg) was dried down in a glass tube, covered loosely with aluminum foil, and allowed to oxidize by air for five to twelve days (182). PLPC (1mg) was dried down in a glass tube, covered loosely with aluminum foil, and allowed to oxidize by air for three to four weeks. PAPE (1mg) was dried down in a glass tube, covered loosely with aluminum foil, and allowed to oxidize by air for three to five days. Qualitative direct inject-mass spectrometry analysis and quantitative liquid chromatography-mass spectrometry was used to monitor the oxidation status.

The final mixtures of phospholipids were referred to as OxPAPC, OxPLPC, or OxPAPE and were re-suspended in cell culture media (RPMI with 10% fetal bovine serum, 2% HEPES, and 1% Antibiotic-Antimycotic) for cell treatment.

2.2.2 Classification of oxidized phospholipids

We broadly defined species as either "**full-length**" or "**truncated**" based on the extent of arachidonic acid or linoleic acid oxidation in the sn-2 position and previously defined conventions (128, 183). Species that we classified in the full-length group include: HETE-PC, HPETE-PC, PECPC, PEIPC, H2-IP-PC, and F2-IP-PC. Species we classified in the truncated group include: POVPC, PGPC, PONPC, PAzPC, HOOA-PC, KOOA-PC, HOdiA-PC, KOdiA-PC, and LysoPC. Of the 13 species of OxPAPC and 2 species of OxPLPC we detected, all have been previously identified, allowing us to assign them to one of four classes based on the structure of the oxidized moiety and previously characterized biological activity (109, 128, 184). Of the full-length species, we defined the class of "**HETE/HPETE**" to encompass species of arachidonic acid containing either a hydroxide or hydroperoxide functional group, such as the species HETE-PC and HPETE-PC. These species have been shown to be produced through action of lipoxygenases (for HPETEs) and subsequent action of glutathione peroxidase (for HETEs), but also through simple air oxidation (128). These species have a variety of biological activities, including but not limited to regulating macrophage response to apoptotic cells (24) and inducing platelet aggregation (185). Next, of the full-length species measured, we defined a class based on the oxidized moiety's structural similarity to prostaglandins, which we refer to as "**isoprostane**". Members of this group include F2-IP-PC, H2-IP-PC, PEIPC, and PECPC. Watson et al. first described PEIPC (29), shown to be a pro-inflammatory mediator (186) thought to activate the NLRP3 inflammasome in a Caspase-11-dependent manner (30). PECPC, containing a cyclopentenone group and bears a strong structural resemblance to Prostaglandin J2, and has been reported to be an activator of Nrf2 (32, 148, 187). Of the truncated species, the "**carbonyl**" class

denotes the presence of an aldehyde or carboxylic acid on the oxidized moiety, and contains POVPC, PGPC, PONPC, and PAzPC. The species in the carbonyl group have previously been described to have mild pro-inflammatory activity (188, 189), LPS-inhibiting activity (101, 102), and Nrf2-activating ability. Another class of truncated OxPLs we define as "**γ-keto/hydroxyl**" are α-β unsaturated γ-ketone or γ-hydroxyl containing species, including HOOA-PC, HOdiA-PC, KOOA-PC, and KOdiA-PC. The γ-keto/hydroxyl compounds were discovered by Podrez and Hazen, who coined them as $OxPC_{CD36}$ for their ability to bind the CD36 scavenger receptor on macrophages to promote foam cell formation and atherogenesis (20, 21).

2.3 BONE MARROW ISOLATION AND CULTURE

The bone marrow from the hind legs of mice was extracted and incubated for 5 minutes with 0.83% ammonium chloride, to clear erythrocyte progenitors. The bone marrow was cultured with RPMI media supplemented with 10% fetal bovine serum (Atlanta Biologicals), 5% HEPES (Gibco), 1% antibiotic-antimitotic, (Gibco), and 10% L929-conditioned media (L929 cells purchased from ATCC). The culture continued for 7 days, with media changes every 3 to 4 days, after which, the media was exchanged for one lacking L929-conditioned media. On day 7, the bone marrow-derived macrophages (BMDMs) were gently separated from Petri dishes using 0.25% trypsin (Gibco), followed by centrifugation and media replacement. Finally, BMDMs were plated on non-tissue culture treated Petri dishes for various treatments and analyses.

2.4 METABOLOMICS

For each sample, the bone marrow from the hind legs of one mouse was harvested and cultured into BMDMs. These BMDMs were then treated with OxPAPC, LTA, or IL4 for 6 hours to polarize them to Mox, classically activated M1, or alternatively activated M2 macrophages, respectively. Trypsin was used to dislodge the cells from their plates, and each sample was

centrifuged at 600x*g* for 5 minutes to pellet the cells. The supernatant was vacuumed off and the cell pellet was stored at -80 °C prior to transport to Metabolon, Inc. who performed the global metabolomic analysis.

2.5 CERAMIDE MEASUREMENT BY LC-MS

To measure ceramides, 200µL of chloroform was added to 100µL homogenate, and the homogenate was incubated overnight at 48 °C. After cooling to room temperature, 20µL of 1M KOH in methanol was added, and the samples were incubated at 37 °C for 2h. Lipids were neutralized with 5µL of glacial acetic acid. 1.5mL of HPLC-grade chloroform and 2 mL of H_2O (Fisher) were added to each sample, vortexed, and centrifuged at 600×*g* for 10 min to separate the organic and aqueous phases. The organic phase was dried under argon prior to resuspension in mobile phase solvent containing 97% acetonitrile, 2% methanol, and 1% formic acid (v/v/v) supplemented with 5mM ammonium formate. Using a Sciex 4000 QTrap, a triple quadrupole mass spectrometer, coupled to a Shimadzu LC-20AD LC system equipped with a Supelcosil LC-NH2 HPLC column (3µm, 50 cm×2.1 mm) samples were subjected to normal phase LC-MS/MS. We employed a multiple reaction monitoring scheme for naturally occurring species of saturated and unsaturated ceramides, ranging from Cer16:0 to Cer24:2. Data was acquired as previously described, and quantification was carried out by integrating peak areas for each individual analyte using Analyst 1.5.1 software. Recovery was assessed using internal standards, and values were normalized to protein content measured by a Bradford Assay.

2.6 MITOCHONDRIAL AND GLYCOLYTIC STRESS TESTS

Extracellular flux analysis was performed as previously described (182, 190). Briefly, cells were seeded into a Seahorse 24-well tissue culture plate (Agilent Technologies). The cells adhered for a minimum of 1 hour prior to treatment. For assessing respiratory capacity, cells were subjected

to a mitochondrial stress test (MST) as established previously (190), briefly described here. At the beginning of the assay, the media was changed to DMEM with pyruvate (Thermo-Fisher Cat#:12800017, pH=7.35 at 37°C) and cells equilibrated for 30 minutes. Oxygen consumption rate (OCR) from the cell media was measured using four-minute measurement periods, represented in units of pmol O_2/min, using a Seahorse XF24 Flux Analyzer (Agilent Technologies, Santa Clara, CA). After three basal OCR measurements, compounds to modulate cellular respiratory function [1μM Oligomycin (Sigma-Aldrich); 2μM BAM15 (Cayman Chemical Company); 1μM Antimycin A & 100nM Rotenone (Sigma-Aldrich)] were injected into the plate, after every three measurements, in order. Basal respiration was calculated by subtracting the average of the post-Antimycin A and Rotenone measurements from the average of the first three measurements. Maximum respiratory capacity was calculated by subtracting the average of the post- Antimycin A & Rotenone measurements from the average of the post-BAM15 measurements. The reserve capacity was calculated by subtracting the average of the basal measurements from the average of the post-BAM15 measurements. For assessing the glycolytic capacity of the cells, a glycolytic stress test (GST) was performed to measure extracellular acidification rate (ECAR), representing the secretion of lactate into the extracellular media. The GST was used in lieu of measuring ECAR concurrently during an MST. The media used for the GST (unbuffered, glucose-free DMEM; Sigma-Aldrich Cat#: D5030, pH=7.35 at 37°C; supplemented with 143mM NaCl and 2mM glutamine) has fewer buffering agents than the media used for the MST, allowing for greater sensitivity in measuring ECAR. After three basal ECAR measurements, compounds to modulate glycolysis [20mM Glucose; 1μM Oligomycin; 80mM 2-Deoxyglucose (Sigma-Aldrich)] were injected after every four measurements and ECAR was measured using three-minute measurement periods. Basal glycolysis was calculated by subtracting the average of the post- 2-Deoxyglucose measurements from the average of the post-Glucose measurements. Glycolytic capacity was calculated by subtracting the average of the post- 2-Deoxyglucose measurements from the average of the post-Oligomycin measurements.

Finally, XF Phenograms (Agilent Technologies), or bioenergetics plots, were created using the maximum respiratory capacity from MST (y-axis) and the glycolytic capacity from GST (x-axis) from parallel experiments in which the cells received identical treatments.

2.7 SEPARATION OF OXIDIZED PHOSPHOLIPID CLASSES

Using a solid phase extraction procedure of separating lipid classes (191), we separated full-length and truncated OxPAPC species. We loaded 1mg of OxPAPC in chloroform on HyperSep amino-propyl cartridges. First, the column was washed with 4mL of hexanes. Next, 200µL of 5mg/mL OxPAPC in chloroform was added to the column. The column was then eluted with 4mL methanol to recover Fraction FL (containing predominantly full-length species), followed by 4mL of 420:350:100:50:0.5 hexanes:isopropanol:ethanol:water:formic acid with 3.75% phosphoric acid to recover Fraction T (containing predominantly truncated species). The fractions were then dried down under argon and suspended in solvent A (69% methanol, 31% water, 10mM ammonium acetate) for LC-MS analysis or in cell culture media (RPMI with 10% FBS, 2% HEPES, and 1% anti-anti) for cell treatment.

2.8 OXIDIZED PHOSPHOLIPID MEASUREMENT BY LC-MS/MS

Lipids from samples were extracted by a modified Bligh-Dyer extraction. The tissue was manually homogenized and then mixed in a glass tube with 750µL HPLC-grade chloroform and 250µL HPLC-grade methanol supplemented with at least 0.01% butylated hydroxytoluene (BHT; Sigma) and 189nmol of the internal standard for phosphatidylcholines (PC), di-nonanoyl-phosphatidylcholine (DNPC; Avanti Polar Lipids, Inc). 1mL of HPLC-grade water was added and the mixture was vigorously vortexed for 60 seconds. Next, the mixture was centrifuged (1000rpm for 10min) to separate the fractions and the organic layer (bottom) was removed and placed into a fresh glass tube. 1mL of chloroform was added to the aqueous fraction and the

extraction was performed once more. The organic layer of the second extraction was combined with the first, and then dried down under nitrogen. After complete evaporation of the organic solvent, the lipids were suspended in 300µL of Solvent A (69% water; 31% methanol; 10mM ammonium acetate), vortexed vigorously, and stored at -80°C. The determination and quantification of both non-oxidized and oxidized PC species was performed by liquid chromatography-linked electrospray ionization (ESI) mass spectrometry using a Sciex 4000 QTrap (See **Table 2-1** for species-specific parameters). Of the oxidized species listed, the isoprostane-PC species H2-IP-PC and F2-IP-PC have isobaric species, consisting of multiply hydroxylated and peroxylated PAPC, which are currently unable to be resolved by fragmentation or liquid chromatography. Separation of the phospholipids was achieved by loading samples onto an EVO C18 column (Kinetex 5µm, 100 x 4.6mm; Phenomenex). Elution of the phospholipids was achieved using a binary gradient with Solvent A (69% water; 31% methanol; 10mM ammonium acetate) and Solvent B (50% methanol; 50% isopropanol; 10mM ammonium acetate) as the mobile phases, with the oxidized species eluting earlier than the non-oxidized species. Detection for PC species was conducted using multiple reaction monitoring (MRM) in positive mode by identification of two transition states for each analyte. Quantification of each PC analyte was performed based on the peak area of the positively charged 184 m/z fragment ion.

Table 2-1: LC-MS parameters for identification and quantification of OxPL

Identification Parameters			Machine Parameters		
OxPL Species	m/z (M+H)[‡]	Retention Time (min)	Declustering Potential (eV)	Collision Energy (eV)	Cell Exit Potential (eV)
DNPC	538.50		120	54	10
PAPC	782.50	6.66	96	47	16
PLPC	758.59	6.68	136	43	12
Truncated Species					
LysoPC	495.50	5.28, 5.37	81	35	12
POVPC[§]	594.50	5.30,5.38	116	39	16
PGPC[§]	610.50	4.84, 4.96	111	37	14
PONPC[ǂ]	650.52	5.22, 5.59	126	43	12
PAzPC[ǂ]	666.42	5.23	106	41	10
HOOA-PC[§]	650.40	5.30	120	54	10
KOOA-PC[§]	648.38	5.32	120	54	10
HOdiA-PC[§]	666.39	5.15, 5.26	120	54	10
KOdiA-PC[§]	664.38	4.83	120	54	10
HODA-PC[ǂ]	706.46	5.05	101	43	14
KODA-PC[ǂ]	704.41	5.54	146	47	10
HDdiA-PC[ǂ]	722.41	5.05, 5.16	136	45	10
KDdiA-PC[ǂ]	720.42	5.05	136	43	12
Full-length Species					
HPETE-PC[§]	814.56	6.26, 6.37	120	30	10
HETE-PC[§]	798.56	6.27, 6.44	120	30	10
PECPC[§]	810.49	6.00	156	53	14
PEIPC[§]	828.50	5.73, 5.92, 6.07	71	49	14
H2-IP-PC[§]	830.55	6.02	120	30	10
F2-IP-PC[§]	832.57	5.81	120	54	10
HODE-PC[ǂ]	774.38	6.39, 6.68	166	47	10
HPODE-PC[ǂ]	790.46	6.05, 6.14, 6.39	131	47	10
PLPC+3O[ǂ]	806.52	5.75, 6.00	151	51	10
PLPC+4O[ǂ]	822.55	5.75	96	51	10

[‡] All species were quantified on the common 184.1 fragment

[§] Represents PAPC-derived species

[ǂ] Represents PLPC-derived species

2.9 ISOLATION OF THE STROMAL VASCULAR FRACTION FROM ADIPOSE TISSUE

The stromal vascular fraction was collected as previously described (192). The adipose tissue was excised from the mouse and minced with scissors. The tissue was then digested for 30 minutes in a solution containing 2mg/mL collagenase type II solution at 37℃. After digestion, the tissue was filtered through a nylon mesh (100µm) and washed with buffer containing high salt concentration and 1% BSA. The filtered cells were allowed to separate, with the adipocytes floating on top of the buffer. The infranatant was collected, centrifuged (1500rpm for 5 minutes) and incubated with 0.83% NH_4Cl for 5 minutes to remove red blood cells. Finally the cells were washed, centrifuged, and re-suspended in various buffers or media, depending on the subsequent analysis.

2.10 FLOW CYTOMETRIC ANALYSIS OF ADIPOSE TISSUE MACROPHAGES

Cell preparation for flow cytometry was performed as previously described (192). Cells were suspended in FACS buffer (0.5% BSA, 2mM EDTA, and 0.18% NaN_3 in PBS). Cells were first stained with Live/Dead Yellow dye, then fixed using 4% paraformaldehyde. Cell surface Fc receptors were blocked with CD16/32 for 20 minutes in FACS buffer to prevent non-specific binding of antibodies to surface receptor. Cells were washed in FACS buffer and stained for surface markers (CD45, F4/80, CD11b, CD11c, and CX3CR1) for 30 minutes. Cells were washed and made permeable with 0.1% saponin. Cells were then stained for intracellular markers (HO1, TXNRD1, and CD206) in FACS buffer containing 0.1% saponin for 30 minutes. Cells were washed 3-4 times with FACS buffer containing 0.1% saponin to dilute and remove non-bound antibodies. Finally, cells were washed and suspended in FACS buffer for final analysis. The flow-cytometer used was the BD LSRFortessa, and data was analyzed using FlowJo v10 (FlowJo,

LLC). Compensation was performed in FlowJo using single stain and fluorescence-minus-one (FMO) controls, as well as compensation beads.

2.11 Statistical Analysis

Data is represented as mean ± SEM, unless otherwise specified. Unpaired Welch's t-test determined statistical significance between two groups, due to the unequal variance between control and treatment conditions as calculated by an F-test. One-way ANOVA with post-hoc Dunnet's corrected unpaired t-tests determined statistical significance between multiple groups. For oxidized phospholipid species measurement during high-fat diet feeding, two-way ANOVA and Tukey corrected multiple t-tests determined statistical significance. Linear regression and calculation of Pearson's correlation coefficient determined correlation between two parameters.

2.12 Quantitative Real Time-PCR

RNEasy Mini Kit (Qiagen) was used to isolate RNA from 300 to 500 thousand cells. The iScript cDNA Synthesis Kit (Biorad) was used to produce complementary DNA (cDNA) libraries. Quantitative real-time PCR (qRT-PCR) was set up using 250ng of cDNA and SensiMix SYBR & Fluorescein Kit. Primer sequences can be found in **Table 2-2**. Primers were designed with Primer Blast and validated using melt curve analysis. Quantitative real-time polymerase chain reaction (qRT-PCR) was performed as previously described (182).

Table 2-2: Primer Sequences for qRT-PCR

Gene	Forward/Reverse	Sequence 5'-3'
B2m	F	GCTATCCAGAAAACCCCTCAAATTCA
	R	GCAGGCGTATGTATCAGTCTCAGTG
Tfam	F	ATTCCGAAGTGTTTTTCCAGCA
	R	TCTGAAAGTTTTGCATCTGGGT
Ndufa10	F	ACCTTTCACTACCTGCGGATG
	R	GTACCCAGGGGCATACTTGC
Sdhaf2	F	GCGGTGGTCACCTTGATCC
	R	CCTCTGTAGAAGCGTCTGAATG
Cox5b	F	TTCAAGGTTACTTCGCGGAGT
	R	CGGGACTAGATTAGGGTCTTCC
Atp5f1	F	AGTTCCTTTACCCTAAGACTGGT
	R	TTCATGCTCGACTGCTTTACTT
Glut1	F	CGAGGGACAGCCGATGTG
	R	TGCCGACCCTCTTCTTTCAT
Gclm	F	TGGAGCAGCTGTATCAGTGG
	R	AGAGCAGTTCTTTCGGGTCA
Ho1	F	GCCACCAAGGAGGTACACAT
	R	TGGGCCAAAGCTTCTGCTGT
Srxn1	F	ACGGTGCACAACGTACCAAT
	R	CTTGGCAGGAATGGTCTCTC
Txnrd1	F	GGCTCAGAGGCTGTATGGAG
	R	TTCCAATGGCCAAAAGAAAC
Nos2	F	CCTGGTACGGGCATTGCT
	R	GCTCATGCGGCCTCCTT
Arg1	F	AAGACAGCAGAGGAGGTGAAGAG
	R	TGGGAGGAGAAGGCGTTTGC
Pgd	F	CTCCTCGACTCTGCTTCGTC
	R	CGGCATCTTCTTGTCGTGTC
G6pd	F	TGCACTTTGTCCGGAGTGAT
	R	AGGACAAAATGGCGGTCCAA
Taldo	F	CAGATGCCTGCCTACCAAGA
	R	GGAAAGCCTTGCATCAACTTCT
Il1b	F	TACCAGTTGGGGAACTCTGC
	R	CAAAATACCTGTGGCCTTGG
Vegf	F	CCTCCGAAACCATGAACTTTCTGCTC
	R	CAGCCTGGCTCACCGCCTTGGCTT
Cxcl1	F	CCGAAGTCATAGCCACACTCAA
	R	GCAGTCTGTCTTCTTTCTCCGTTAC
Il6	F	CCACGGCCTTCCCTACTTCA
	R	TGCAAGTGCATCATCGTTGTTC
Cox2	F	CGGAGAGAGTTCATCCCTGA
	R	ACCTCTCCACCAATGACCTG
Cers1	F	CCACCACACACATCTTTCGG
	R	GGAGCAGGTAAGCGCAGTAG
Cers2	F	ATGCTCCAGACCTTGTATGACT
	R	CTGAGGCTTTGGCATAGACAC
Cers3	F	TTCAAGCATTCCACAAGCAAAC
	R	CAACCTGGCGCTCTGTCAA
Cers4	F	TACCCACATCAGACCCTGAAT
	R	TGAAGTCCTTGCGTTTGACATC
Cers5	F	CGGGGAAAGGTGTCTAAGGAT
	R	GTTCATGCAGTTGGCACCATT
Cers6	F	GATTCATAGCCAAACCATGTGCC
	R	AATGCTCCGAACATCCCAGTC

Disclaimer

Portions of this chapter (text and figures) were written as published in Serbulea V, Upchurch CM, Ahern KW, Bories G, Voigt PE, Deweese DE, Meher AK, Harris TE, Leitinger N. Macrophages sensing oxidized DAMPs reprogram their metabolism to support redox homeostasis and inflammation through a TLR2-Syk-ceramide dependent mechanism. *Molecular Metabolism*. 2017 Nov 7. doi: 10.1016/j.molmet.2017.11.002. and in Serbulea V, Upchurch CM, Schappe MS, Voigt PE, Deweese DE, Desai BN, Meher AK, Leitinger N. Macrophage phenotype and bioenergetics are controlled by oxidized phospholipids identified in lean and obese adipose tissue. Under review at *PNAS.*

3 CHAPTER 3: MACROPHAGES SENSING OXIDIZED DAMPS REPROGRAM THEIR METABOLISM TO SUPPORT REDOX HOMEOSTASIS AND INFLAMMATION THROUGH A TLR2-SYK-CERAMIDE DEPENDENT MECHANISM

3.1 ABSTRACT

Macrophages control tissue homeostasis and inflammation by sensing and responding to environmental cues. However, the metabolic adaptation of macrophages to oxidative tissue damage and its translation into inflammatory mechanisms remains enigmatic. Here we identify the critical regulatory pathways that are induced by endogenous oxidation-derived DAMPs (oxidized phospholipids, OxPL) *in vitro* leading to formation of a unique redox-regulatory metabolic phenotype (Mox), which is strikingly different from conventional classical (M1) or alternative (M2) macrophage activation. Unexpectedly, metabolomic analyses demonstrated that Mox heavily rely on glucose metabolism and the pentose phosphate pathway (PPP) to support GSH production and Nrf2-dependent antioxidant gene expression. While the metabolic adaptation of macrophages to OxPL involved transient suppression of aerobic glycolysis, it also led to upregulation of inflammatory gene expression. In contrast to classically activated (M1) macrophages, Hif1α mediated expression of OxPL-induced Glut1 and VEGF, but was dispensable for Il1β expression. Mechanistically, we show that OxPL suppress mitochondrial respiration via TLR2-dependent ceramide production, redirecting TCA metabolites to GSH synthesis. Finally, we identify spleen tyrosine kinase (Syk) as a critical downstream signaling mediator that translates OxPL-induced effects into ceramide production and inflammatory gene regulation. Together, these data demonstrate the metabolic and bioenergetic requirements that enable macrophages to translate tissue oxidation status into either antioxidant or inflammatory

responses via sensing OxPL. Targeting dysregulated redox homeostasis in macrophages could therefore lead to novel therapies to treat chronic inflammation.

3.2 INTRODUCTION

Macrophages have been shown to play essential roles in maintenance of tissue homeostasis, as well as in regulating induction and resolution of inflammation in response to tissue injury or infection (178, 193). The functional plasticity of macrophages has been tied to changes in their cellular metabolism (172–174). In general, inflammation-promoting classically activated (M1) macrophages rely on aerobic glycolysis and succinate-driven Hif1α-dependent glycolytic gene expression, which is necessary for bacterial ligand-induced pro-inflammatory cytokine production (175). On the other hand, anti-inflammatory alternatively activated (M2) macrophages rely on oxidative phosphorylation (OXPHOS) with a possible role for fatty acid oxidation in phenotypic polarization and sustained function (176, 177). We have previously identified phenotypically polarized macrophages in atherosclerotic lesions, coined Mox, that respond to oxidized phospholipids (OxPLs) by upregulating Nrf2-dependent antioxidant enzymes (146). However, the cellular metabolism of Mox macrophages has not been described.

OxPL have been identified as endogenous danger associated molecular patterns (DAMPs), characteristic of oxidatively damaged tissue, and they were shown to be key players in cardiovascular disease. The Copenhagen General Population Study revealed that OxPLs are risk factors for calcific aortic valve disease (194). This study also showed a close correlation of OxPLs and lipoprotein(a), which has been previously associated with calcific aortic valve disease and atherosclerosis in humans and mice (114, 195, 196). Chronic inflammatory diseases like atherosclerosis are macrophage-driven diseases, which may involve the action of OxPLs, making it essential to better understand the signaling pathways that are induced by OxPLs in macrophages.

OxPAPC is a mixture of individual OxPL species derived from free radical-induced oxidation of 1-palmitoyl-2-arachidonoyl-sn-glycero-3-phosphatidylcholine (PAPC)) (28, 197–199). In macrophages, OxPAPC has been shown to drive TLR2-dependent pro-inflammatory (98, 183) and Nrf2-dependent antioxidant responses (31, 146, 149, 148, 200). Furthermore, OxPAPC has been shown to inhibit classic LPS-driven TLR4-dependent inflammatory responses (102, 110, 183), but also to induce non-canonical Caspase11-driven inflammasome activation (30). Although OxPL induce inflammatory gene expression, they do not induce NF-κB signaling (109). Mounting evidence suggests that spleen tyrosine kinase (Syk), target of the drug fostamatinib (201), is downstream of TLR2 signaling induced by a variety of ligands (202–206). Syk has been shown to play a crucial role in the action of oxidized cholesteryl esters on macrophages (62–64), and treatment with the orally available Syk inhibitor, fostamatinib, prevented atherogenesis in LDLR-receptor deficient mice fed a high-fat diet (207).

Here we show that macrophages sense OxPL to reprogram their metabolism towards a redox-regulatory phenotype accompanied by antioxidant and inflammatory gene expression, via a mechanism involving TLR2 and Syk-driven ceramide accumulation. Together, we provide a new model for macrophage adaptation to oxidative tissue damage, revealing unexpected roles of TLR2, ceramides, and Hif1a in cellular metabolic reprogramming and translation into inflammatory gene expression.

3.3 RESULTS

3.3.1 OxPLs induce a metabolic shift to glutathione (GSH) synthesis in macrophages

Recently, the metabolomic profiles of M1 and M2 macrophages have been described (177), demonstrating a shift to a highly glycolytic metabolism in M1 (175, 208) and a dependence on oxidative phosphorylation in M2 macrophages (176). To investigate the cellular metabolism of

Mox macrophages, we performed metabolomic analyses (Metabolon, Inc.) on bone marrow-derived macrophages (BMDMs) that had been treated with either vehicle, OxPAPC, the TLR2 agonist lipoteichoic acid (LTA), or interleukin-4 (IL4) for 4 hours, to induce M0, Mox, M1, or M2 phenotypic polarization, respectively (**Figure 3-1A)** (146). Comparison of the phenotypes revealed that Mox macrophages displayed a metabolomic profile strikingly different from M1 or M2 macrophages, characterized by 104 uniquely regulated metabolites **(Figure 3-1B**). Volcano plots illustrated that most of the metabolites that were uniquely and most significantly changed in Mox macrophages belonged to energy metabolism and antioxidant production pathways (**Figure 3-1C**) and included cysteine, cysteine-glutathione disulfide, and γ-glutamyl-cysteine (**Figure 3-1D**), essential components of the glutathione synthesis pathway. Furthermore, only in Mox macrophages were glutamate levels significantly decreased, consistent with its use for glutathione synthesis (**Figure 3-1D**). Together, these data demonstrate that the glutathione synthesis pathway is specifically upregulated in Mox (**Figure 3-1E**), but not in M1 or M2 macrophages (**Figure 3-2A**).

In order to alleviate oxidative stress, initially depleted glutathione needs to be replenished over time to restore redox homeostasis, as has been shown in macrophages treated with oxidized LDL (209). We found that treatment of macrophages with OxPAPC significantly decreases reduced glutathione (GSH) levels after 6 hours (**Figure 3-1F**), but after 24-hours GSH levels returned to normal, indicative of *de novo* GSH production (**Figure 3-1F**). On the other hand, in LTA-treated macrophages GSH levels remained unchanged after 6 and 24 hours (**Figure 3-2B**).

Taken together, these data demonstrate that macrophages uniquely respond to phospholipid oxidation products by initially channeling their metabolism to adopt a redox-regulating phenotype.

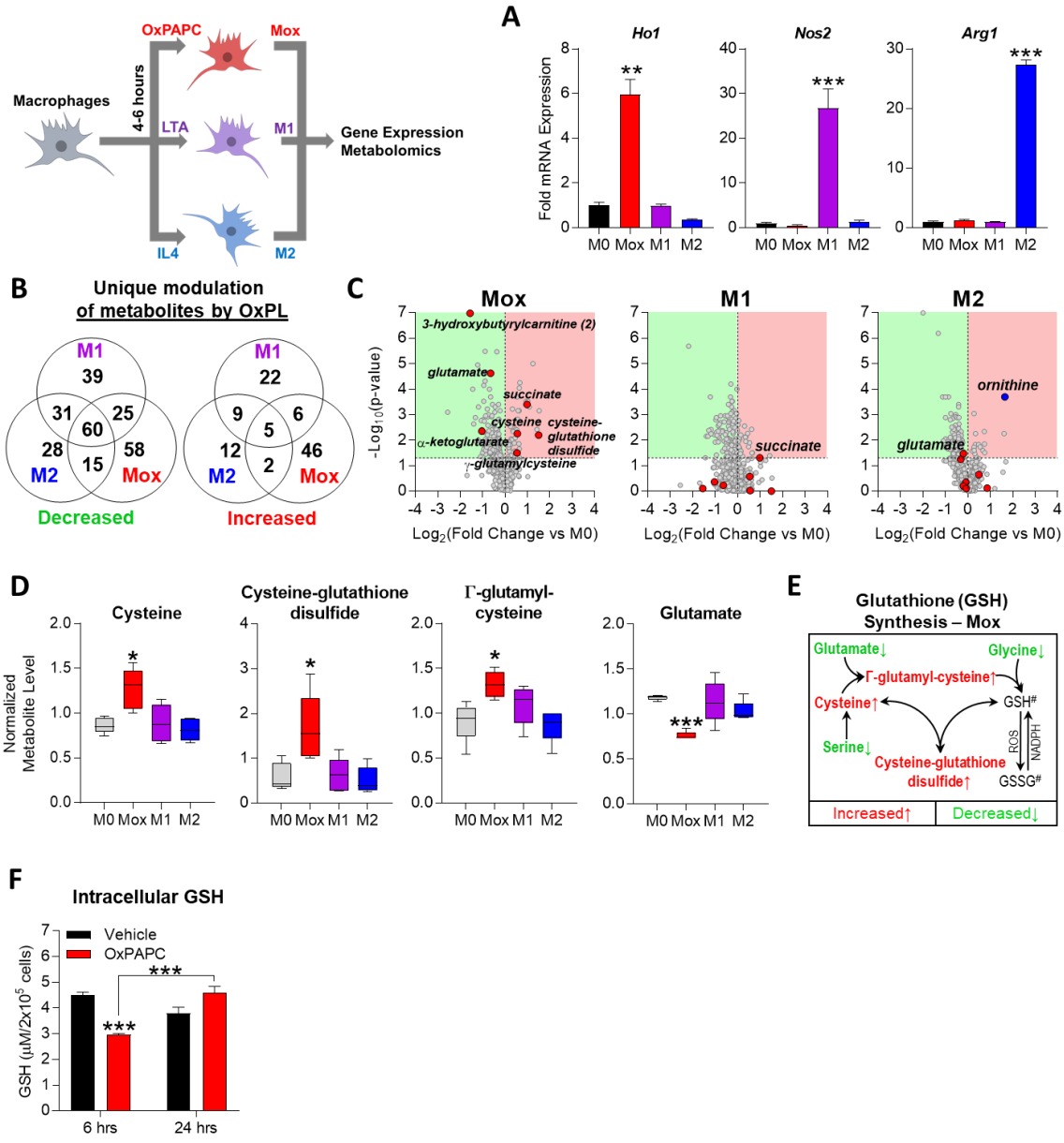

Figure 3-1: OxPLs induce a metabolic shift to glutathione (GSH) synthesis in macrophages

Figure 3-1 Legend

A. mRNA expression by qPCR measured in BMDMs treated with 1µg/mL LTA (M1), 10ng/mL IL4 (M2), or 10µg/mL OxPAPC (Mox) for 4 hours. Genes measured are *Nos2* (iNOS; M1 marker), *Arg1* (M2 marker), and *Ho1* (Mox marker). ($n \geq 3$)

B. Metabolomics was performed on bone marrow-derived macrophages (BMDMs; harvested and cultured from C57BL/6 mouse hind legs) after 6 hour treatment with M0 (vehicle, RPMI media), M1 (1µg/mL LTA), M2 (10ng/mL IL4), and Mox (10µg/mL OxPAPC) stimuli (n = 5). Of a total of 512 metabolites of known identity, following normalization to protein concentration by Bradford assay, Welch's two-sample t-test was used to identify metabolites that differed significantly between experimental groups. A summary of the numbers of metabolites that achieved statistical significance (Welch's 2-sided t-test, $p \leq 0.05$) either uniquely per individual treatment or commonly between treatments, represented in a Venn diagram. (n = 5)

C. Volcano plots produced using data from metabolomics of polarized BMDMs (see A) highlighting significantly ($p \leq 0.05$) increased (red) or decreased (green) metabolites per group. Metabolites related to energy metabolism and redox homeostasis significantly changed in Mox (OxPAPC-treated) BMDMs are highlighted as red circles in each panel. Ornithine is highlighted in the M2 (IL4-treated) BMDMs as a positive control.

D. Quantification of individual metabolites involved in the glutathione synthesis pathway in BMDMs represented by box and whisker plots. The highest and lowest bars represent the maximum distribution, while the upper, middle, and lower lines of the box represent the first quartile, median, and third quartile, respectively. (n = 5)

E. Glutathione synthesis pathway in Mox BMDMs (10µg/mL OxPAPC, 6 hours). $^{\#}$GSH (reduced glutathione) and GSSG (oxidized glutathione) levels were not measured.

F. Intracellular reduced glutathione (GSH) levels in BMDMs treated for 6 or 24 hours with vehicle (RPMI media) or 10µg/mL OxPAPC, measured using the GSH/GSSG Ratio Detection Assay Kit (Abcam; ab138881). (n = 4)

Data are expressed as mean ± SEM. Biological replicates indicated by (n). Statistical significance calculated by Welch's 2-sided t-test ($^{*}p \leq 0.05$; $^{**}p < 0.01$; $^{***}p < 0.001$).

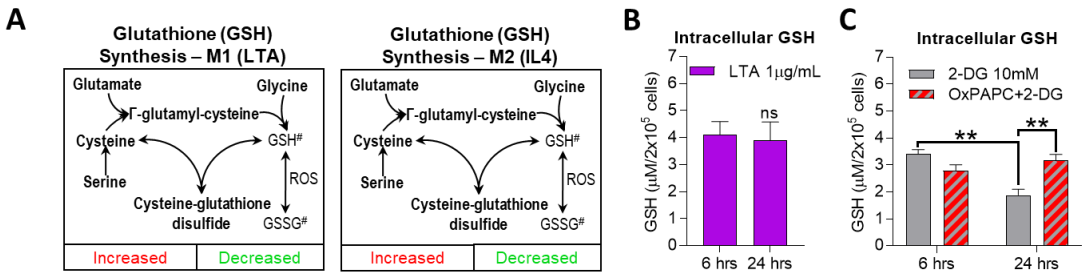

Figure 3-2: Supplement to Figure 3-1 and Figure 3-3

Figure 3-2 Legend

A. Glutathione synthesis pathway in M1 (1µg/mL LTA, 6 hours) and M2 (10ng/mL IL4, 6 hours) BMDMs. #GSH (reduced glutathione) and GSSG (oxidized glutathione) levels were not measured. (n = 5)

B. Intracellular reduced glutathione (GSH) levels in BMDMs treated for 6 or 24 hours with 1µg/mL LTA, measured using the GSH/GSSG Ratio Detection Assay Kit (Abcam; ab138881). (n = 4)

C. Intracellular reduced glutathione (GSH) levels in BMDMs treated for 6 or 24 hours with 10mM 2-DG or with 10mM 2-DG and 10µg/mL OxPAPC, measured using the GSH/GSSG Ratio Detection Assay Kit (Abcam; ab138881). (n = 4)

Data are expressed as mean ± SEM. Biological replicates indicated by (n). Statistical significance calculated by Welch's 2-sided t-test (*$p \leq 0.05$; **$p < 0.01$; ***$p < 0.001$).

3.3.2 OxPL-treated macrophages induce the pentose phosphate pathway while relying on glucose metabolism for antioxidant gene expression.

M1 macrophages utilize glucose and M2 macrophages use fatty acids for energy production (175, 176); however, the fuel source for Mox macrophages is not known. Metabolomic analysis demonstrated that glucose levels significantly increased in OxPAPC-treated macrophages (**Figure 3-3A**), suggesting that Mox macrophages utilize glucose as fuel for cellular functions. Indeed, treatment of BMDMs with OxPAPC for 6 hours resulted in a concentration-dependent increase of intracellular glucose levels, comparable to effects of the TLR2 ligand LTA or insulin (**Figure 3-3B**). Furthermore, OxPAPC induced expression of *Glut1* mRNA in BMDMs in a concentration- and time-dependent manner (**Figure 3-3C**). Next, we investigated whether glucose metabolism is required for the OxPAPC-induced expression of Nrf2-dependent enzymes. We found that pre-treatment of BMDMs with 10mM 2-deoxyglucose (2-DG), a competitive inhibitor of hexokinase (given at half the concentration of glucose in the culture medium), blocked OxPAPC-induced *Gclm*, *Ho1*, *Srxn1*, and *Txnrd1* expression (**Figure 3-3D**). Furthermore, we found that the OxPAPC and 2-DG co-treated macrophages did not recover GSH levels after 24 hours (**Figure 3-2C**), although GSH levels were still significantly higher than in macrophages treated with 2-DG alone. These data show that glucose metabolism plays an essential role in glutathione synthesis in Mox macrophages.

Many of the Nrf2-dependent enzymes, such as those involved in GSH synthesis, require NADPH as a reducing equivalent (210–214), which is primarily produced by the pentose phosphate pathway (PPP) (215, 216). We found that 6-hour treatment of macrophages with OxPAPC significantly depleted NADPH (**Figure 3-3E**), and 6 and 24-hour treatment with OxPAPC induced gene expression of enzymes involved in the PPP, including *Pgd, G6pd,* and *Taldo,* in a time- and concentration-dependent manner (**Figure 3-3F**). These data demonstrate

that a redox-regulatory metabolism in Mox macrophages is fueled by glucose with a concomitant shift to the PPP to support newly expressed antioxidant genes and GSH production.

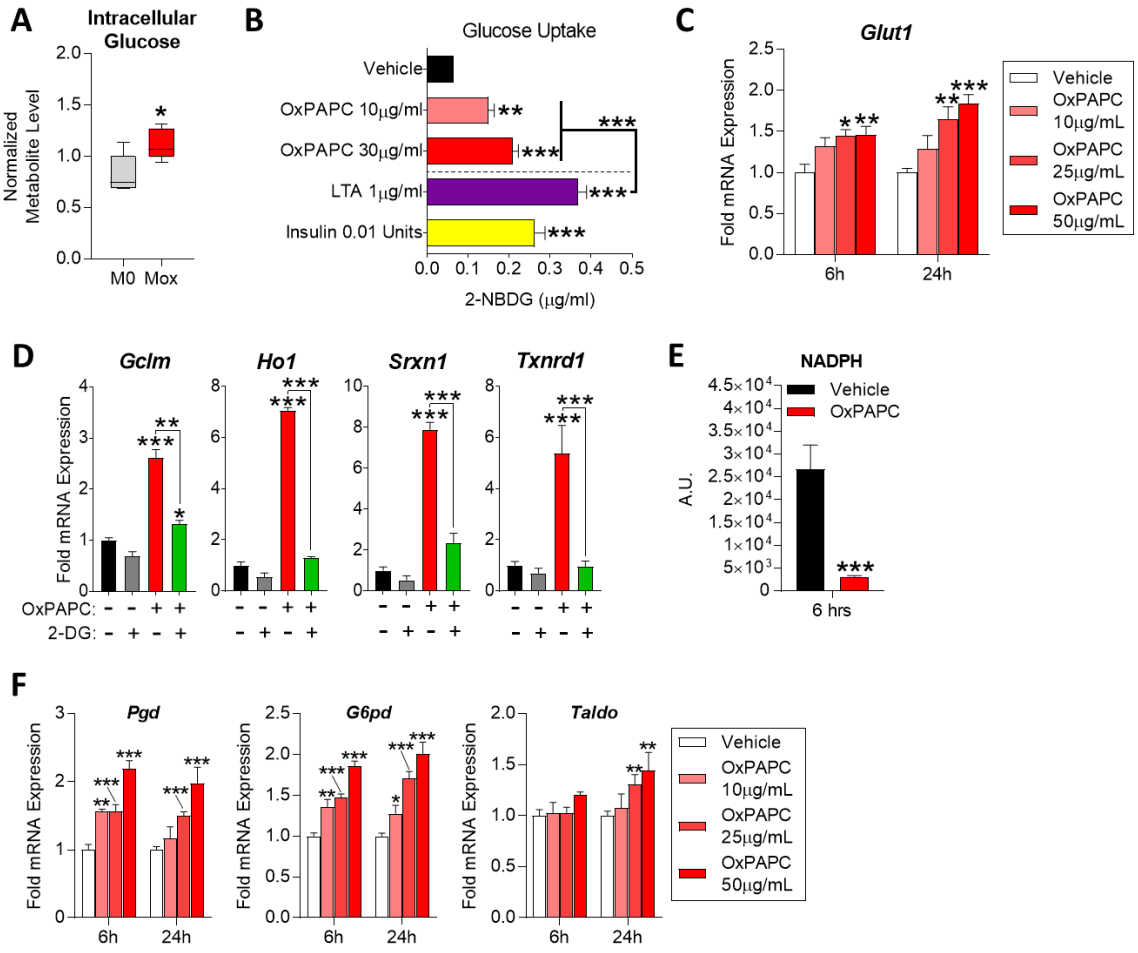

Figure 3-3: OxPL-treated macrophages induce the pentose phosphate pathway while relying on glucose metabolism for antioxidant gene expression

Figure 3-3 Legend

A. Intracellular glucose levels from metabolomics of polarized BMDMs represented by box and whisker plots. (n = 5)
B. Glucose uptake in BMDMs treated with vehicle (RPMI media), 10-30µg/mL OxPAPC, 1µg/mL LTA, or 0.01 units of insulin for 6 hours. Uptake measured by fluorescence quantification of 2-NBGD (2-(N-(7-nitrobenz-2-oxa-1,3-diazol-4-yl)amino)-2-deoxy-glucose; fluorescent 2-deoxy-glucose analog). (n = 4)
C. *Glut1* mRNA expression as measured by qPCR in RAW264.7 cells after 6 and 24 hour treatment with vehicle (RPMI media) or 10-50µg/mL OxPAPC. (n = 4)
D. mRNA expression of redox homeostasis genes measured by qPCR in BMDMs after 4 hour treatment with 10µg/mL OxPAPC and/or 10mM 2-deoxy-D-glucose (2-DG). (n = 3)
E. Intracellular NADPH levels in BMDMs treated with 10µg/mL OxPAPC for 6 hours, measured using the NADP/NADPH Assay Kit (Abcam; ab65349). (n = 4)
F. mRNA expression of pentose phosphate pathway genes measured by qPCR in RAW264.7 cells treated with 10-50µg/mL OxPAPC for 6 or 24 hours. Genes measured include *Pgd*, *G6pdx*, and *Taldo*. (n = 4)
G. mRNA expression of metabolism-related genes measured by qPCR in BMDMs after 24 hour treatment with 6.4µM (50µg/mL) OxPAPC, OxPAPE, or OxAA. (n = 3)

Data are expressed as mean ± SEM. Biological replicates indicated by (n). Statistical significance calculated by Welch's 2-sided t-test (*$p \leq 0.05$; **$p < 0.01$; ***$p < 0.001$).

3.3.3 The macrophage metabolic adaptation to OxPLs involves transient suppression of aerobic glycolysis accompanied by Hif1α-dependent and independent gene expression

While homeostatic energy production of resting immune cells is primarily dependent on oxidative phosphorylation, stress conditions and inflammatory stimulation induce a metabolic state that heavily relies on glycolytic bioenergetics (175, 217, 218). Phenotypic polarization to pro-inflammatory M1 macrophages involves a switch to Warburg metabolism (aerobic glycolysis) leading to lactate secretion and a succinate-dependent upregulation of inflammatory genes via Hif1α (175). However, in Mox macrophages, metabolomic analysis showed that intracellular lactate is significantly decreased, strikingly different from LTA-induced M1 macrophages (**Figure 3-4A**). Moreover, metabolites of the glycolytic pathway, including fructose-1,6-bisphosphate, dihydroxyacetone phosphate (DHAP), and pyruvate are decreased in Mox, again, strikingly different from LTA-induced M1 and IL4-induced M2 macrophages (**Figure 3-4B**). Together, metabolomic analysis indicated that aerobic glycolysis is suppressed in Mox macrophages. Supporting this notion, extracellular flux analysis of BMDMs and RAW264.7 cells demonstrated that OxPAPC significantly decreased basal and stressed extracellular acidification rate (ECAR), reflecting decreased lactate production (**Figure 3-4C**; **Figure 3-5A**). Strikingly, treatment with OxPAPC for 4 hours inhibited ECAR not only in naïve, but also in M1-polarized BMDMs that had been pre-treated with LPS for 16 hours (**Figure 3-4D**). Together, these data point to a novel acute metabolic reprogramming of macrophages in response to OxPLs that is characterized by suppression of aerobic glycolysis.

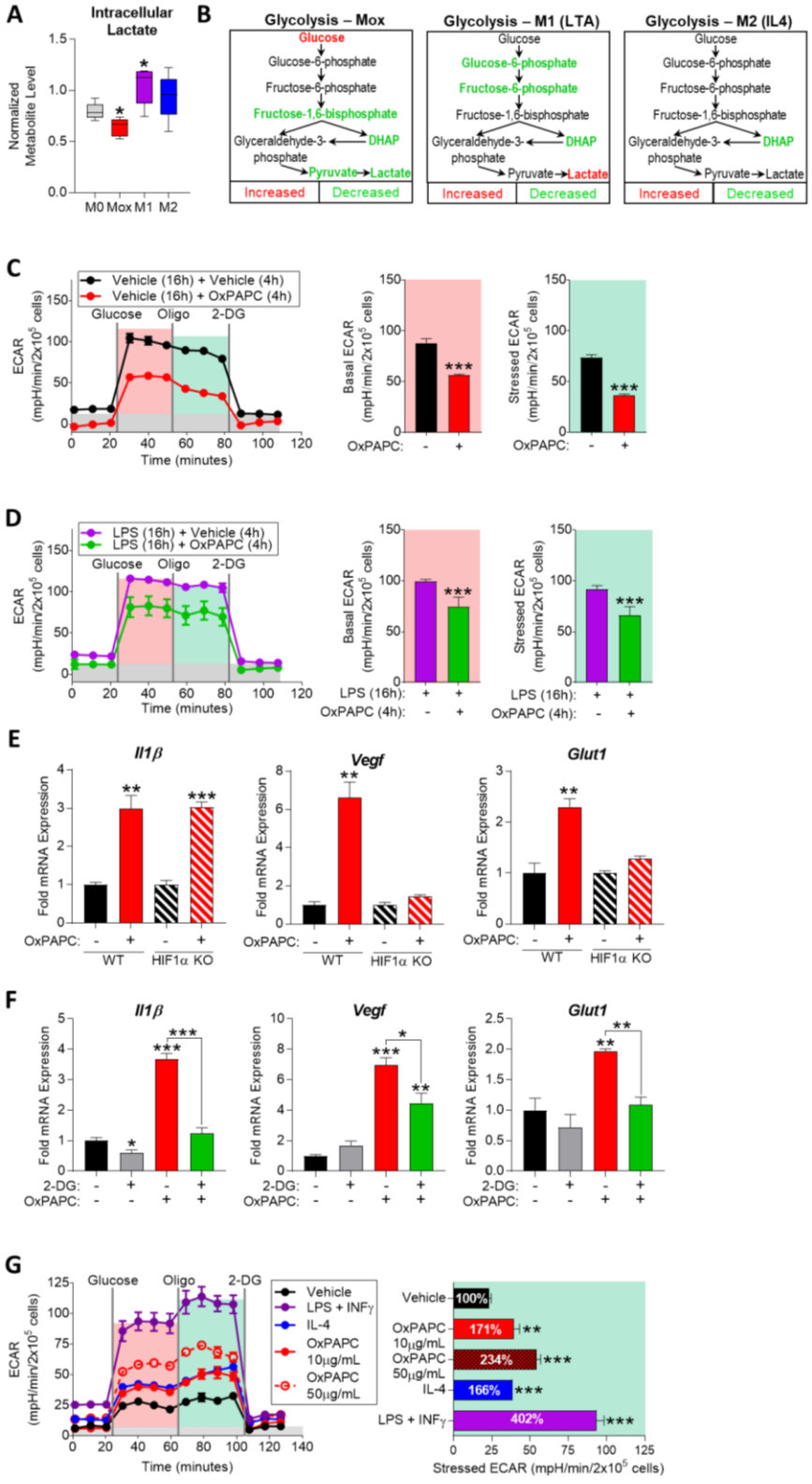

Figure 3-4: The macrophage metabolic adaptation to OxPLs involves transient suppression of aerobic glycolysis and Hif1α-dependent and independent gene expression

Figure 3-4 Legend

A. Intracellular lactate from metabolomics of M0 (vehicle, RPMI media), Mox (10μg/mL OxPAPC), M1 (1μg/mL LTA), and M2 (10ng/mL IL4) BMDMs (6 hours) represented by box and whisker plots. (n = 5)
B. Glycolysis pathway in Mox, M1, and M2 BMDMs (6 hours). (n = 5)
C. Glycolytic stress test (GST) of BMDMs treated with vehicle (RPMI media) or 10μg/mL OxPAPC for 4 hours (n = 4). The extracellular acidification rate (ECAR) was measured after injection of 20mM glucose, 1μM oligomycin, and 80mM 2-DG addition to produce the basal (red), stressed (teal), and background (gray) ECAR, respectively. Basal and stressed ECAR were calculated by subtracting the mean ECAR of the post-glucose (basal) or post-Oligomycin (stressed) measurements from the mean ECAR of the post-2-DG measurements.
D. GST of BMDMs treated with 1μg/mL LPS for 16 hours to induce M1 polarization, followed by 4 hour treatment of vehicle (RPMI media) or 10μg/mL OxPAPC (n = 4).
E. mRNA expression of *Il1β*, *Vegf*, and *Glut1* measured by qPCR in WT and HIF1α-KO BMDMs treated with vehicle or 50μg/mL OxPAPC for 6 hours. (n = 4)
F. mRNA expression of *Il1β*, *Vegf*, and *Glut1* measured by qPCR in WT BMDMs treated with 10mM 2-DG and/or 10μg/mL OxPAPC for 4 hours. (n = 3)
G. GST of BMDMs treated with vehicle, 1μg/mL LPS (M1), 10ng/mL IL4 (M2), or 10-50μg/mL OxPAPC (Mox) for 24 hours. (n = 4)

Data are expressed as mean ± SEM. Biological replicates indicated by (n). Statistical significance calculated by Welch's 2-sided t-test (*$p \leq 0.05$; **$p < 0.01$; ***$p < 0.001$).

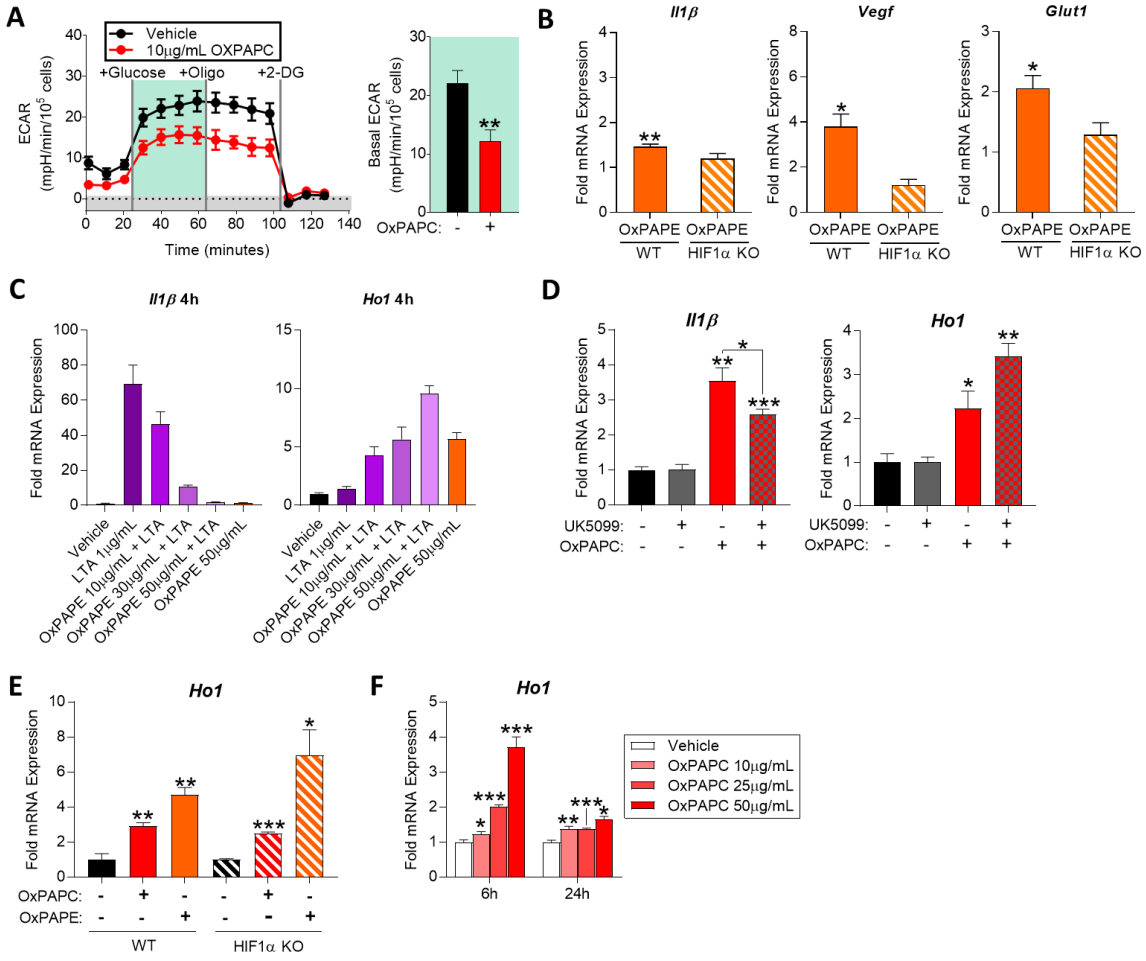

Figure 3-5: Supplement to Figure 3-4

Figure 3-5 Legend

A. Glycolytic stress test (GST) of RAW264.7 cells treated with vehicle (RPMI media) or 10μg/mL OxPAPC for 4 hours (n = 4). The extracellular acidification rate (ECAR) was measured after injection of 20mM glucose, 1μM oligomycin, and 80mM 2-DG addition to produce the basal (red), stressed (teal), and background (gray) ECAR, respectively. Basal and stressed ECAR were calculated by subtracting the mean ECAR of the post-glucose (basal) or post-Oligomycin (stressed) measurements from the mean ECAR of the post-2-DG measurements.

B. mRNA expression of *Il1β*, *Vegf*, and *Glut1* measured by qPCR in WT and HIF1α-KO BMDMs treated with 50μg/mL OxPAPE for 4 hours. (n = 4)

C. mRNA expression of *Il1β* and *Ho1* as measured by qPCR in BMDMs treated with vehicle, 1μg/mL LTA, 50μg/mL OxPAPE, or both LTA and 10-50μg/mL OxPAPE for 4 hours. (n = 4)

D. mRNA expression of *Il1β* and *Ho1* as measured by qPCR in BMDMs treated with vehicle, 20μM UK5099 (inhibitor of pyruvate transport to mitochondria), 10μg/mL OxPAPC, or both UK5099 and OxPAPC for 4 hours. (n = 4)

E. mRNA expression of *Ho1* measured by qPCR in WT and HIF1α-KO BMDMs treated with vehicle, 50μg/mL OxPAPC, or 50μg/mL OxPAPE for 6 hours. (n = 4)

F. mRNA expression of *Ho1* measured by qPCR in RAW264.7 cells treated with 10-50μg/mL OxPAPC for 6 or 24 hours. (n = 4)

Data are expressed as mean ± SEM. Biological replicates indicated by (n). Statistical significance calculated by Welch's 2-sided t-test (*$p \leq 0.05$; **$p < 0.01$; ***$p < 0.001$).

In M1 macrophages, increased aerobic glycolysis has been linked to inflammatory gene expression including *Il1β*, by a mechanism involving Hif1α (175). However, using BMDMs isolated from Hif1α-deficient mice (219), we found that OxPAPC-induced *Il1β* expression was independent of Hif1α, while OxPAPC-induced expression of *Glut1* and *Vegf* required Hif1α (**Figure 3-4E**). Nevertheless, OxPAPC-induced *Glut1*, *Vegf* and *Il1β* all were dependent on glycolysis, since inhibition of glucose phosphorylation blocked OxPAPC-induced expression of these genes (**Figure 3-4F**). Inhibition of pyruvate transport into mitochondria significantly reduced OxPAPC-induced *Il1β*, while increasing Nrf2-dependent *Ho1* gene expression (**Figure 3-5D**), which did not require Hif1α (**Figure 3-5E**) and was restricted to early time points (**Figure 3-5F**). In contrast, OxPAPC-induced expression of genes involved in glycolysis and the PPP was sustained for up to 24 hours (**Figure 3-3C; Figure 3-3F**), indicating metabolic adaptation of macrophages to these oxidation-derived DAMPs. To further investigate the long-term adaptation of macrophages to OxPLs, we treated BMDMs with OxPAPC for 24 hours and then analyzed ECAR to assess aerobic glycolysis. Compared to the vehicle control, long-term exposure of macrophages to OxPAPC significantly increased ECAR in a concentration-dependent manner (**Figure 3-4G**). As previously reported, alternatively activated M2 polarization by IL4 for 24 hours also increased lactate production (220) and classically activated M1 polarization using LPS & INFγ resulted in the expected strong shift towards aerobic glycolysis (**Figure 3-4G**).

Taken together, these data demonstrate that, through suppression of aerobic glycolysis, OxPLs acutely reprogram glucose metabolism in macrophages to support production of NADPH, antioxidant enzymes, and antioxidant metabolites. The results implicate different metabolic requirements for Hif1α and Nrf2-dependent gene expression in Mox macrophages and also raise the possibility that different OxPL species present in OxPAPC selectively induce inflammatory versus metabolic and antioxidant gene expression. Long-term adaptation to OxPLs, once GSH levels return to normal, results in a sustained, elevated use of glucose that may be eventually

converted to lactate. Furthermore, the fact that glucose taken up by Mox macrophages is not initially converted to lactate, as in M1 macrophages, implies that it is instead converted to pyruvate, which enters the TCA cycle.

3.3.4 OxPLs redirect TCA metabolism and inhibit macrophage respiratory capacity

Analysis of TCA cycle metabolites revealed that α-ketoglutarate levels were significantly lower in Mox macrophages, compared to M0, M1 or M2 macrophages (**Figure 3-6A**). α-ketoglutarate can be metabolized to glutamate, one of the essential substrates for GSH synthesis (43), by aspartate transaminase (AST or *Got1*) (221). In support of this mechanism, we have previously shown that *Got1* is significantly upregulated in Mox, but not in M1 or M2 macrophages (146). These findings indicate that OxPLs impact TCA metabolism. Analyses of mitochondrial gene expression demonstrated significantly lower expression of *Cox5b*, a complex IV component after 4 hours of treatment with OxPAPC (**Figure 3-7A**). Moreover, we found that succinate levels were significantly increased (**Figure 3-6B**), while succinate dehydrogenase (SDH; a component of TCA cycle and electron transport chain) mRNA levels were significantly decreased (**Figure 3-6C**) and protein levels trended to be lower in Mox macrophages (**Figure 3-7B**). Levels of methylmalonate, an inhibitor of SDH (222), were significantly increased in Mox macrophages (**Figure 3-6D**). In addition, we found that levels of a variety of carnitines, molecules essential for β-oxidation through facilitation of mitochondrial fatty acid transport, were significantly decreased in Mox macrophages (**Table 3-1**). Together, these data demonstrate that in contrast to M1 and M2 macrophages, Mox macrophages redirect the flux of TCA intermediates towards GSH synthesis at the level of SDH (**Figure 3-6E**), indicating a unique glucose utilization mechanism supporting redox homeostasis.

To examine the consequences of this metabolic switch for oxidative phosphorylation (OXPHOS) in Mox macrophages, we treated BMDMs with OxPAPC and measured respiratory capacity by analyzing oxygen consumption rate (OCR). We found that OxPAPC inhibited

macrophage respiration after 4 hours, demonstrated by a depressed basal and maximal OCR (**Figure 3-6F**). OxPAPC also inhibited OCR in RAW264.7 macrophages (**Figure 3-7C**). This effect was replicated in BMDMs with OxPAPE, suggesting that this effect is not phospholipid head group dependent (**Figure 3-6G**). To test whether the oxidized moiety is the structural component of OxPL responsible for the effects seen, we treated BMDMs non-enzymatically oxidized arachidonic acid (OxAA) and found that the antioxidant, inflammatory, and metabolic gene expression were induced to the same extent as with OxPAPC and OxPAPE (**Figure 3-7D**). This effect was dependent on oxidative modification of the phospholipid, since neither PAPC nor dimystiroyl-phosphatidylcholine (DMPC, a phospholipid containing saturated fatty acids and thus cannot be oxidized) inhibited respiratory capacity (**data not shown**). The inhibition of respiratory capacity of LysoPC was not to the same extent as OxPAPC, or POVPC and PGPC, nor did LysoPC inhibit the glycolytic capacity of macrophages (**Figure 3-7E**). To test whether the effect of OxPLs on mitochondrial respiration was immediate, we directly injected OxPAPC to the cells during the stress test. While exposure to OxPAPC did not affect basal OCR within the first 2 hours, the maximal OCR was significantly inhibited (**Figure 3-6H**), indicating that the electron transport chain within mitochondria is affected. M2 polarization with IL4 was shown to increase OCR (176), however, we found that OxPAPC inhibits respiratory capacity of M2-polarized macrophages, essentially overriding the effect of IL4 (**Figure 3-6I**).

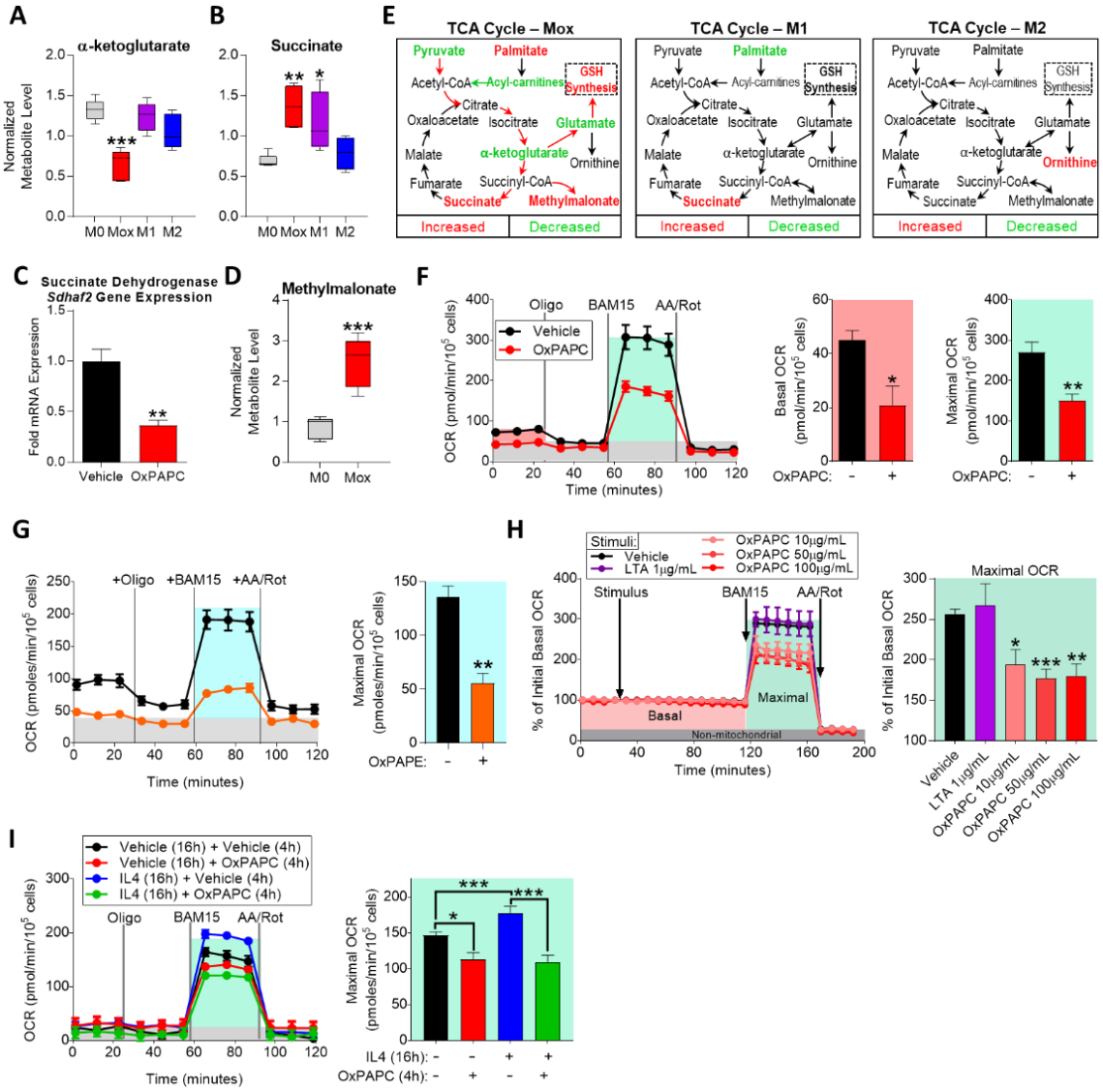

Figure 3-6: OxPLs redirect TCA metabolism and inhibit macrophage respiratory capacity

Figure 3-6 Legend

A. Intracellular α-ketoglutarate from metabolomics of M0 (vehicle, RPMI media), Mox (10μg/mL OxPAPC), M1 (1μg/mL LTA), and M2 (10ng/mL IL4) BMDMs (6 hours) represented by box and whisker plots. (n = 5)
B. Intracellular succinate from metabolomics of M0, Mox, M1, and M2 BMDMs (6 hours) represented by box and whisker plots. (n = 5)
C. mRNA expression of nuclear-encoded complex II subunit, *Sdhaf2*, as measured by qPCR in BMDMs treated with vehicle or 10μg/mL OxPAPC for 4 hours. (n = 4)
D. Fold change of intracellular succinate dehydrogenase inhibitor, methylmalonate, in Mox BMDMs compared to M0 as found by metabolomics. (n = 5).
E. The tri-carboxylic acid (TCA) cycle in Mox, M1, and M2 BMDMs, highlighting metabolites significantly changed from M0. (n = 5)
F. Mitochondrial stress test (MST) of BMDMs treated with vehicle (RPMI media) or 10μg/mL OxPAPC for 4 hours (n = 4). The oxygen consumption rate (OCR) was measured initially (basal; red), and after injection of 1μM oligomycin, 2μM of the uncoupler BAM15 (maximal; teal), and 10μM antimycin A & 1μM rotenone (AA/Rot; gray; non-mitochondrial). Basal and maximal OCR were calculated by subtracting the mean OCR of the first three (basal) or post-BAM15 (maximal) measurements from the mean OCR of the post-AA/Rot measurements.
G. MST of BMDMs treated with vehicle (RPMI media) or 30μg/mL OxPAPE for 4 hours. (n = 4)
H. Basal and maximal oxygen consumption rate (OCR) measured in BMDMs treated acutely with vehicle, 1μg/mL LTA, or 10-100μg/mL OxPAPC. Treatment was injected into wells containing BMDMs after 30 minutes of unstimulated measurement. OCR was measured for 2 hours (basal) after which 2μM BAM15 was injected to assess maximal OCR. Antimycin A and rotenone were injected to determine the non-mitochondrial OCR (background). Data represented as %OCR, where 100% refers to the unstimulated basal OCR. (n = 4)
I. MST of BMDMs treated with vehicle (RPMI media) or 10ng/mL IL4 for 16 hours, followed by vehicle (RPMI media) or 10μg/mL OxPAPC for 4 hours. (n = 4)

Data are expressed as mean ± SEM. Biological replicates indicated by (n). Statistical significance calculated by Welch's 2-sided t-test (*$p \leq 0.05$; **$p < 0.01$; ***$p < 0.001$).

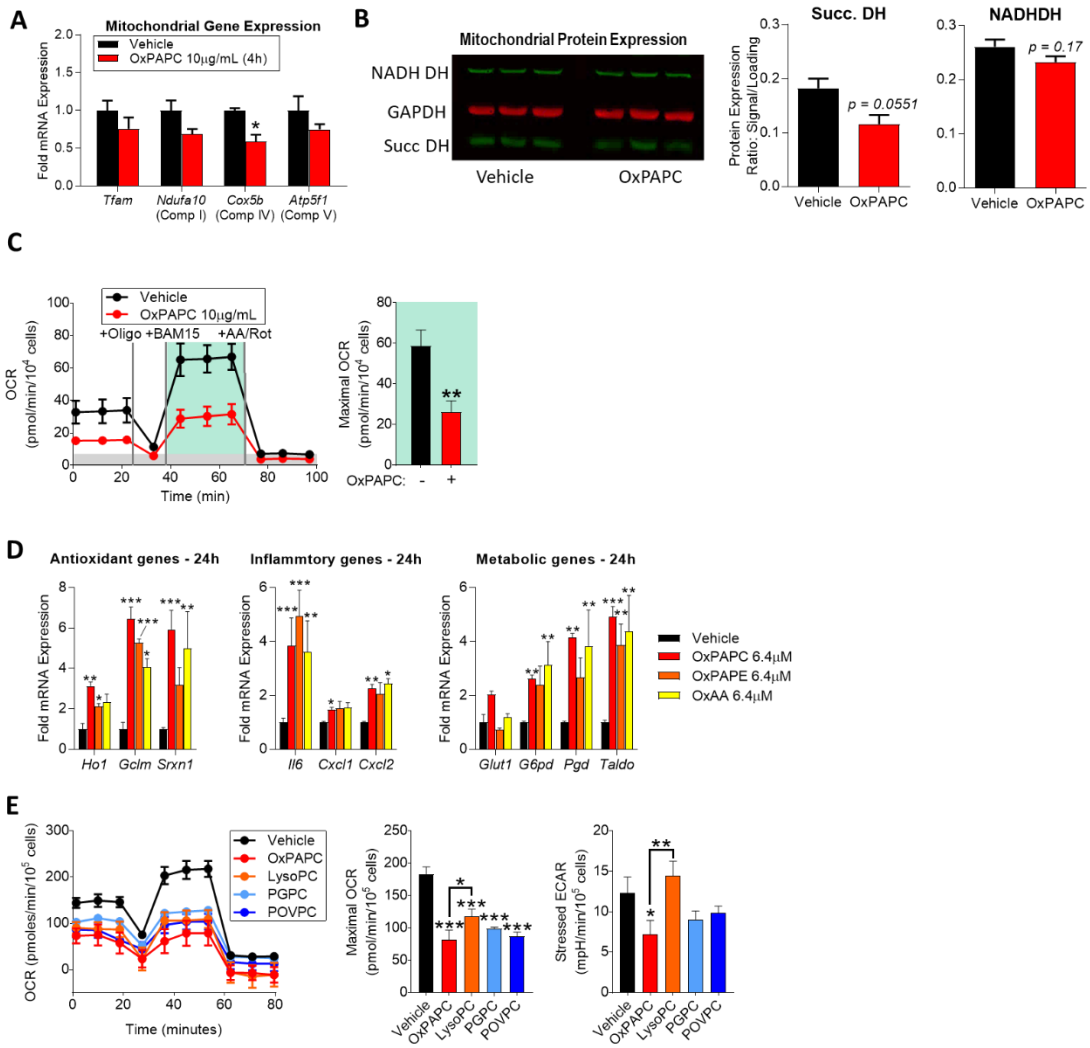

Figure 3-7: Supplement to Figure 3-6

Figure 3-7 Error! Reference source not found. **Legend**

A. mRNA expression of nuclear-encoded mitochondrial transcription factor and complex subunits as measured by qPCR in BMDMs treated with vehicle or 10µg/mL OxPAPC for 4 hours. Genes include *Tfam*, *Ndufa10*, *Cox5b*, and *Atp5f1*. (n = 4)

B. Western blot of total protein isolated from BMDMs treated with vehicle and 10µg/mL OxPAPC for 8 hours. Antibodies for mitochondrial complexes I and II (NADHDH and Succ. DH, green) and GAPDH (red) used to assess mitochondrial protein content. Quantification performed using densitometry, taking the ratio of mitochondrial protein and loading control (GAPDH). (n = 3)

C. Mitochondrial stress test (MST) of RAW264.7 cells treated with vehicle or 10µg/mL OxPAPC for 4 hours. (n = 4)

D. Ceramide accumulation as measured by liquid chromatography-mass spectrometry (LC-MS) of WT BMDMs treated with vehicle or 10µg/mL OxPAPC for 4 hours (n = 5). Ceramides were quantified on an individual species basis, using the integrated peak area of the ion count. The integrated peak area of each analyte was normalized to the internal standard, Cer17:0, and to the protein content of each sample as determined by a Bradford assay. Significance was determined by Welch's 2-sided t-test of the ion count peak area.

E. mRNA expression of ceramide synthase genes as measured by qPCR in BMDMs treated with vehicle, 10µg/mL OxPAPC, or 10µg/mL PGPC for 4 hours. N.D. refers to genes too lowly expressed to be detected. (n = 4)

F. MST of BMDMs treated with vehicle, 10nM myriocin, 10µg/mL OxPAPC, or both for 4 hours. ($n \geq 4$)

Data are expressed as mean ± SEM. Biological replicates indicated by (n). Statistical significance calculated by Welch's 2-sided t-test (*$p \leq 0.05$; **$p < 0.01$; ***$p < 0.001$).

Table 3-1: Analysis of Acyl-carnitine levels in polarized macrophages

Metabolite	Condition	Mean	Standard Deviation	Significance
Carnitine	Mox	0.816	0.062	***
	M1	0.863	0.135	n.s.
	M2	0.973	0.111	n.s.
3-hydroxybutyrylcarnitine (1)	Mox	0.617	0.071	***
	M1	1.362	1.233	n.s.
	M2	1.444	1.151	n.s.
3-hydroxybutyrylcarnitine (2)	Mox	0.343	0.033	***
	M1	1.597	2.319	n.s.
	M2	1.820	2.128	n.s.
Acetylcarnitine	Mox	0.676	0.073	***
	M1	1.028	0.097	n.s.
	M2	1.033	0.081	n.s.
Deoxycarnitine	Mox	0.990	0.053	n.s.
	M1	0.783	0.080	**
	M2	0.824	0.146	*
Linoleoylcarnitine	Mox	0.644	0.073	***
	M1	0.735	0.343	n.s.
	M2	0.788	0.342	n.s.
Myristoylcarnitine	Mox	0.751	0.099	*
	M1	0.936	0.295	n.s.
	M2	1.019	0.192	n.s.
Oleoylcarnitine	Mox	0.751	0.093	**
	M1	0.804	0.342	n.s.
	M2	0.827	0.245	n.s.
Palmitoleoylcarnitine	Mox	0.537	0.068	***
	M1	0.921	0.307	n.s.
	M2	1.006	0.269	n.s.
Propionylcarnitine	Mox	0.821	0.159	n.s.
	M1	1.065	0.375	n.s.
	M2	1.087	0.411	n.s.
Palmitoylcarnitine	Mox	0.889	0.199	n.s.
	M1	0.640	0.170	**
	M2	0.800	0.159	n.s.
Stearoylcarnitine	Mox	0.919	0.149	n.s.
	M1	0.542	0.138	***
	M2	0.554	0.080	***

† Represented as fold change vs. M0 from metabolomics analysis
* $p < 0.05$
** $p < 0.01$
*** $p < 0.001$

3.3.5 Mitochondrial inhibition by OxPLs requires TLR2-dependent ceramide accumulation

We have previously shown that OxPL-induced inflammatory gene expression is dependent on TLR2 (98). To test whether TLR2 also mediates inhibition of OCR by OxPLs, we used BMDMs isolated from TLR2 deficient mice, which were resistant to OxPAPC-induced *Cxcl1* expression (**Figure 3-8A**). In contrast, OxPAPC-induced *Ho1* expression, which is known to be mediated by Nrf2 (98, 146), was independent of TLR2 (**Figure 3-8A**). We demonstrate that mitochondrial inhibition by OxPAPC was also attenuated in TLR2-deficient macrophages (**Figure 3-8B**), but not in Nrf2-deficient macrophages (**Figure 3-8C**).

Ceramides, products of sphingosine and sphingomyelin metabolism, were shown to directly affect cellular metabolism by inhibiting mitochondrial function (223), and it was previously shown that OxPLs induce ceramide accumulation in RAW264.7 macrophages (224). Using liquid chromatography-mass spectrometry (LC-MS), we demonstrate here that OxPAPC induced significant ceramide accumulation in BMDMs as early as 4 hours (**Figure 3-9A**). Furthermore, we found that OxPAPC did not induce ceramide accumulation in TLR2-deficient macrophages (**Figure 3-8D**).

Further investigation of the mechanism involved in OxPL-induced ceramide production revealed that neither OxPAPC nor its component PGPC significantly affected gene expression of any of the 6 ceramide synthases (*CerS1-6*) (**Figure 3-9B**), indicating that activation of enzymatic activity mediates increased ceramide levels. Ceramide synthesis occurs by two pathways: 1) de novo ceramide synthesis and 2) sphingomyelin recycling (**Figure 3-8E**), which can be assessed using the serine palmitoyltransferase inhibitor myriocin or the neutral sphingomyelinase inhibitor 3-O-methyl-sphingomyelin (3OMS), respectively. We found that inhibition of neutral sphingomyelinase abolished, while inhibition of serine palmitoyltransferase only partially affected the inhibitory effect of OxPAPC on respiratory capacity (**Figure 3-8F; Figure 3-9C**).

Together, these data show that macrophages sense OxPL species via TLR2 to suppress mitochondrial function and OXPHOS, primarily through a neutral sphingomyelin recycling mechanism of ceramide accumulation.

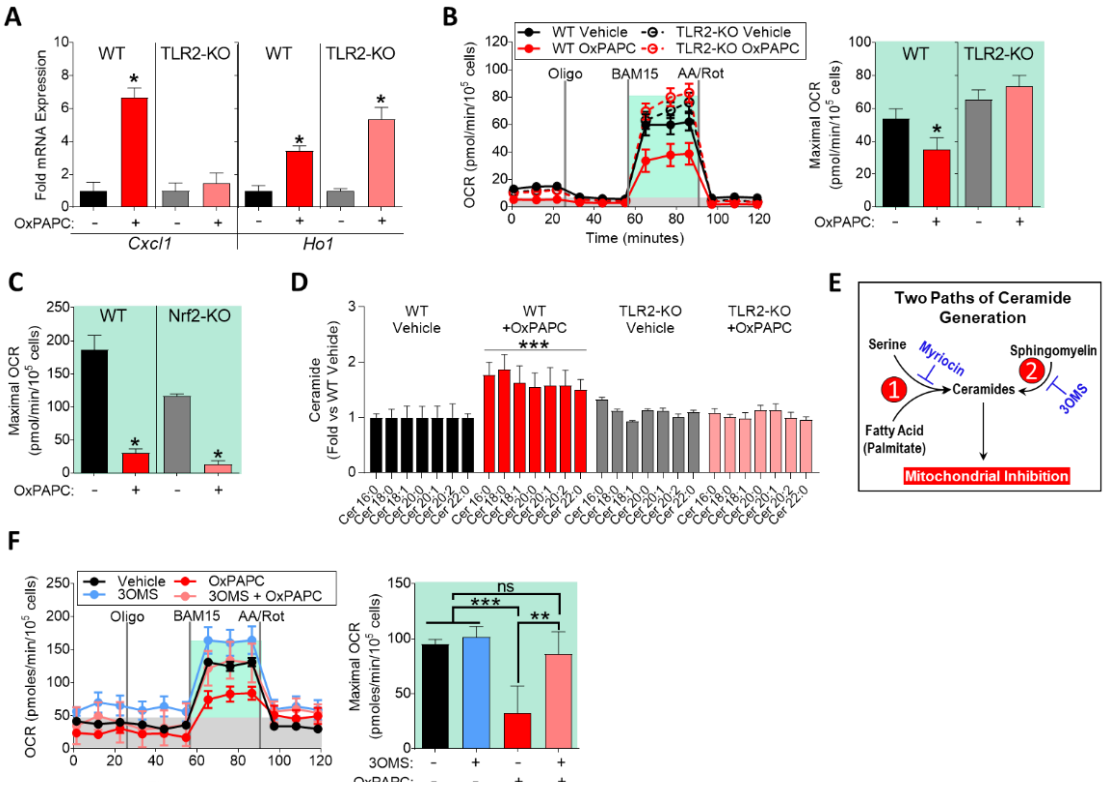

Figure 3-8: Mitochondrial inhibition by OxPLs requires TLR2-dependent ceramide accumulation

Figure 3-8 Legend

A. mRNA expression of *Cxcl1* and *Ho1* measured by qPCR in WT or TLR2-KO BMDMs treated with vehicle or 10µg/mL OxPAPC for 4 hours. (n = 3)
B. MST of WT or TLR2-KO BMDMs treated with vehicle or 10µg/mL OxPAPC for 4 hours. (n = 4)
C. Maximal OCR calculated from the MST of WT (C57BL/6) or Nrf2-KO BMDMs treated with 10µg/mL OxPAPC for 4 hours. (n = 4)
D. Fold change in ceramide accumulation as measured by liquid chromatography-mass spectrometry (LC-MS) of WT or TLR2-KO BMDMs treated with vehicle or 30µg/mL OxPAPC for 16 hours (n = 5). Ceramides were quantified on an individual species basis, using the integrated peak area of the ion count. The integrated peak area of each analyte was normalized to the internal standard, Cer17:0, and to the protein content of each sample as determined by a Bradford assay. Significance was determined by two-way ANOVA of the ion count peak area. Data represented in as fold change compared to WT vehicle control.
E. Summary of two pathways leading to ceramide generation in cells. Pathway 1, referred to as de novo ceramide biogenesis, contains the rate-limiting enzyme serine-palmitoyl-transferase1, which is inhibited by myriocin. Pathway 2, referred to as sphingomyelin recycling, contains acidic and neutral sphingomyelinases as the rate-limiting enzymes. 3-O-methyl-sphingomyelin (3OMS) inhibits neutral sphingomyelinase.
F. MST of WT BMDMs treated with 10µg/mL OxPAPC and/or 1µM 3-O-methyl-sphingomyelin (3OMS), an inhibitor of neutral sphingomyelinase, for 4 hours. (n = 4)

Data are expressed as mean ± SEM. Biological replicates indicated by (n). Statistical significance calculated by Welch's 2-sided t-test (*$p \leq 0.05$; **$p < 0.01$; ***$p < 0.001$).

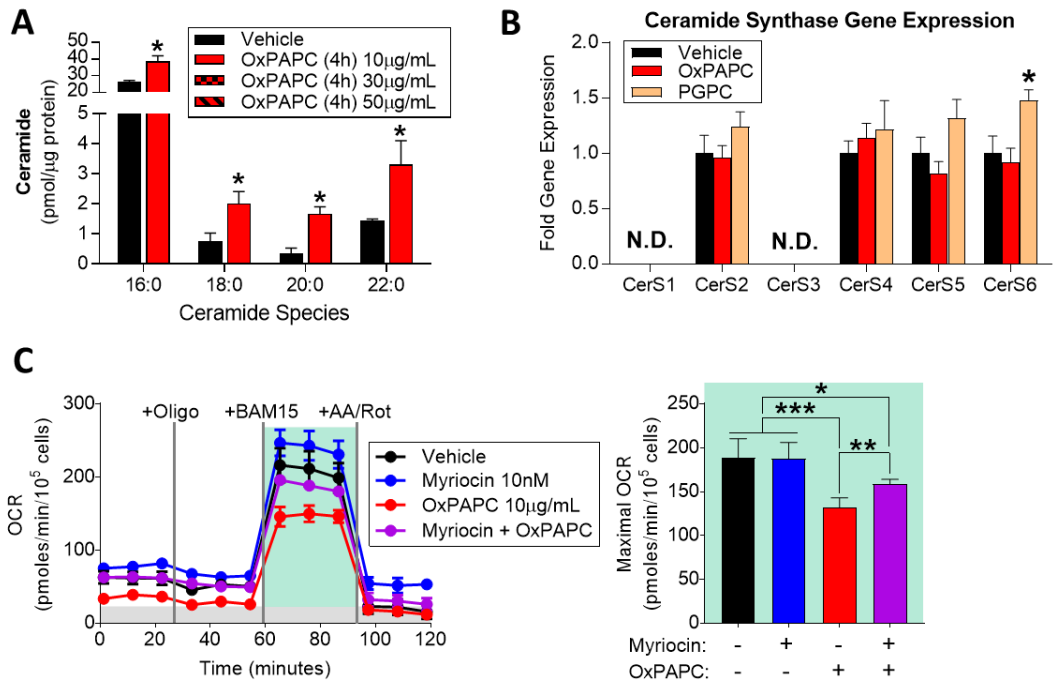

Figure 3-9: Supplement to Figure 3-8

Figure 3-9 Legend

A. Ceramide accumulation as measured by liquid chromatography-mass spectrometry (LC-MS) of WT BMDMs treated with vehicle or 10μg/mL OxPAPC for 4 hours (n = 5). Ceramides were quantified on an individual species basis, using the integrated peak area of the ion count. The integrated peak area of each analyte was normalized to the internal standard, Cer17:0, and to the protein content of each sample as determined by a Bradford assay. Significance was determined by Welch's 2-sided t-test of the ion count peak area.

B. mRNA expression of ceramide synthase genes as measured by qPCR in BMDMs treated with vehicle, 10μg/mL OxPAPC, or 10μg/mL PGPC for 4 hours. N.D. refers to genes too lowly expressed to be detected. (n = 4)

C. MST of BMDMs treated with vehicle, 10nM myriocin, 10μg/mL OxPAPC, or both for 4 hours. ($n \geq 4$)

Data are expressed as mean ± SEM. Biological replicates indicated by (n). Statistical significance calculated by Welch's 2-sided t-test (*$p \leq 0.05$; **$p < 0.01$; ***$p < 0.001$).

3.3.6 Spleen tyrosine kinase (Syk) is a key mediator of OxPL-induced inflammatory gene expression, ceramide accumulation, and mitochondrial inhibition

Recently, Syk has been implicated in TLR2 signaling (202–204). To test if Syk is involved in OxPL-induced inflammatory gene expression and mitochondrial inhibition, we treated wild-type and Syk-KO BMDMs with OxPAPC. We found that inflammatory gene expression was significantly blunted in Syk-KO macrophages, while antioxidant gene expression was not affected (**Figure 3-10A**). Furthermore, treatment with the Syk inhibitor piceatannol inhibited OxPAPC-induced inflammatory gene expression (**Figure 3-10B**). To test whether inhibition of Syk would affect OxPL-induced ceramide accumulation in macrophages, we used the Syk inhibitor R406 (the active version of the prodrug fostamatinib). We found that R406 ablated OxPAPC-induced ceramide accumulation and restored mitochondrial function in macrophages (**Figure 3-10C,D**). Taken together, these data demonstrate that Syk is a crucial mediator for OxPL-induced cellular signaling and they indicate that Syk inhibition is a viable approach to inhibiting OxPL-driven inflammatory gene expression and mitochondrial inhibition.

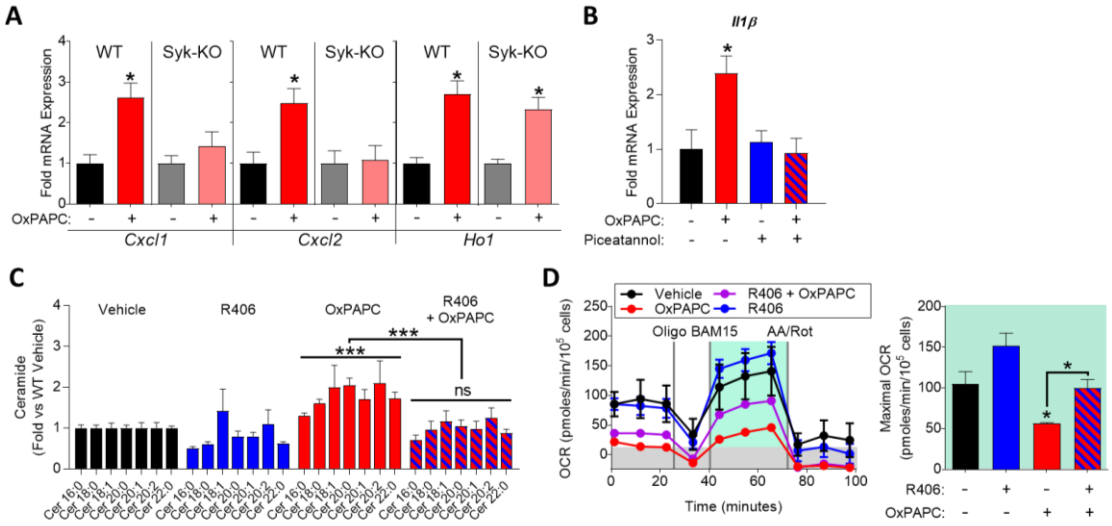

Figure 3-10: Spleen tyrosine kinase (Syk) is a key mediator of OxPL-induced inflammatory gene expression, ceramide accumulation, and mitochondrial inhibition

Figure 3-10 Legend

A. mRNA expression of *Cxcl1*, *Cxcl2*, and *Ho1* measured by qPCR in WT or Syk-KO BMDMs treated with vehicle or 10µg/mL OxPAPC for 4 hours. (n = 3)
B. mRNA expression of *Il1* measured by qPCR in RAW264.7 macrophages treated with vehicle or 10µg/mL OxPAPC for 4 hours. (n = 3)
C. Fold change in ceramide accumulation as measured by liquid chromatography-mass spectrometry (LC-MS) of BMDMs treated with vehicle or 30µg/mL OxPAPC or 50nM R406 (Syk inhibitor) for 16 hours ($n \geq 4$). Ceramides were quantified on an individual species basis, using the integrated peak area of the ion count. The integrated peak area of each analyte was normalized to the internal standard, Cer17:0, and to the protein content of each sample as determined by a Bradford assay. Significance was determined by two-way ANOVA of the ion count peak area. Data represented in as fold change compared to vehicle control.
D. MST of BMDMs treated with 10µg/mL OxPAPC and/or 5µM R406 for 4 hours. (n = 4)

Data are expressed as mean ± SEM. Biological replicates indicated by (n). Statistical significance calculated by Welch's 2-sided t-test (*$p \leq 0.05$; **$p < 0.01$; ***$p < 0.001$).

3.4 CONCLUSION & DISCUSSION

Cellular metabolism of immune cells has risen to the forefront of immunology research, with landmark studies showing that classically activated pro-inflammatory macrophages rely on aerobic glycolysis (175), while alternatively activated anti-inflammatory macrophages require oxidative phosphorylation (176). Here we show for the first time that in response to OxPLs, which are oxidation-derived DAMPs, macrophages reprogram their metabolism to either support redox-regulatory or inflammatory mechanisms. We further identify Syk as a common downstream mediator that is involved in both OxPL-induced ceramide production and inflammatory gene expression.

We find that OxPLs drive production of glutathione in macrophages in a glucose-dependent manner. The production of glutathione, supported by Nrf2-dependent enzyme expression, is unique to Mox macrophages when compared to M1 and M2 macrophages. OxPLs initially deplete glutathione as well as NADPH in macrophages, but glutathione is eventually replenished through a mechanism requiring functional glucose metabolism. This effect is not regulated by TLR2 stimulation alone, as macrophages did not produce glutathione after stimulation with the TLR2 ligand LTA.

Furthermore, we show that PPP enzymes are upregulated and sustained after OxPAPC treatment, providing a source of NADPH necessary to produce glutathione and the function of Nrf2-dependent antioxidant enzymes. The switch to aerobic glycolysis (referred to as the Warburg effect) has been shown to be necessary for pro-inflammatory cytokine production by M1 macrophages (175). In contrast, OxPAPC acutely inhibits lactate production in both naïve (M0) and already glycolytic (M1 and RAW264.7) macrophages. Surprisingly, Mox macrophages still upregulate pro-inflammatory gene expression, and we have shown that they secrete IL1β

(98). We find that OxPAPC induces expression of the glucose transporter *Glut1* via Hif1α, and that Mox macrophages indeed have increased glucose uptake.

After long-term exposure to OxPAPC (24 hours), Mox macrophages switch to lactate production. Concurrently, long-term exposure of macrophages to OxPAPC leads to the restoration of glutathione levels and the abrogation of Nrf2-dependent gene expression while the glucose uptake and PPP-related gene expression remains sustained, indicating an increased potential for glucose metabolism. The two main fates of the glucose-derived metabolite pyruvate are to be converted to lactate or to be transported to the mitochondria for use in the TCA cycle. OxPAPC-treated cells do not acutely promote pyruvate conversion to lactate, given the dramatic decrease we see in ECAR. Instead, our data are consistent with pyruvate being shuttled to the mitochondria for further processing. A striking observation was that Mox macrophages have significantly lower levels of α-ketoglutarate (a Hif1α-repressor (225) and component of the TCA cycle), while having significantly increased levels of succinate (a Hif1α-stabilizer) (225, 226), which may explain how metabolism in Mox macrophages is linked to Hif1α-dependent gene expression.

It has previously been reported that OxPLs induce ceramide accumulation in macrophages (103, 224). Here we find that OxPAPC induced ceramide accumulation in macrophages by a mechanism involving TLR2. Inhibition of mainly sphingomyelin recycling, but also inhibition of *de novo* ceramide synthesis, abrogated OxPAPC-induced mitochondrial inhibition. Ceramide accumulation has been linked to mitochondrial dysfunction, and we find that macrophages deficient in TLR2, but not Nrf2, were protected against OxPAPC-induced mitochondrial dysfunction.

Finally, we identify Syk as a key mediator of OxPL-induced effects that are downstream of TLR2. Genetic deletion or pharmacologic inhibition of Syk abrogated OxPL-induced inflammatory gene expression, ceramide accumulation, and mitochondrial inhibition, without

inhibiting antioxidant gene expression. Syk inhibitors are being tested in preclinical and clinical studies for the treatment of chronic inflammatory disorders (201, 227, 228) and based on our findings, Syk may be a viable therapeutic target to inhibit the perceived negative effects of OxPL in the context of cardiometabolic diseases as well.

Taken together, we show that OxPLs, through a TLR2 and Syk-driven mechanism, reprogram macrophage metabolism, which together with Nrf2-dependent gene expression, is required for production of antioxidant metabolites. In addition, we discovered that metabolic changes in Mox macrophages are tightly linked to redox-regulatory and inflammatory gene expression. Our study provides novel insight into the immunometabolic mechanisms that regulate the translation of oxidative tissue damage into chronic inflammatory responses.

Disclaimer

The work described in this chapter was performed by myself in conjunction with the following team members: Clint Upchurch, Katelyn W. Ahern, Paxton Voigt, Dory DeWeese, Gael Bories, and Akshaya Meher

Portions of this chapter (text and figures) were written as published in Serbulea V, Upchurch CM, Ahern KW, Bories G, Voigt PE, Deweese DE, Meher AK, Harris TE, Leitinger N. Macrophages sensing oxidized DAMPs reprogram their metabolism to support redox homeostasis and inflammation through a TLR2-Syk-ceramide dependent mechanism. *Molecular Metabolism*. 2017 Nov 7. doi: 10.1016/j.molmet.2017.11.002.

4 CHAPTER 4: MACROPHAGE PHENOTYPE AND BIOENERGETICS ARE CONTROLLED BY OXIDIZED PHOSPHOLIPIDS IDENTIFIED IN LEAN AND OBESE ADIPOSE TISSUE

4.1 ABSTRACT

Adipose tissue macrophages (ATMs) adapt their metabolic phenotype either to maintain lean tissue homeostasis or drive inflammation and insulin resistance in obesity. However, the factors in the adipose tissue microenvironment that control ATM phenotypic polarization and bioenergetics remain unknown. We have recently shown that oxidized phospholipids (OxPL) uniquely regulate gene expression and cellular metabolism in *Mox* macrophages, but the presence of the *Mox* phenotype in adipose tissue has not been reported. Here we show, using extracellular flux analysis, that ATMs isolated from lean mice are metabolically inhibited. We identify a unique population of CX3CR1^{neg}/F4/80^{low} ATMs that resemble the *Mox* (Txnrd1^{+}HO1^{+}) phenotype to be the predominant ATM phenotype in lean adipose tissue. In contrast, ATMs isolated from obese mice had characteristics typical of the *M1*/*M2* (CD11c^{+}CD206^{+}) phenotype with highly activated bioenergetics. Quantifying individual OxPL species in the stromal vascular fraction of murine adipose tissue, using targeted liquid chromatography-mass spectrometry, revealed that high fat diet-induced adipose tissue expansion led to a disproportional increase in *full-length* over *truncated* OxPL species. *In vitro* studies showed that macrophages respond to *truncated* OxPL species by suppressing bioenergetics and up-regulating antioxidant programs, mimicking the *Mox* phenotype of ATMs isolated from lean mice. Conversely, *full-length* OxPL species induce pro-inflammatory gene expression and an activated bioenergetic profile that mimics ATMs isolated from obese mice. Together, these data identify a redox-regulatory Mox macrophage phenotype to be predominant in lean adipose tissue and demonstrate that individual

OxPL species that accumulate in adipose tissue instruct ATMs to adapt their phenotype and bioenergetic profile to either maintain redox homeostasis or to promote inflammation.

4.2 INTRODUCTION

Macrophages sense pathogen-associated molecular patterns (PAMPs) as well as endogenously formed danger-associated molecular patterns (DAMPs) derived from cell and tissue damage to adapt their functional phenotype and cellular metabolism (193, 229). Since oxidative stress is a hallmark of highly metabolic healthy as well as inflamed tissue, the formation of oxidation-derived DAMPs is an important signal for macrophage adaptation to oxidative tissue damage (94, 182).

In adipose tissue, accumulating evidence supports a role for adipose tissue macrophages (ATMs) in regulating tissue-specific glucose homeostasis and inflammation (167–171). Both insulin sensitivity and obesity-associated insulin resistance are affected by tissue redox homeostasis and oxidative stress (155–157). However, if ATMs play a role in regulating tissue redox homeostasis, and how ATMs adapt to tissue oxidation status is unknown. Metabolic activation of macrophages in obesity has been implied based on *in vitro* stimulation and was demonstrated to be distinct from classical *M1* metabolism (181). However, the bioenergetic profile of murine ATMs remains enigmatic since data from isolated, live ATMs are not available. Furthermore, the endogenously produced DAMPs responsible for promoting metabolic changes and inflammation in adipose tissue have not been identified.

We have previously shown that oxidized phospholipids (OxPL) induce the formation of the Mox phenotype in macrophages by inducing Nrf2-dependent gene expression (146). Recently, we found that OxPL redirect macrophage metabolism and bioenergetics to support production of antioxidant metabolites (182), but also promote a low level of inflammation via

TLR2 (98). Others have shown that certain OxPL species induce Caspase-11/CD14-dependent inflammasome activation in macrophages (30, 230), and that lipoxygenase (LOX)-generated OxPL species orchestrate ferroptosis, a hydroperoxy-OxPL driven form of cell death centered around mitochondrial dysfunction (231–234, 53). Indeed, individual OxPL species promote different cellular responses (21, 67, 133, 186, 235), dependent on their head group, structure, presence of functional groups, as well as chain length in the *sn*-2 position (36, 98, 109, 236). This implies that the relative abundance of individual OxPL species within tissues determines cellular responses and metabolic adaptation.

Here we characterize the bioenergetic profile of ATMs from lean and obese mice. We used flow cytometry to link the ATM bioenergetics profile to established *in vitro* macrophage polarization states (i.e. pro-inflammatory M1, anti-inflammatory M2, or antioxidant Mox). Furthermore, quantification of individual OxPL species in whole blood and the ATM-containing stromal vascular fraction (SVF) of adipose tissue allowed us to define the unique OxPL compositions present in physiological and pathological states of obesity. Finally, we tested the different OxPL compositions that we found *in vivo* on their ability to differentially reprogram macrophage bioenergetics and phenotypic polarization states *in vitro*.

4.3 RESULTS

4.3.1 Adipose tissue macrophages from lean mice are metabolically inhibited while those from obese mice are highly energetic

Adipose tissue macrophages (ATMs) were shown to regulate obesity-associated adipose tissue dysfunction and insulin resistance (171). Metabolic activation of macrophages in obesity has been implied based on *in vitro* stimulation (181), yet measurement of the actual bioenergetic profile of resident or infiltrating ATMs *ex vivo* has not been reported. Previous studies suggest that ATMs

from lean mice are of the anti-inflammatory *M2* phenotype (162, 237), which would indicate heavy reliance on oxidative phosphorylation and mitochondrial function (176), while in the context of obesity, a shift in ATM polarization to pro-inflammatory *M1* macrophages was proposed (162, 237), which would rely heavily on aerobic glycolysis (175). We used extracellular flux assays, which allow for direct evaluation of cellular bioenergetic profiles *ex vivo* by measuring oxygen consumption rate (OCR, measure of oxidative phosphorylation) and extracellular acidification rate (ECAR, measure of aerobic glycolysis), to test the hypothesis that ATMs from lean mice exhibit a high OCR and low ECAR (*M2* metabolism), while ATMs from obese mice show a low OCR and high ECAR (*M1* metabolism). To analyze ATM metabolism in lean and obese adipose tissue, we fed C57BL/6 mice chow diet or high-fat diet (HFD) for 12 weeks. Next, we isolated the stromal vascular fraction (SVF) from the epididymal fat pads for bioenergetic profiling (**Figure 4-1A**) and assessed OCR and ECAR in SVF cells using extracellular flux analysis (238, 239). Unexpectedly, we found that both the respiratory capacity (OCR) and aerobic glycolysis (ECAR) of SVF isolated from lean mice were low, while they were both significantly increased in SVF cells isolated from obese mice (**Figure 4-1B**). This result indicates that SVF cells isolated from lean mice exist in a relatively low bioenergetic state, while SVF cells in obesity adopt an *energetic* (high respiratory capacity, high glycolysis) metabolic phenotype. Since the SVF isolated from adipose tissue contains a variety of cell types, we enriched the SVF for $CD11b^+$ cells (which are predominantly macrophages) using magnetic beads coupled to an anti-CD11b antibody. Surprisingly, $CD11b^+$ cells isolated from adipose tissue of lean mice exhibit a strikingly suppressed OCR and ECAR, resulting in a bioenergetic profile reminiscent of a quiescent state (**Figure 4-1C**). Remarkably, the respiratory capacity (OCR) of $CD11b^+$-enriched SVF from obese mice was almost 3 times greater than lean mice, where glycolysis (ECAR) was 4 times greater than CD11b+ SVF from lean mice. Together, these data show that $CD11b^+$ ATMs maintain a *quiescent* metabolic phenotype (low respiratory capacity and glycolysis) in lean adipose tissue, but in obesity, $CD11b^+$ cells exert a highly

energetic metabolic phenotype. Moreover, this is in striking difference from what would be expected for *M2* polarized macrophages (high OCR) or *M1* macrophages (high ECAR). This unexpected finding led us to further investigate the polarization state of resident ATMs in lean mice and to monitor changes during obesity.

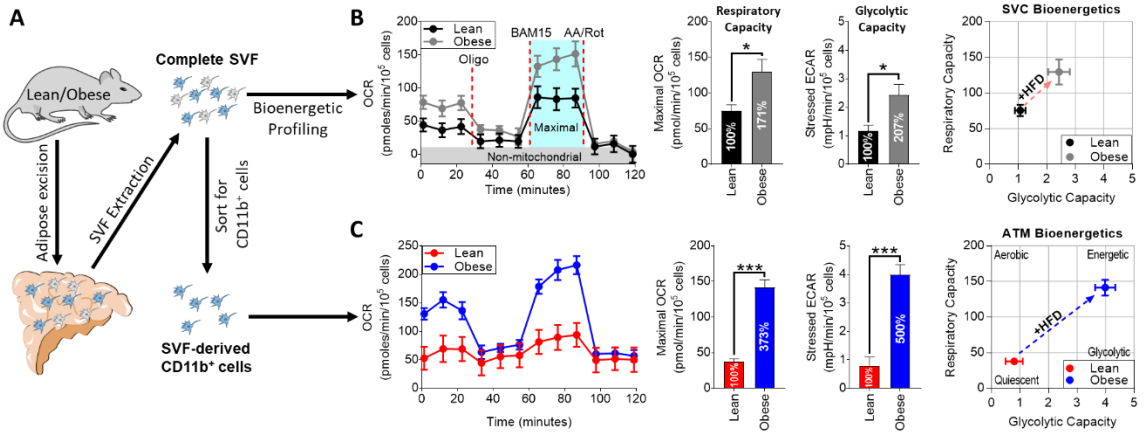

Figure 4-1: Adipose tissue macrophages from lean mice are metabolically inhibited compared to those from obese mice which are highly energetic

Figure 4-1 Legend

A. Schematic showing experimental setup. Briefly, gonadal adipose tissue was excised from mice fed a chow (lean) or high-fat diet (HFD; obese) for 12 weeks. Stromal vascular fraction (SVF) was isolated and either immediately subjected to bioenergetic profiling or further enriched for $CD11b^+$ cells.

B. Mitochondrial stress test (MST) of SVF cells isolated from lean or obese (12 week HFD-fed) mice. Bioenergetics plot relates the cells' respiratory capacity (based on maximal OCR, y-axis) to the glycolytic capacity (based on stressed ECAR, x-axis). (n = 5)

C. MST and bioenergetic profile of SVF cells isolated from lean and obese mice, enriched for adipose tissue macrophages (ATM) using CD11b-magnetic bead purification. (n = 5) Data are expressed as mean ± SEM. Statistical significance calculated by Welch's t-test (*$p < 0.05$; **$p < 0.01$; ***$p < 0.001$).

4.3.2 A population of CX3CR1^{-} / F4/80^{lo} cells is predominant in lean adipose, while obesity induces accumulation of CX3CR1^{+} / F4/80^{hi} cells in adipose tissue.

To examine the relationship between ATM phenotypic polarization and the respective cellular bioenergetic profiles in obesity we placed mice on a HFD for 8 and 16 weeks to induce adipose tissue expansion and immune cell infiltration (**Figure 4-2A**). We isolated the SVF from the epididymal fat pads of each mouse and analyzed the macrophage content by flow cytometry using CD45, F4/80, and CD11b as markers for ATM (179, 180, 240) (see **Figure 4-2B** for gating strategy). Within the F4/80^{+}CD11b^{+} ATM population, we identified two distinct populations that were distinguished by CX3CR1 expression (**Figure 4-3A**). In lean mice, approximately 6% of ATMs were CX3CR1^{+}, however, this percentage increased to over 60% and over 80% after 8 and 16 weeks of HFD feeding, respectively (**Figure 4-3B**). We observed that CX3CR1 expression coincided with high expression of F4/80 and accordingly identified two ATM populations characterized as F4/80^{lo} and F4/80^{hi} (**Figure 4-3C, D**). Similarly, two populations of macrophages have been previously characterized based on their F4/80 and CD11b expression in other tissues, and have been referred to as F4/80^{hi}CD11b^{lo} and F4/80^{lo}CD11b^{+} (also F4/80^{lo}CD11b^{mid}) (179, 180, 240, 241). Like the CX3CR1^{-} population (**Figure 4-3C**), the F4/80^{lo} population was predominant in lean adipose tissue (83%), and doubled in number after 8 weeks of HFD (from 1.1x10^{5} to 2.5x10^{5} cells per fat pad), but decreased in percentage (83% in lean, 55% after 8 weeks and 12% after 16 weeks HFD) (**Figure 4-3D**). In contrast, F4/80^{hi} macrophages drastically increased in number during the HFD (from 0.2x10^{5} to 8.4x10^{5} cells per fat pad; 17% in lean, 53% after 8 weeks and 84% after 16 weeks HFD) (**Figure 4-3E**). These results indicate that resident ATMs are predominantly CX3CR1^{-}F4/80^{lo} and that ATMs infiltrating during obesity are primarily CX3CR1^{+}F4/80^{hi}.

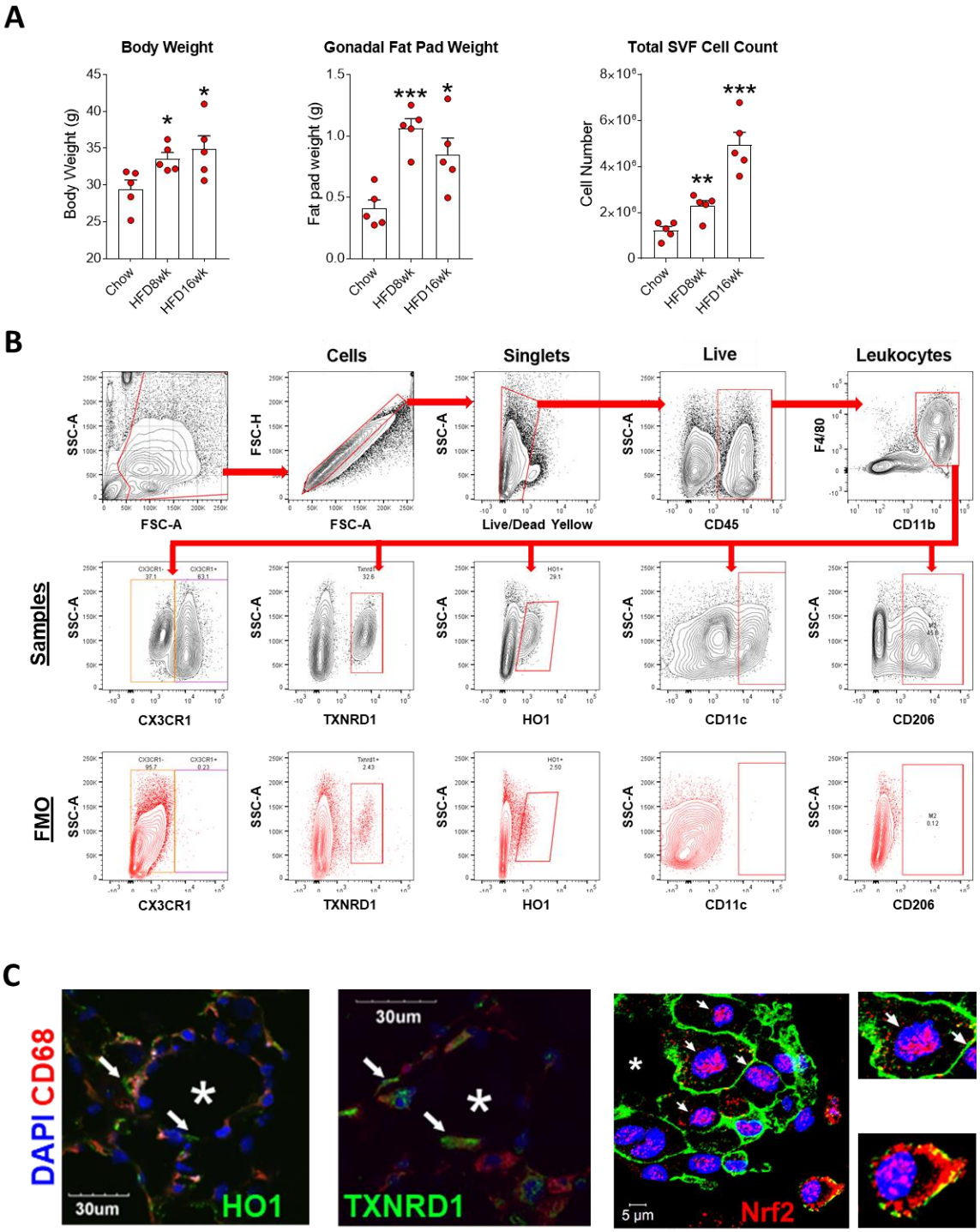

Figure 4-2: Supplement to Figure 4-3 and Figure 4-4

Figure 4-2 Legend

A. Whole body weight, epididymal fat pad weight, and total stromal vascular fraction (SVF) cell count from respective fat pad of lean mice or mice fed a high fat diet (HFD) for 8 or 16 weeks. (n = 5)

B. Gating strategy used to identify adipose tissue macrophages (ATMs). Dead cells were excluded using Live/Dead Yellow dye. ATMs were identified as $CD45^{+}F4/80^{+}CD11b^{+}$. Fluorescence-minus-one (FMO) controls shown for CX3CR1, TXNRD1, HO1, CD11c, and CD206.

C. Immunofluorescence of an epididymal adipose tissue section taken from a mouse fed a HFD for 12 weeks. Left and middle sections were stained with DAPI (nuclei; blue), CD68 (macrophage; red), and (left) HO1 or (middle) TXNRD1 (Mox; green). Sections (right) were stained with DAPI (blue), F4/80 (macrophage; green), and Nrf2 (Mox transcription factor; red). Image highlights localization of Nrf2 to the nucleus of crown-like structure macrophages.

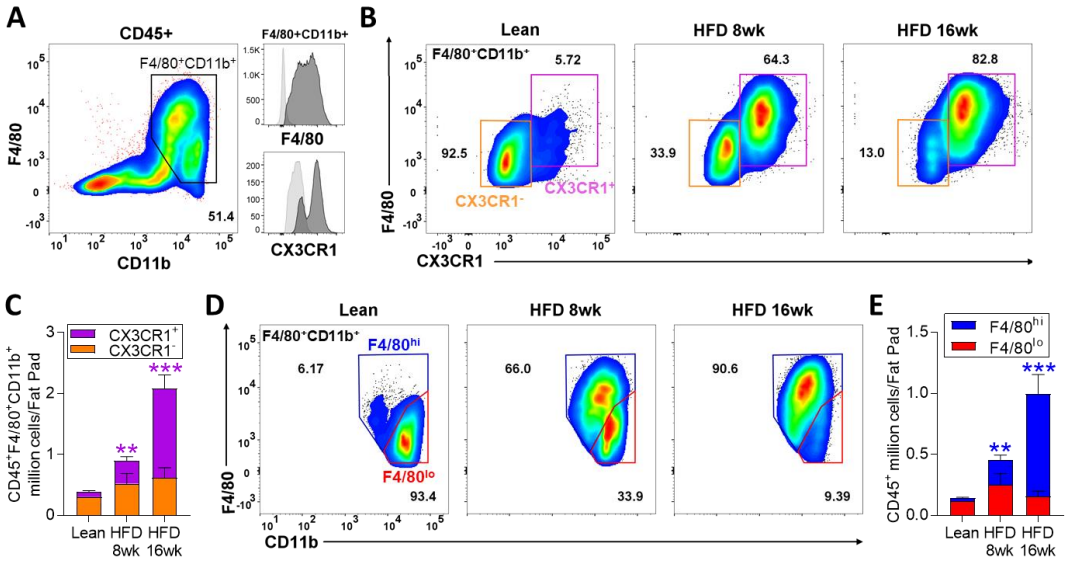

Figure 4-3: Resident CX3CR1^{-} and F4/80^{lo} ATMs are replaced by CX3CR1^{+} and F4/80^{hi} ATMs during obesity

Figure 4-3 Legend

A. Flow cytometry analysis of live $CD45^+$ SVF cells, showing the spread of F4/80 expression and two distinct populations of macrophages discriminated by CX3CR1 expression. Representative sample from 8 week HFD-fed mice shown.
B. Expression of F4/80 and CX3CR1 by live $CD45^+F4/80^+CD11b^+$ cells isolated from SVF of lean, 8 week, and 16 week HFD-fed mice, showing two distinct macrophage populations ($CX3CR1^+$ and $CX3CR1^-$). ($n \geq 4$)
C. Absolute number of total $CD45^+F4/80^+CD11b^+$ macrophages in SVF that are $CX3CR1^+$ (purple, top) or $CX3CR1^-$ (orange, bottom). ($n \geq 4$)
D. Expression of F4/80 and CD11b by live $CD45^+F4/80^+CD11b^+$ cells isolated from SVF of lean, 8 week, and 16 week HFD-fed mice, showing two distinct macrophage populations labeled $F4/80^{hi}$ and $F4/80^{lo}$. ($n \geq 4$)
E. Absolute number of total live $CD45^+$ cells in SVF that are $F4/80^{hi}$ (blue, top) and $F4/80^{lo}$ (red, bottom). ($n \geq 4$)

Data are expressed as mean ± SEM. Statistical significance calculated by Welch's t-test (*$p < 0.05$; **$p < 0.01$; ***$p < 0.001$).

4.3.3 The majority of resident ATMs are positive for *Mox* markers and are out-populated by *M1*/*M2* ATMs during obesity

To further investigate phenotypic polarization of ATMs, we interrogated the F4/80^{lo} and F4/80^{hi} ATM populations for macrophage phenotypic polarization. We used the established markers CD11c for *M1* (162) and CD206 for *M2* (242, 243) ATMs. Additionally, we used redox homeostatic enzymes Txnrd1 and HO1 (whose expression is driven by the transcription factor Nrf2) for *Mox*, a macrophage polarization state previously identified in atherosclerotic lesions (146). We found that expression of the *Mox* markers Txnrd1 and HO1 was exclusively associated with the resident F4/80^{lo} (also CX3CR1^{-}) population, while expression of CD11c and CD206 appears almost exclusively in the F4/80^{hi} (also CX3CR1^{+}) population (**Figure 4-4A**), reminiscent of the inflammatory macrophage phenotype found in human obesity (164). The total number of *Mox* remained constant (1.2x10^5 in lean, 1.4x10^5 after 8 week, and 1.0x10^5 after 16 week HFD-fed mice) and consistent with the numbers of F4/80^{lo} macrophages, while CD11c^{+}, CD206^{+}, and CD11c^{+}CD206^{+} cells significantly increased after HFD feeding (**Figure 4-4B**). Remarkably, while in lean mice 84% of F4/80^{+}CD11b^{+} cells expressed the *Mox* markers HO1 and Txnrd1, *Mox* still comprised 47% and 13% of all macrophages after 8 and 16 weeks of HFD (**Figure 4-4C**). Together, over the course of HFD-induced cell infiltration into the SVF of adipose tissue, the dynamics of macrophage phenotypic polarization reflects a relative decrease of the *Mox* macrophage population, with concomitant increases of the M1/M2 hybrid and M2 populations (**Figure 4-4D**). However, these results also support the notion that sufficient numbers of *Mox* macrophages are present in adipose tissue of not only lean, but also obese mice. Indeed, we find that crown-like structures contain *Mox* macrophages, characterized by expression of HO1^{+} and Txnrd1^{+}, as well as Nrf2 that has translocated to the nucleus (**Figure 4-2C**).

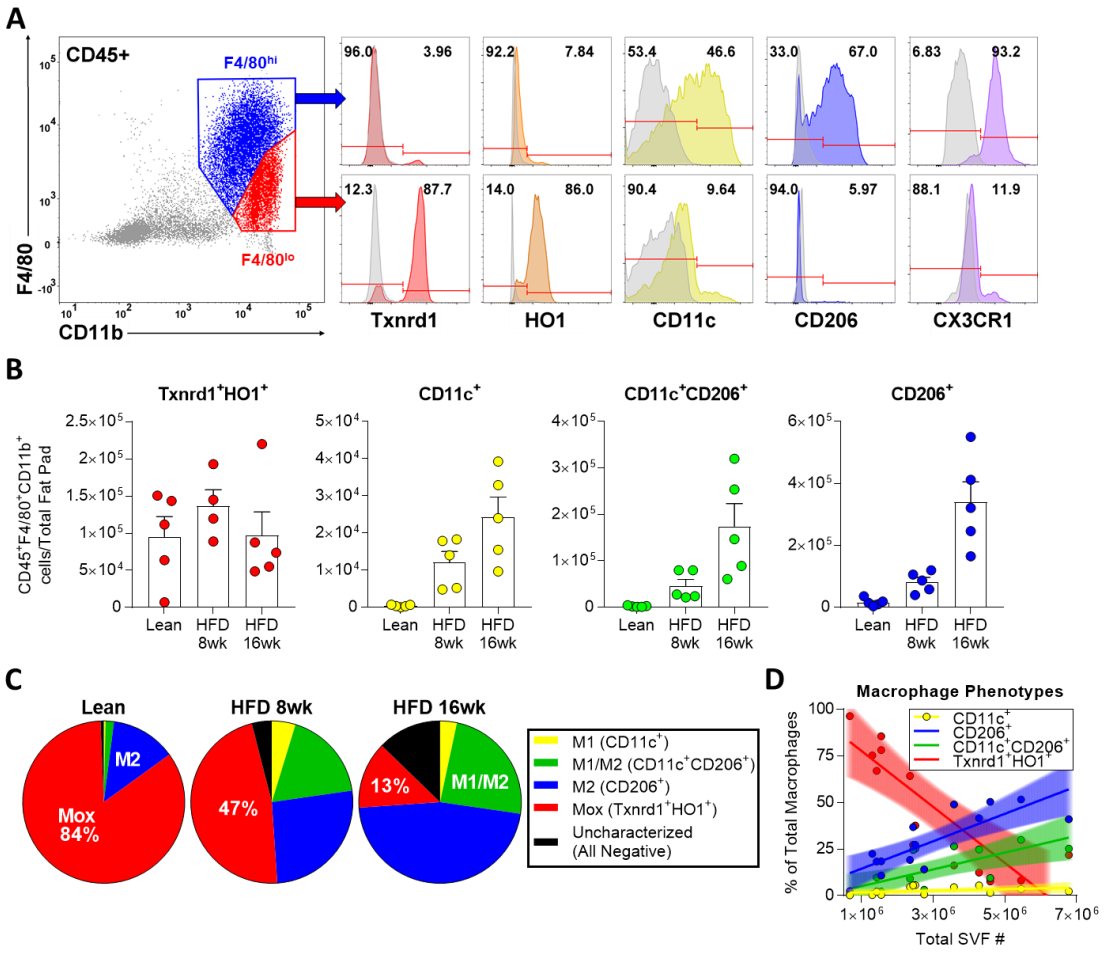

Figure 4-4: The majority of resident ATMs are positive for Mox markers and are out-populated by M1/M2 ATMs during obesity

Figure 4-4 Legend

A. Characterization of $F4/80^{hi}$ and $F4/80^{lo}$ populations by Txnrd1, HO1, CD11c, CD206, and CX3CR1, as shown through histograms. Representative sample from 8 week HFD-fed mice shown.
B. Absolute number of live $CD45^+F4/80^+CD11b^+$ cells in SVF that are $Txnrd1^+HO1^+$ (Mox), $CD11c^+$ (M1), $CD11c^+CD206^+$ (M1/M2), or $CD206^+$ (M2). ($n \geq 4$)
C. Relative levels of ATMs ($CD45^+F4/80^+CD11b^+$) that are $Txnrd1^+HO1^+$ (Mox), $CD11c^+$ (M1), $CD11c^+CD206^+$ (M1/M2), $CD206^+$ (M2), or Total Negative (population that $CD45^+F4/80^+CD11b^+$ but negative for Txnrd1, HO1, CD11c, and CD206). ($n \geq 4$)
D. Correlation between abundance of individual ATM populations and total number of SVF cells per epididymal fat pad.

Data are expressed as mean ± SEM. Statistical significance calculated by Welch's t-test (*$p < 0.05$; **$p < 0.01$; ***$p < 0.001$).

4.3.4 Analysis of full-length and truncated OxPAPC species in blood from lean and obese mice

To analyze individual OxPL species we developed a targeted liquid chromatography-mass spectrometry (LC-MS) approach (modified from (244, 245)), aimed at quantifying the levels of oxidation products derived from 1-palmitoyl-2-arachidonoyl-3-*sn*-glycero-phosphatidylcholine (PAPC) and 1-palmitoyl-2-linoleoyl-3-*sn*-glycero-phosphatidylcholine (PLPC), collectively referred to as OxPAPC and OxPLPC (246, 247). In order to better characterize the relative abundance of individual classes of phospholipid oxidation products, we assigned 15 of the previously identified species of OxPAPC (and OxPLPC) to one of four groups based on the structure of the oxidized moiety and previously characterized biological activity (20, 109, 128, 184, 236). *Full-length* species were divided into the *HETE/HPETE* and the *Isoprostane* classes, and *truncated* species into the *Carbonyl* (including PLPC oxidation products PONPC and PAzPC) and the *γ-Keto/Hydroxyl* classes, based on criteria described in Materials and Methods (**Figure 4-5A, Figure 4-6A**). From an *in vitro*-oxidized OxPAPC and OxPLPC mixtures (28) we measured 15 species by direct-inject MS and optimized the parameters for quantification (**Figure 4-5B, Figure 4-6B,** Error! Reference source not found.). Establishing an LC method with more polar lipids eluting earlier and less polar lipids eluting later in the run allowed us to reliably monitor the air-oxidation of PAPC over time (**Figure 4-5C, D, Figure 4-6C**), quantitatively representing relative amounts of each OxPAPC class present at different time points (**Figure 4-5E**).

To quantify the levels of OxPAPC species in whole blood from lean and obese mice, we used mice that had been fed chow or a HFD for 9 or 17 weeks, resulting in a significant increase in body weights over time (**Figure 4-7A**). In whole blood, LysoPC (specifically 16:0), which can be derived from both phospholipid oxidation (248) and phospholipase A2 (PLA2) activity (**Figure 4-5A**), was highly abundant and significantly increased with HFD, and remarkably,

significantly correlated with body weight (**Figure 4-8A**). While the levels of full-length OxPAPC species (HETE/HPETE and isoprostane groups) and the γ-keto/hydroxyl-PCs increased with the duration of HFD feeding, interestingly, the level of carbonyl species significantly dropped (**Figure 4-8B, C**). Overall, the oxidized fraction of PAPC (i.e. the sum of all OxPAPC species including LysoPC in relation to native PAPC) in blood increased from 14% in lean to 26% and 35% after 9 and 17 weeks of HFD, respectively (**Figure 4-8D**). The relative level of full-length OxPAPC species increased at the expense of the truncated species (**Figure 4-8E**), resulting in a strong positive correlation of the HETE/HPETE-PCs with body weight, while the carbonyl-PCs showed a negative correlation (**Figure 4-8F**).

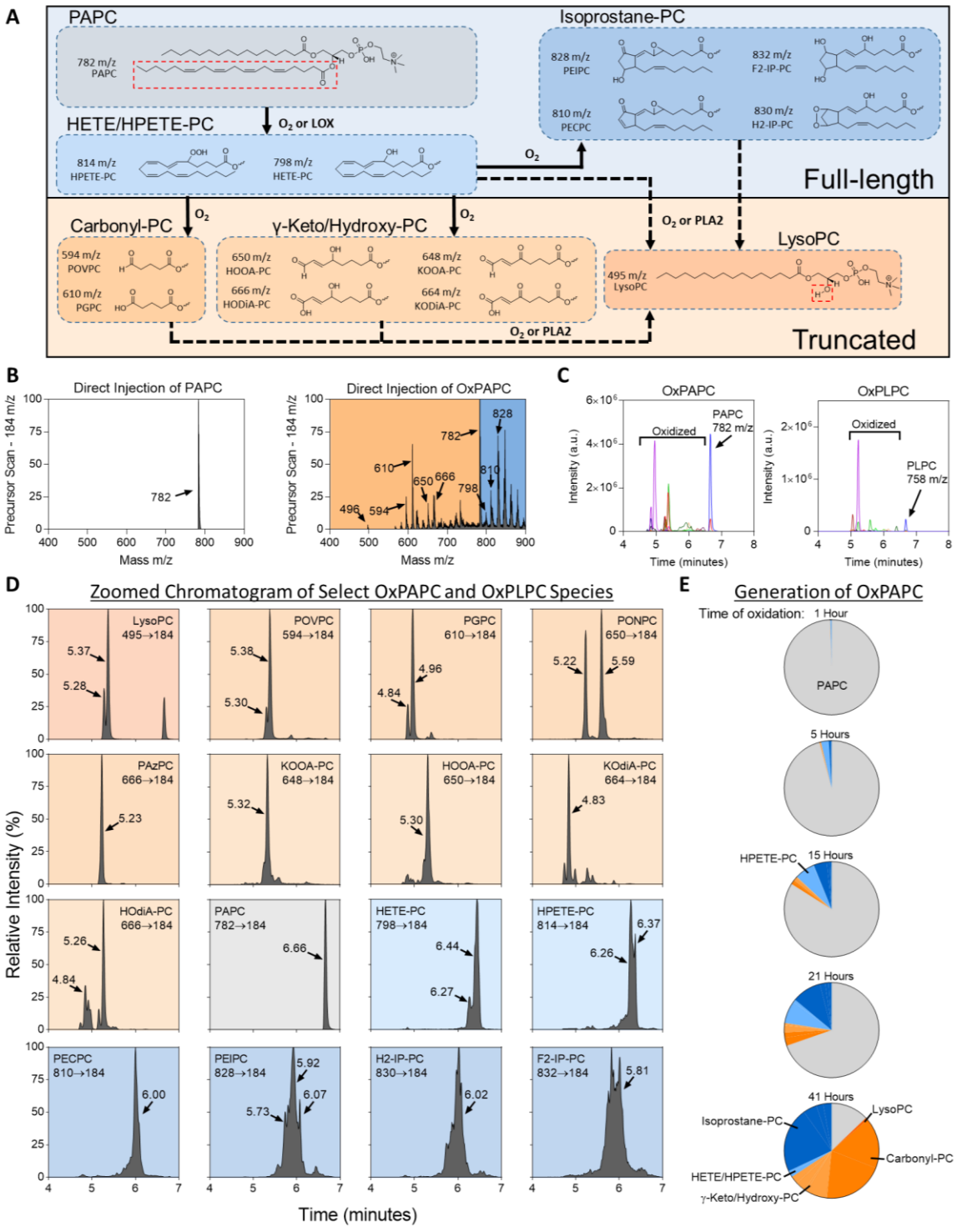

Figure 4-5: LC-MS/MS approach for quantifying full-length and truncated OxPAPC species

Figure 4-5 Legend

A. Schematic outlining the oxidation products of PAPC, the dotted red line highlighting the arachidonic acid, which is susceptible to oxidation. The predicted oxidation products were first assigned into two broad groups, full-length or truncated, based on mass to charge ratio (m/z) that is larger or smaller than PAPC (782 m/z), respectively. Next, they were subdivided into 4 classes, based on chemical moieties and biological activity. Finally, the product of terminal oxidation or enzymatic cleavage is LysoPC (495 m/z)

B. Ion scans for precursors of fragment 184 of PAPC (782 m/z) and OxPAPC (collective mixture of PAPC oxidation products) obtained using direct-inject mass spectrometry (MS) analysis, allowing for qualitative assessment of individual species presence. The blue highlight represents ions pertaining to the full-length group, while the orange highlight covers the ions associated with the truncated group.

C. Liquid chromatograms of OxPAPC and OxPLPC, allowing for quantification on an individual species basis using the integrated peak area of the ion count, normalized to internal standard DNPC.

D. Zoomed chromatograms of PAPC and the 13 OxPAPC and 2 OxPLPC species measured, scaled to the highest intensity for each species.

E. The oxidation of PAPC by air exposure over 41 hours to generate OxPAPC, as represented by pie charts showing the relative amount of each class (isoprostane-dark blue; HETE/HPETE-light blue; γ-keto/hydroxyl-light orange; carbonyl-dark orange).

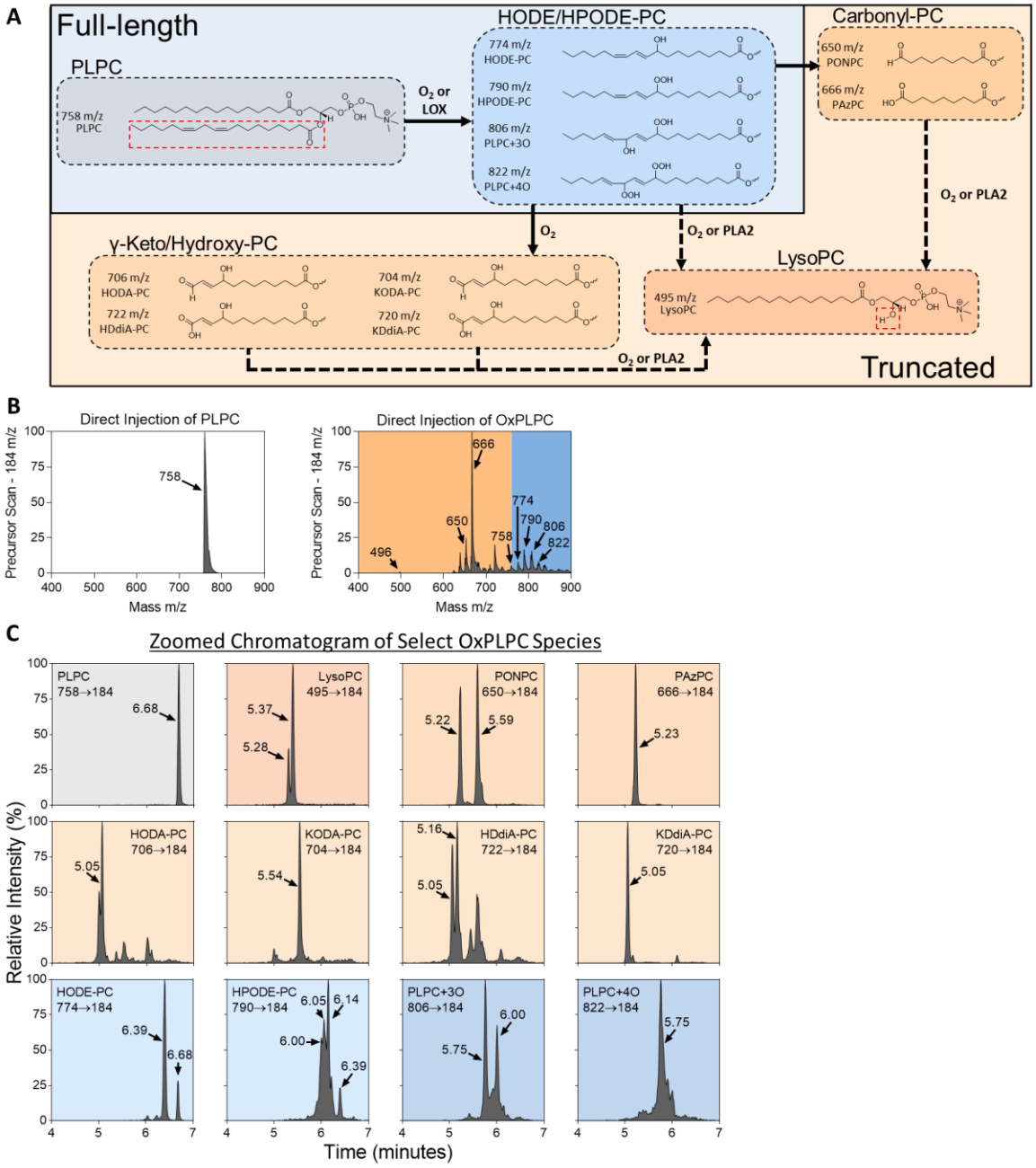

Figure 4-6: Supplement to Figure 4-5

Figure 4-6 Legend

A. Schematic outlining the oxidation products of PLPC, the dotted red line highlighting the arachidonic acid, which is susceptible to oxidation. The predicted oxidation products were first assigned into two broad groups, full-length or truncated, based on mass to charge ratio (m/z) that is larger or smaller than PLPC (758 m/z), respectively. Next, they were subdivided into 4 classes, based on chemical moieties and biological activity. Finally, the product of terminal oxidation or enzymatic cleavage is LysoPC (495 m/z)

B. Ion scans for precursors of fragment 184 of PLPC (758 m/z) and OxPLPC (collective mixture of PLPC oxidation products) obtained using direct-inject mass spectrometry (MS) analysis, allowing for qualitative assessment of individual species presence. The blue highlight represents ions pertaining to the full-length group, while the orange highlight covers the ions associated with the truncated group.

C. Zoomed chromatograms of PLPC and the 12 OxPLPC species measured, scaled to the highest intensity for each species.

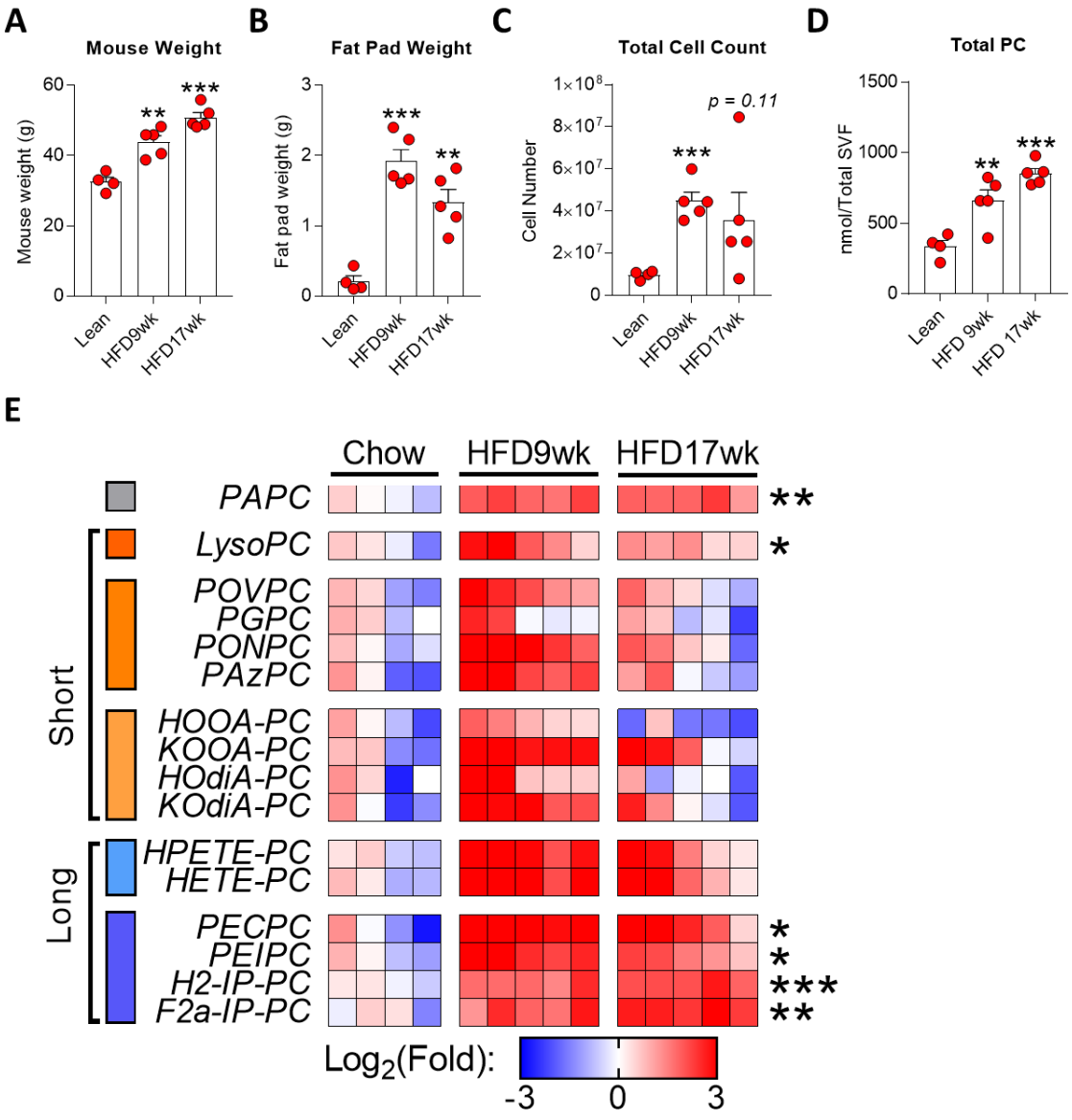

Figure 4-7: Supplement to Figure 4-8 and Figure 4-9

Figure 4-7 Legend

A. Whole body weight of lean mice or mice fed a high fat diet (HFD) for 9 or 17 weeks. ($n \geq 4$)

B. Epididymal fat pad weight of lean mice or mice fed a high fat diet (HFD) for 9 or 17 weeks. ($n \geq 4$)

C. Total stromal vascular cell (SVF) cell count from respective fat pad of lean mice or mice fed a high fat diet (HFD) for 9 or 17 weeks. ($n \geq 4$)

D. Total PC levels in total epididymal SVF of lean mice or mice fed a high fat diet (HFD) for 9 or 17 weeks ($n \geq 4$). Total levels of PC were calculated by summation of the integrated ion peak areas of each individual PC species. ($n \geq 4$)

E. Fold change in individual OxPAPC species as measured by liquid chromatography-mass spectrometry (LC-MS) of epididymal SVF from lean mice and mice fed a HFD for 9 or 17 weeks ($n \geq 4$). Phospholipids were quantified on an individual species basis, using the integrated peak area of the ion count. The integrated peak area of each analyte was normalized to the internal standard, DNPC. Significance was determined by two-way ANOVA of the ion count peak area. Post-hoc statistical significance of individual species was determined by Welch's 2-sided t-test. Data represented in a heat map showing $\log_2$ of the fold change compared to lean mice.
Data are expressed as mean ± SEM. Statistical significance calculated by Welch's 2-sided t-test unless otherwise specified (*$p < 0.05$; **$p < 0.01$; ***$p < 0.001$).

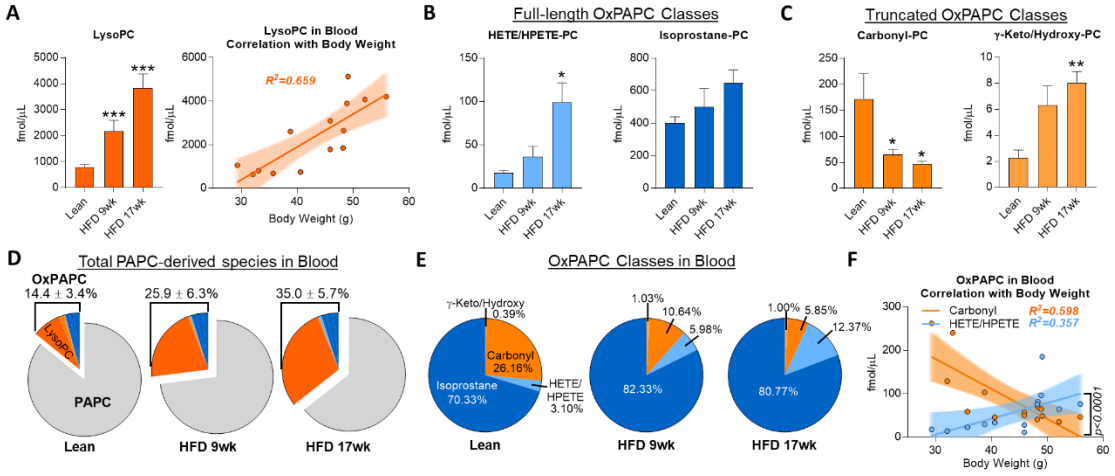

Figure 4-8: Increase in full-length at the expense of truncated OxPAPC species in blood of mice fed high-fat diet

Figure 4-8 Legend

A. Accumulation of 16:0 LysoPC normalized to blood volume of lean mice and 9 or 17 week HFD-fed mice ($n \geq 4$). Assessment of correlation between LysoPC in blood and murine body weight.
B. Accumulation of full-length OxPAPC classes HETE/HPETE-PC and Isoprostane-PC normalized to blood volume of lean mice and 9 or 17 week high-fat diet (HFD)-fed mice. ($n \geq 4$) Phospholipids were quantified on an individual species basis, using the integrated peak area of the ion count. The integrated peak area of each analyte was normalized to the internal standard, dinonanoyl-phosphatidylcholine (DNPC) and to the volume of blood used for analysis.
C. Accumulation of truncated OxPAPC classes Carbonyl-PC and γ-Keto/Hydroxy-PC normalized to blood volume of lean mice and 9 or 17 week HFD-fed mice. ($n \geq 4$)
D. Pie charts representing relative levels of PAPC and PAPC-derived oxidation products (OxPAPC). Percentages represent the fraction of total PAPC-derived species that are OxPAPC.
E. Distribution of OxPAPC classes in blood of lean or HFD-fed mice. Carbonyl-PC (orange), γ-Keto/Hydroxy-PC (light orange), HETE/HPETE-PC (light blue), and Isoprostane-PC (dark blue) are presented in clockwise fashion.
F. Assessment of correlation between OxPL classes Carbonyl-PC (orange) and HETE/HPETE-PC (blue) in blood and murine body weight.

Data are expressed as mean ± SEM. Statistical significance calculated by Welch's t-test unless otherwise specified (*$p < 0.05$; **$p < 0.01$; ***$p < 0.001$).

4.3.5 HFD-feeding leads to a disproportional increase of full-length compared to truncated OxPAPC species in adipose SVF

Increased oxidative stress is a hallmark of metabolically active tissue, resulting in the formation of lipid oxidation products (156). Furthermore, HFD-feeding is known to cause oxidative stress and increased lipid oxidation (249). However, it is not known if OxPLs are present in adipose tissue and whether HFD-feeding affects the absolute or relative abundance of individual OxPL species. Immunostaining of adipose tissue from obese mice using the E06 antibody that recognizes oxidized phosphatidylcholines (23, 116, 117) demonstrates that oxidation-specific epitopes derived from phospholipid oxidation are abundant in macrophage-containing crown-like structures (**Figure 4-9A**). Next we analyzed the composition of native, non-oxidized, and oxidized PC species in the stromal compartment of adipose tissue, after isolating the stromal vascular fraction (SVF) from the epididymal fat pads of lean or obese mice fed a HFD for 9 or 17 weeks. HFD-fed mice had increased fat pad weights and numbers of stromal cells (**Figure 4-7B, C**), and as expected, as the adipose tissue expands in response to HFD, the total PC content in the SVF also increased (**Figure 4-7D**). Analysis of PAPC and its oxidation products revealed that the total amount of PAPC increased during HFD, as did the PAPC-derived oxidation products (**Figure 4-7E**). Even in lean mice, 7.7% of the total PAPC in the SVF was oxidized, which doubled to 14.2% at 9 weeks and dropped to 8.3%, after 17 weeks of HFD (**Figure 4-9B**). Interestingly, the degree of PAPC oxidation in SVF did not correlate with body weight (R^2 = 0.0019; slope was effectively zero, p = 0.8798), but significantly correlated with fat pad weight (R^2 = 0.3145; slope was significantly non-zero, p = 0.0369) (**Figure 4-9C**).

The changes in abundance of individual OxPAPC species in adipose SVF during HFD were different for the 4 classes (**Figure 4-7E, Figure 4-9D**). At 9 weeks of HFD, members of all 4 groups were significantly increased, while after 17 weeks of HFD we found, in addition to LysoPC, a shift towards full-length species (HETE/HPETE-PCs and isoprostane-PCs). Both

truncated and full-length PAPC-derived species are present in SVF of lean mice, however, the relative amounts of full-length species increased at a greater rate than truncated species as the adipose tissue expanded (**Figure 4-9E**). These results show that phospholipid oxidation is a feature of lean adipose tissue, and HFD feeding induces significant changes in the phospholipidome in the adipose SVF, characterized by a shift in relative abundance from truncated OxPL species to full-length species.

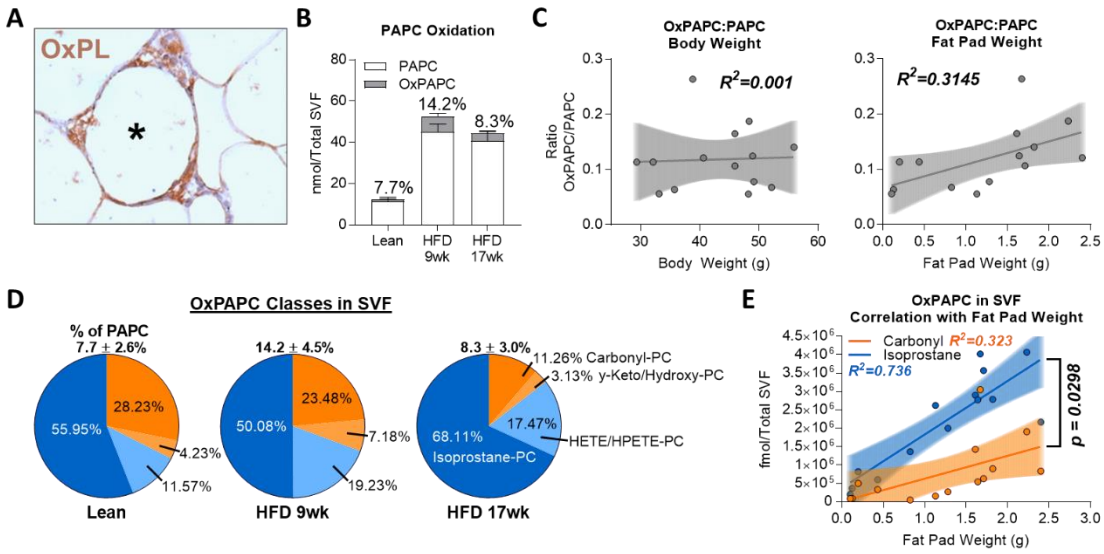

Figure 4-9: High-fat diet feeding leads to a greater increase of full-length compared to truncated OxPAPC species in adipose stromal vascular fraction

Figure 4-9 Legend

A. Histology section of gonadal fat pad from a mouse fed a high-fat diet (HFD) for 12 weeks. Immunohistochemistry using the E06 antibody, an IgM recognizing oxidized phosphatidylcholines, is shown in brown. *****denotes an adipocyte at the center of a crown-like structure.

B. Lean mice or mice fed a HFD for 9 or 17 weeks had the epididymal fat pad removed, and the stromal vascular fraction (SVF) purified. A Bligh-Dyer lipid extraction was performed on the SVF, and the lipids were subjected to LC-MS analysis. Total SVF levels of PAPC and its summed oxidation products were quantified on an individual species basis using the integrated peak area of the ion count, normalized to internal standard DNPC.

C. Assessment of the relationship between the ratio of OxPAPC to PAPC in SVF and body weight shows no correlation. Assessment of the relationship between the ratio of OxPAPC to PAPC in SVF and fat pad weight shows a positive correlation.

D. Distribution of OxPAPC classes in SVF of lean or HFD-fed mice. LysoPC (dark orange), Carbonyl-PC (orange), γ-Keto/Hydroxy-PC (light orange), HETE/HPETE-PC (light blue), and Isoprostane-PC (dark blue) are presented in clockwise fashion.

E. Correlation between OxPAPC classes and fat pad weight shows a disproportional increase in Isoprostane-PC species over Carbonyl-PC species.

Data are expressed as mean ± SEM. Statistical significance calculated by Welch's t-test unless otherwise specified (*$p < 0.05$; **$p < 0.01$; ***$p < 0.001$).

4.3.6 Truncated OxPAPC species inhibit macrophage mitochondrial function and promote antioxidant gene expression while full-length species promote inflammatory gene expression

We have recently demonstrated that OxPAPC depresses OCR in macrophages (182). To identify the OxPL species within OxPAPC that are responsible for inhibiting OCR in macrophages, we used solid phase extraction (191) to separate OxPAPC into fractions highly enriched for either full-length (*Fraction FL*) or truncated (*Fraction T*) OxPAPC species (**Figure 4-10A**). Quantification of each fraction using LC-MS/MS showed that we successfully enriched for both full-length (**Figure 4-10B**) and truncated species (**Figure 4-10C**) in their respective fractions. Treatment of BMDMs with each fraction demonstrated that the truncated, but not the full-length, OxPAPC species inhibited macrophage respiratory capacity, as measured by maximal OCR (**Figure 4-10D**). This finding is corroborated by data we have previously published demonstrating that individually synthesized truncated species present in OxPAPC, including PGPC, POVPC, and LysoPC, significantly inhibited respiratory capacity (182). In contrast, full-length, but not truncated OxPAPC species, induced the glycolytic capacity of BMDMs, as measured by stressed ECAR (**Figure 4-10D**).

OxPLs induce different cellular programs in macrophages, including induction of pro-inflammatory as well as antioxidant gene expression (109, 183). However, the structural requirements of OxPLs for induction of these diverse cellular programs in macrophages are not known. Following treatment of BMDMs with either Fraction FL or Fraction T we found that full-length, but not truncated, OxPAPC species induced pro-inflammatory gene expression in macrophages, demonstrated by increased expression of *Il1β*, *Il6*, and *Cxcl1* (**Figure 4-10E**). In contrast, truncated, but not full-length OxPAPC species induced antioxidant gene expression, as evidenced by increased expression of *Ho1*, *Txnrd1*, and *Gclm* (**Figure 4-10F**). Furthermore, we observed that the fraction containing truncated OxPAPC species significantly induced *Glut1* gene

expression, suggesting that the truncated OxPLs contribute to the metabolic reprogramming of macrophages to support antioxidant production. Interestingly, mRNA expression of cyclooxygenase 2 (*Cox2*) was induced by both the full-length and truncated OxPAPC fractions.

Together, these data show that the truncated species of OxPAPC induce reprogramming of macrophage metabolism to support antioxidant production, while the full-length OxPAPC species induce pro-inflammatory gene expression. These findings suggest that the relative abundance of truncated and full-length OxPL species in oxidatively damaged tissue determines the metabolic and inflammatory polarization of macrophages.

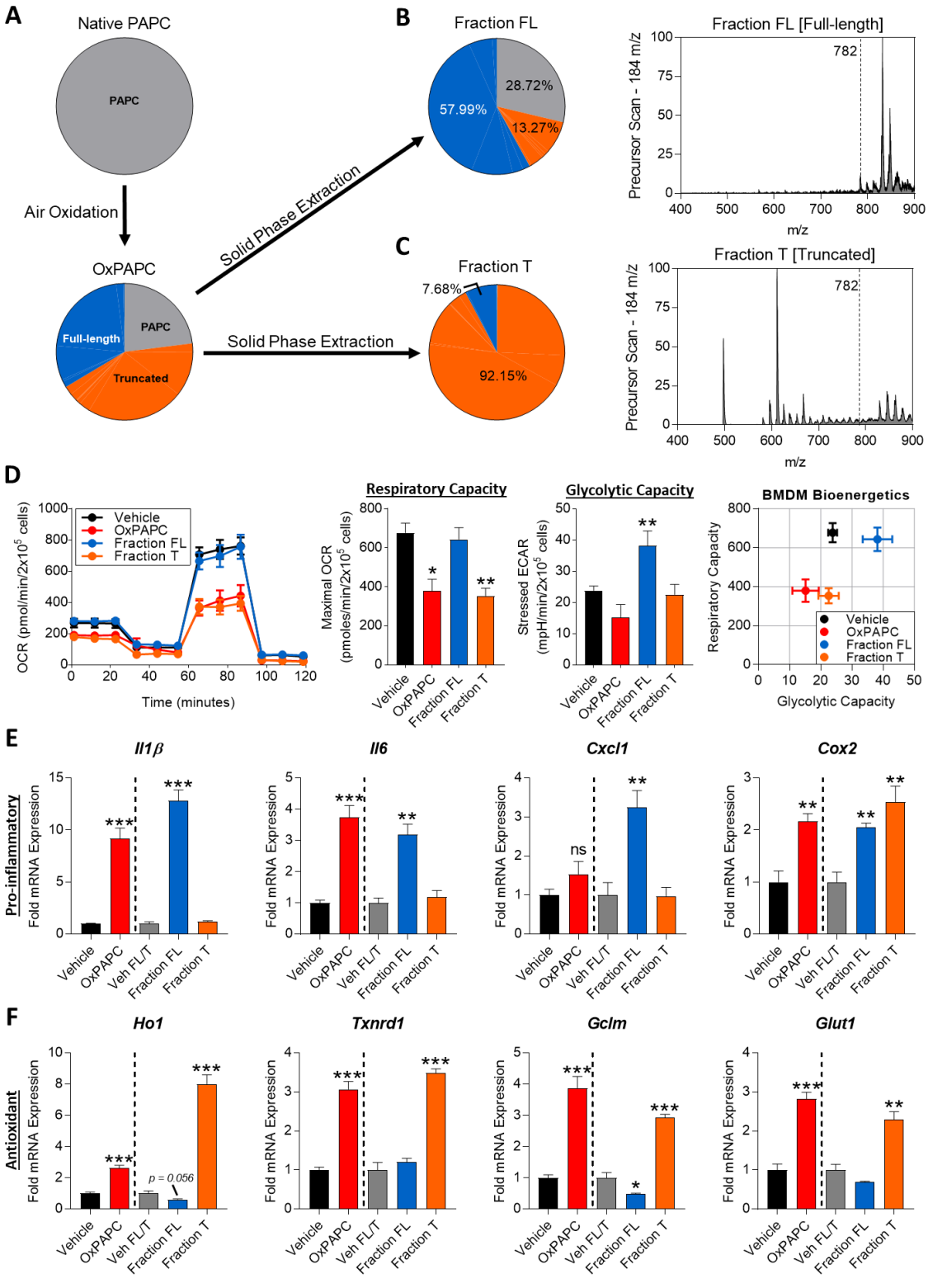

Figure 4-10: Truncated OxPAPC species promote a quiescent metabolism and antioxidant gene expression while full-length stimulate metabolism and pro-inflammatory gene expression

Figure 4-10 Legend

A. Schematic representing the generation of OxPAPC from native PAPC followed by solid phase extraction-based separation of full-length (FL) and truncated (T) OxPAPC species.
B. Fraction FL, is shown using a pie chart for relative species abundance (left) and a precursor ion scan for 184 (right).
C. Fraction T, is shown using a pie chart for relative species abundance (left) and a precursor ion scan for 184 (right).
D. MST of BMDMs treated with vehicle (RPMI media), 10µg/mL OxPAPC, Fraction FL, or Fraction T for 4 hours. Maximal OCR (respiratory capacity) and stressed ECAR (glycolytic capacity) also presented, with the results summarized in a bioenergetics chart (right).
E. mRNA expression of pro-inflammatory genes *Il1β*, *Il6*, *Cxcl1*, and *Cox2* measured by qPCR in BMDMs treated with vehicle (RPMI media), 10µg/mL OxPAPC, vehicle FL/T (combined eluents from column loaded with only chloroform, dried down and re-suspended with RPMI media), 10µg/mL Fraction FL, or Fraction T for 4 hours.
F. mRNA expression of redox homeostasis genes *Ho1*, *Txnrd1*, and *Gclm*, and glucose transporter *Glut1* measured by qPCR in BMDMs treated with vehicle (RPMI media), 10µg/mL OxPAPC, vehicle FL/T (combined eluents from column loaded with only chloroform, dried down and re-suspended with RPMI media), 10µg/mL Fraction FL, or Fraction T for 4 hours.

Data are expressed as mean ± SEM. Statistical significance calculated by Welch's 2-sided t-test (*$p < 0.05$; **$p < 0.01$; ***$p < 0.001$).

4.4 CONCLUSION & DISCUSSION

Cellular metabolism of immune cells has risen to the forefront of immunology research, with landmark studies showing that classic pro-inflammatory macrophages (M1) rely on aerobic glycolysis (175), while anti-inflammatory macrophages (M2) require oxidative phosphorylation (176). We have shown that antioxidant macrophages (Mox) require regular energy metabolism to be suppressed, to produce the antioxidant glutathione (182). The switch to aerobic glycolysis (referred to as the Warburg effect) in response to classic pro-inflammatory stimuli has been shown to be necessary for cytokine production by M1 macrophages (175). In adipose tissue, M1 macrophages are thought to be essential for the pathogenesis of obesity, but phenotypic and bioenergetic changes of macrophages in lean adipose tissue and during obesity are poorly understood.

We show here that specific OxPLs differentially reprogram macrophage metabolism. We found that truncated OxPLs inhibit macrophage respiratory capacity, an indicator of mitochondrial function and oxidative phosphorylation. Additionally, truncated OxPLs induce expression of genes involved in redox homeostasis. In contrast, the full-length OxPLs induce pro-inflammatory gene expression and do not inhibit respiration, instead, promoting aerobic glycolysis. Together these experiments clearly show the varying effects that different OxPL classes have on macrophage phenotypic and bioenergetic polarization.

Numerous studies have confirmed that adipose tissue, being a highly metabolic tissue, experiences oxidative stress. The majority of these studies focus on oxidative stress that develops during obesity (155, 250), however, some studies suggest that there is already a notable basal level of oxidative stress in lean adipose tissue, in otherwise healthy mice (155). As a product of oxidative stress, OxPLs have been shown to be present in oxidized LDL particles (23), on the surface of apoptotic cells (22, 251), in multiple sclerosis (11), in atherosclerotic lesions (252), and

in the plasma of patients with cardiovascular disease (253–256), demonstrated by using the E06 antibody, a mouse IgM antibody that recognizes oxidized phosphatidylcholines (23, 114, 117, 257). To identify individual OxPL species and to measure their abundance during disease progression, we developed an LC-MS/MS method based on previously published works (141, 231, 244, 245, 258). We grouped individual OxPL species based on the functional oxidized groups and biological activity (109, 128, 183). Similar to the findings of Podrez et al. (141), we found micro-molar levels of OxPL species in murine whole blood, and a significant increase in response to high fat feeding. As has been previously reported, high-fat diet feeding induces phospholipase A2 (PLA2) activity in blood (259) and it has been found that PLA2 preferentially cleaves the *sn*-2 moiety from truncated OxPLs (260), offering an explanation for the increased level of LysoPC at the cost of carbonyl-PC species. On the other hand, LysoPC is also an end product of phospholipid oxidation (248).

Analyzing the macrophage-containing fraction of adipose tissue (the stromal vascular fraction; SVF) from mice fed chow or high-fat diet, we found that the full-length OxPL species increase disproportionally compared to the truncated OxPLs after high-fat diet, providing an endogenously formed class of compounds that promote inflammation. Our data support a scenario where ATM come into contact with mainly truncated OxPLs in lean healthy adipose tissue, while with pro-inflammatory full-length OxPLs in obese adipose tissue. We find that truncated OxPLs strongly inhibit respiratory capacity, while full-length OxPL induce inflammatory gene expression in macrophages. This suggests that the adipose tissue microenvironment in lean mice would maintain bioenergetically inhibited macrophages (*Mox*), while more energetic (*M1/M2*) macrophages predominate during the development of obesity. In the context of atherosclerotic lesions, we have previously identified phenotypically polarized macrophages (*Mox*) that respond to OxPLs by upregulating Nrf2-dependent antioxidant enzymes and increased glutathione production, as well as TLR2-dependent low-level inflammatory gene

expression (98). Assessing the bioenergetic profiles of ATMs *ex vivo* from lean and obese mice we find that ATMs from lean mice are quiescent (low OCR and ECAR) while ATMs from obese mice are highly energetic (high OCR and ECAR). These findings contradict a predicted switch from M2 (high OCR) to M1 (high ECAR and low OCR) macrophages during the development of obesity.

These findings may have important implications for the metabolic state of macrophages in lean and obese individuals. Many reports focus on the macrophage phenotypic switch to a pro-inflammatory phenotype, identified as $CD11c^{+}$ (an accepted marker for M1 macrophages in adipose, or dendritic cells in other tissues) (162). More recent and in-depth studies in mice and humans reported that a plurality of macrophages in obese adipose tissue are $CD11c^{+}CD206^{+}$, interpreted to be hybrid M1/M2 macrophage (164, 165). Furthermore Kratz et al. recently labeled ATMs found in obesity as "metabolically activated," described as macrophages that result from the metabolic environment of obesity, lending them to have both pro- and anti-inflammatory characteristics (181). Here, we identify two distinct populations of ATMs ($CD45^{+}F4/80^{+}CD11b^{+}$) previously observed and coined $F4/80^{hi}$ ($CX3CR1^{+}$) and $F4/80^{lo}$ ($CX3CR1^{-}$), based on differential F4/80 and CX3CR1 expression (241, 261). We find that the $F4/80^{lo}$ population describes the resident ATMs, constituting the majority of macrophages in lean mice, and does not change in abundance after high-fat feeding. The $F4/80^{hi}$ ATMs significantly increase in number after high-fat feeding, identifying them as the infiltrating population. Unexpectedly, we find that the predominant ATM phenotype from lean mice appears to be *Mox* ($F4/80^{lo}HO1^{+}Txnrd1^{+}$), with a fraction being of the *M2* phenotype ($F4/80^{hi}CD206^{+}$). Over the course of high-fat diet feeding and development of obesity, we find that the *Mox* macrophages become outnumbered by macrophages that are *M2* and *M1/M2* hybrids ($F4/80^{hi}CD11c^{+}CD206^{+}$). This was accompanied by a relative loss of truncated OxPL, species we discovered to promote redox homeostasis, after

high-fat diet feeding, and a disproportional increase of full-length OxPL, species we demonstrate to promote an inflammatory macrophage profile.

Taken together, we show that ATM cellular metabolism changes dramatically during obesity. We show that this shift during obesity from a quiescent to an energetic metabolic profile correlates with two more changes: shift from 1) truncated to full-length OxPL species and 2) antioxidant *Mox* to activated *M1/M2* ATMs. Finally, we connect the OxPL microenvironment of SVF to the ATM polarization state by showing that: 1) truncated OxPL induce antioxidant gene expression and quiescent metabolism and 2) full-length OxPL induce pro-inflammatory gene expression and an energetic metabolism. Further study into modulating the metabolism of macrophages in obesity is warranted, as it may offer an important tool for addressing whole-body metabolism-linked pathologies.

Disclaimer

The work described in this chapter was performed by myself in conjunction with the following team members: Clint Upchurch, Michael Schappe, Paxton Voigt, Dory DeWeese, and Akshaya Meher.

Portions of this chapter (text and figures) were written as in Serbulea V, Upchurch CM, Schappe MS, Voigt PE, Deweese DE, Desai BN, Meher AK, Leitinger N. Macrophage phenotype and bioenergetics are controlled by oxidized phospholipids identified in lean and obese adipose tissue. Under review at *PNAS.*

5 CHAPTER 5: OXIDIZED PHOSPHATIDYLETHANOLAMINES SELECTIVELY INDUCE AEROBIC GLYCOLYSIS IN MACROPHAGES, WHILE PROMOTING ANTIOXIDANT GENE EXPRESSION

In this last chapter, we present observations on a developing story centered on phosphatidylethanolamine oxidation products. Though much work remains to be done, the data presented in this chapter supports the hypothesis that the actions of different oxidized lipid products are quite nuanced. This chapter will not have a self-contained conclusion and discussion section, instead, these results are discussed in **Chapter 6: Summary, Conclusions, Discussion, and Future Directions**.

5.1 INTRODUCTION

Amine-containing phospholipids, phosphatidylethanolamines (PEs) and phosphatidylserines (PSs), are found in the cytoplasmic-facing inner leaflet of the plasma membrane, while phosphatidylcholines (PCs) predominate in the outer membrane (17, 262). This is essential because the phospholipids of the plasma membrane are subject to oxidation from either external (environmental) or internal (mitochondrial and enzymatic) sources of reactive oxygen and nitrogen species. Recently, PE oxidation products and derivatives have been identified in several pathological contexts. Carboxyalkylpyrrole-phosphatidylethanolamine derivatives found in hyperlipidemic blood, as well as oxidized phosphatidylethanolamines (OxPEs) found on modified LDL, have been shown to induce platelet activation (91, 263). Compared to PCs, the PEs have a high capacity for binding divalent metal ions, such as copper (Cu^{2+}) and have been reported to be more readily oxidized as a consequence (264). The Krönke group has shown that certain 1-palmitoyl-2-arachidonioyl-sn-glycero-phosphatidylethanolamine (PAPE) oxidation products generated via lipoxygenase 12/15, such as the hydroxide (PAPE-OH) and hydroperoxide (PAPE-

OOH) of PAPE, promote phagocytosis of apoptotic cells by inflammatory monocytes (59). Furthermore, PAPE-OH and PAPE-OOH have been shown to induce ferroptosis of mouse embryonic fibroblasts (231), a cell-death pathway dependent on iron and mitochondrial metabolism (53). This result is similar to what has been shown by the Hazen group with oxidized PS (OxPS), who show that cells abundant with OxPS are phagocytosed by macrophages, while cells with non-oxidized PS remain unhindered (22). On the other hand, macrophages pre-treated with oxidized PCs (OxPC) seem to have inhibited phagocytosis of polystyrene beads and bacteria (265). In Chapter 3, we provided evidence supporting the metabolic reprogramming of macrophages by OxPC species (182). In Chapter 4, we provided evidence for the presence of numerous OxPC species in both whole blood and adipose stromal vascular fraction (SVF). Furthermore, we showed that enriching for truncated OxPC species drives antioxidant polarization along with bioenergetic inhibition. Additionally, we found that enriching for full-length OxPC drives pro-inflammatory polarization, along with promoting aerobic glycolysis. The question remains as to whether OxPE species have a similar activity to the OxPC species. An even more pressing question is identifying whether OxPE species exist in healthy tissue and whether the abundances and ratios of these species change during the development of obesity.

As we have shown in Chapter 4, lipid oxidation is a feature of adipose tissue. Due to its metabolic activity, adipose tissue is a site of increased oxidative stress and lipid oxidation (155). Here we show, for the first time, the presence and increasing abundance of individual OxPE species in murine adipose tissue after high-fat diet feeding. We present evidence that these species affect the transcriptional and metabolic profile of macrophages. The actions of OxPEs on macrophages bear numerous transcriptional similarities to that of OxPCs while promoting a different metabolic profile.

5.2 RESULTS

5.2.1 Full-length OxPE species increase in adipose SVF after high-fat diet feeding.

Recently, Valerian Kagan and colleagues used liquid chromatography-mass spectrometry to identify unique OxPE species as mediators of ferroptosis (231). We built on this approach to measure a subset of previously characterized oxidized acyl chains (109, 183). To develop and validate this approach, we obtained synthetic PAPE, oxidized it by air, and created the many oxidation products collectively referred to as OxPAPE (**Figure 5-1A,B**). We used the same classification system for the OxPE species as we did for OxPC, and assigned each species to one of four groups based on their oxidized acyl chain. Using this method, we detected and quantified the levels of 12 OxPE species found in adipose tissue stromal vascular fraction (SVF) (**Figure 5-2**) and whole blood (**Figure 5-3**) from mice fed a chow or high-fat diet for 9 and 17 weeks. We detected a low abundance of PAPE in blood taken from lean mice, relative to a high level of LysoPE (**Figure 5-3A**). Surprisingly, the abundance of PAPE in blood did not significantly change after high-fat diet feeding (**data not shown**), but the abundance of LysoPE increased (**Figure 5-3A**). As it has been reported before, high-fat diet feeding induces PLA2 activity in blood (259), making it a likely explanation for the increased level of LysoPE. Further analysis revealed that the oxidized fraction of PAPE-derived species, including LysoPE, in blood increases from 45% to 87%after high-fat diet (**Figure 5-3B**). Many of the truncated PE species could not be measured, as they are below the limit of detection for our method. Furthermore, it has been noted that PLA2 preferentially cleaves the sn-2 moiety from truncated OxPL (260).

Next, we used LC-MS to measure multiple non-oxidized PE species in SVF. We found that the total level of PE in adipose SVF increased over 20-fold in after high-fat diet feeding (**Figure 5-2A**). Although total non-oxidized PC was far more abundant than PE, the ratio of PE to PC species increased dramatically (**Figure 5-2B**). We find that total PE levels in SVF correlates

with the increase in the fat pad size (**Figure 5-2C**). PAPE itself is strongly increased in SVF after high-fat diet feeding (4-5 fold), while total OxPE species are only slightly increased (2-2.5 fold) (**Figure 5-2D**). Abundance of both PAPE and total OxPE species correlate with increased fat pad weight (**Figure 5-2E,F**). Each class of OxPE seems to increase, apart from the γ-keto/hydroxy-PE, and with the Isoprostane-PE having the greatest rate of increase (**Figure 5-2G-I**). Finally, high-fat diet feeding leads to a greater relative proportion of full-length OxPE species (**Figure 5-2J**). In summary, both non-oxidized and oxidized PE species accumulate in adipose SVF. These data show high-fat feeding induces significant changes in the phospholipidome of the SVF. Considering that obesity is associated with an influx of macrophages to the adipose tissue, we investigated the effects of OxPE on macrophage polarization.

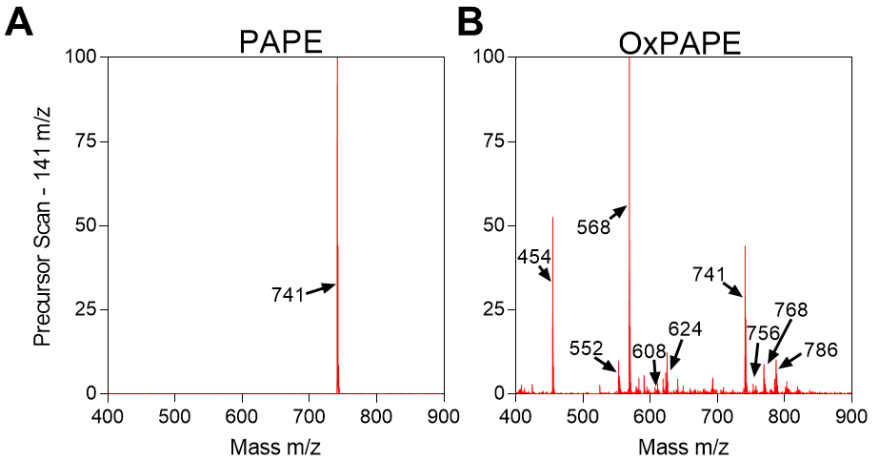

Figure 5-1: Oxidation of PAPE yields many detectable oxidized phospholipids

Figure 5-1 Legend

A. Ion scans for precursors of fragment 184 of PAPC (782 m/z) obtained using direct-inject mass spectrometry (MS) analysis, allowing for qualitative assessment of individual species presence.
B. Ion scans for precursors of fragment 184 of OxPAPE (collective mixture of PAPE oxidation products) obtained using direct-inject mass spectrometry (MS) analysis.

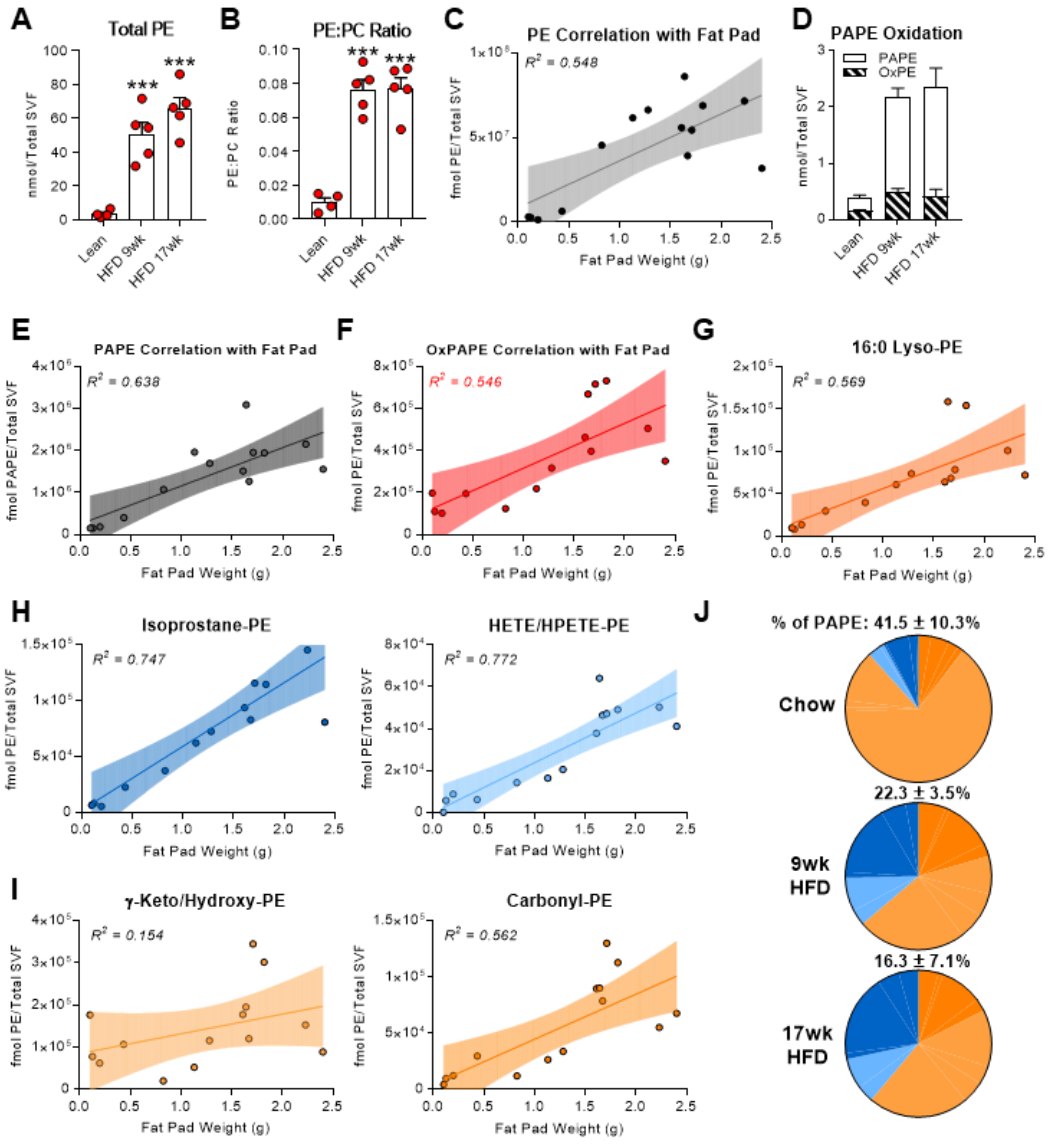

Figure 5-2: Phosphatidylethanolamines increase in adipose SVF, with a preference towards full-length OxPE

Figure 5-2 Legend

A. Total PE levels in total epididymal SVF (stromal vascular fraction) of lean mice or mice fed a high fat diet (HFD) for 9 or 17 weeks ($n \geq 4$). Total levels of PE were calculated by summation of the integrated ion peak areas of each individual PE species. ($n \geq 4$)
B. PE:PC ratio as calculated by dividing the summed integrated PE ion peak areas from the PC peak areas.
C. Accumulation of total PE species in SVF of lean mice and 9 or 17 week HFD-fed mice ($n \geq 4$). Assessment of correlation between total PE in SVF and fat pad weight.
D. Quantification of PAPE and PAPE-derived oxidation products (OxPE) in SVF.
E. Assessment of correlation between PAPE in SVF and fat pad weight.
F. Assessment of correlation between total OxPAPE species in SVF and fat pad weight.
G. Accumulation of 16:0 LysoPC normalized to blood volume of lean mice and 9 or 17 week HFD-fed mice ($n \geq 4$). Assessment of correlation between LysoPE in SVF and fat pad weight.
H. Accumulation of full-length OxPAPE classes HETE/HPETE-PE and Isoprostane-PE in SVF of lean mice and 9 or 17 week high-fat diet (HFD)-fed mice. ($n \geq 4$) Phospholipids were quantified on an individual species basis, using the integrated peak area of the ion count. The integrated peak area of each analyte was normalized to the internal standard, dinonanoyl-phosphatidylcholine (DNPC).
I. Accumulation of truncated OxPAPE classes Carbonyl-PE and γ-Keto/Hydroxy-PE in SVF of lean mice and 9 or 17 week HFD-fed mice. ($n \geq 4$)
J. Distribution of OxPAPE classes in SVF of lean or HFD-fed mice. Carbonyl-PE (orange), γ-Keto/Hydroxy-PE (light orange), HETE/HPETE-PE (light blue), and Isoprostane-PE (dark blue) are presented in clockwise fashion.

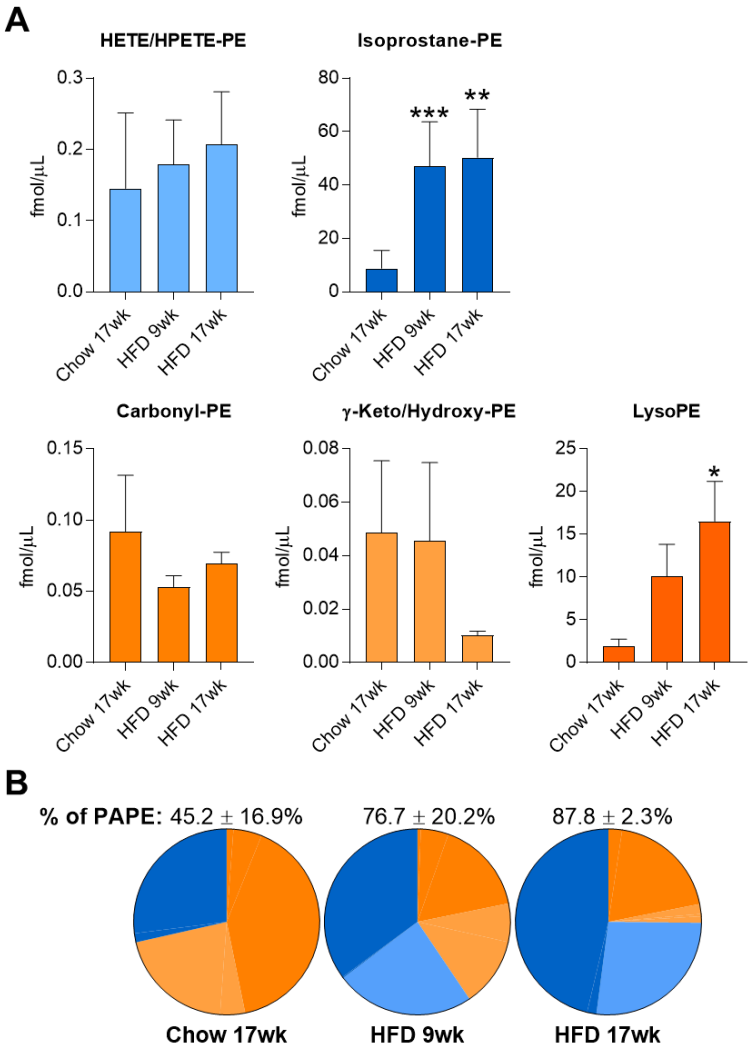

Figure 5-3: Supplement to Figure 5-2. Levels of OxPE in whole blood.

Figure 5-3 Legend

A. Fold change in OxPAPE classes as measured by liquid chromatography-mass spectrometry (LC-MS) in whole blood from lean mice and mice fed a HFD for 9 or 17 weeks ($n \geq 4$). Phospholipids were quantified on an individual species basis, using the integrated peak area of the ion count. The integrated peak area of each analyte was normalized to the internal standard, DNPC. Significance was determined by two-way ANOVA of the ion count peak area. Post-hoc statistical significance of individual classes was determined by Welch's 2-sided t-test. Data represented in a heat map showing $\log_2$ of the fold change compared to lean mice.

B. Distribution of OxPAPE classes in whole blood of lean or HFD-fed mice. Carbonyl-PE (orange), γ-Keto/Hydroxy-PE (light orange), HETE/HPETE-PE (light blue), and Isoprostane-PE (dark blue) are presented in clockwise fashion.
Data are expressed as mean ± SEM. Statistical significance calculated by Welch's 2-sided t-test unless otherwise specified (*$p < 0.05$; **$p < 0.01$; ***$p < 0.001$).

5.2.2 OxPEs abrogate LTA-induced inflammatory gene expression while concurrently promoting weak pro-inflammatory gene expression

We treated bone marrow-derived macrophages (BMDMs) with OxPAPE or LTA (TLR2 ligand used as a positive control) for 4-6 hours, after which we used qPCR to measure gene expression. Relative to the level of LTA-induced pro-inflammatory gene expression, OxPAPE increased *Il1β* and *Itgax* gene expression around 2-fold (**Figure 5-4A**). Itgax is the gene name for CD11c, an integrin commonly used as a marker for dendritic cells and pro-inflammatory adipose tissue macrophages (162, 163). Additionally, we found that OxPAPE significantly induced *Vegf* gene expression, a marker of hypoxia. Furthermore, we found that both OxPAPE and LTA increased expression of the antioxidant gene *Ho1* (**Figure 5-4B**). This finding was initially surprising, as we did not expect LTA to induce Nrf2-depedent genes. Consulting the literature, we found that LTA, via a TLR2-MyD88-Src dependent pathway, induces NADPH oxidase and subsequent reactive oxygen species production, which in turn lead to Nrf2-dependent gene and protein expression (266). OxPLs are known to be powerful anti-inflammatory compounds (102). To test the anti-inflammatory potential of OxPE species, we co-treated BMDMs with LTA and a concentration series of OxPAPE. We found that OxPAPE significantly inhibited *Il1β* gene expression, while inducing *Ho1* gene expression (**Figure 3-5C**).

Next, considering that we found increased *Vegf* gene expression after OxPAPE-stimulation, we asked whether Hif1α was involved in the induction of gene expression. Using Hif1α-KO BMDMs, we found that, indeed, the induction of *Il1β* and *Vegf* was Hif1α-dependent (**Figure 3-5B**), while *Ho1* expression was not (**Figure 3-5E**). O'Neill's group has previously shown that LPS-stimulated macrophages accumulate succinate, which activates Hif1α, which in turn reprograms macrophage metabolism towards aerobic glycolysis (175). We next asked whether OxPAPE reprograms macrophages metabolism towards aerobic glycolysis.

5.2.3 OxPE induce aerobic glycolysis in macrophages, independent of IL1β

Kagan et al. have shown that one may generate intracellular OxPE species by inhibiting glutathione peroxidase 4 (GPX4) using the inhibitor RSL3 (231). We treated BMDMs with OxPAPE and RSL3 and assessed cellular metabolism using extracellular flux analysis. First, the glycolytic stress test showed that both RSL3 and OxPAPE promote aerobic glycolysis (**Figure 5-5B**). Second, the mitochondrial stress test showed that RSL3, but not OxPAPE, inhibited maximal respiratory capacity (**Figure 5-5A**). In Chapter 3, we show that higher concentrations OxPAPE inhibited macrophage respiratory capacity (**Figure 3-6**). Taken together, both OxPAPE and RSL3 lead macrophages to become more glycolytic. Interestingly, we found that Ferrostatin, an inhibitor of ferroptosis, inhibits OxPAPE-induced *Il1β* expression (**Figure 5-6A**), but not antioxidant gene expression such as *Ho1* and *Txnrd1* (**Figure 5-6B**). Furthermore, we found that 50nM RSL3, though it had a dramatic effect on macrophage metabolism, did not seem to induce pro-inflammatory or antioxidant gene expression.

Studies in the literature suggest that most pro-inflammatory mediators or cytokines will induce aerobic glycolysis. Considering that OxPLs promote the production of pro-inflammatory cytokines, namely IL1β, we decided to test whether IL1β itself could make macrophage metabolism more glycolytic. We treated BMDMs with recombinant murine IL1β and IL1-receptor antagonist (IL1RA) and found that, indeed, IL1β through action on the IL1-receptor induces aerobic glycolysis (**Figure 5-7A**). We next tested whether cotreated BMDMs with OxPAPC and IL1RA to test whether OxPAPE-induced IL1β acts in an autocrine fashion to induce glycolysis. We found that cotreatment with IL1RA did not abrogate OxPAPE-induced aerobic glycolysis (**Figure 5-7B**).

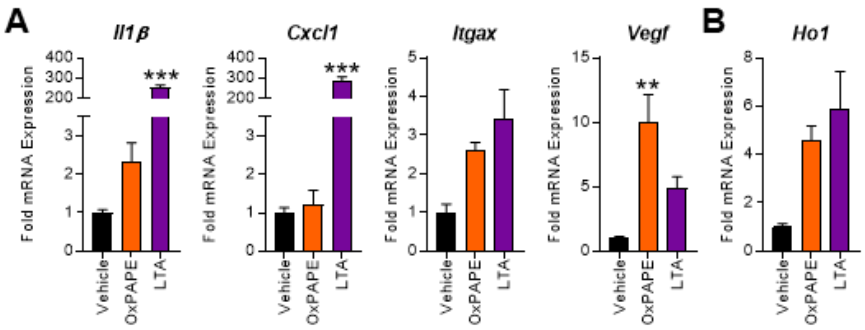

Figure 5-4: OxPE induces weak inflammatory gene expression in macrophages relative to LTA

Figure 5-4 Legend

A. mRNA expression by qPCR measured in BMDMs treated with 1µg/mL LTA or 30µg/mL OxPAPE for 4 hours. Genes measured are *Il1β*, *Cxcl1*, *Itgax* (proinflammatory markers), and *Vegf* (hypoxia marker). ($n \geq 3$)
B. mRNA expression of *Ho1* (antioxidant marker) by qPCR measured in BMDMs treated with 1µg/mL LTA or 30µg/mL OxPAPE for 4 hours. ($n \geq 3$)

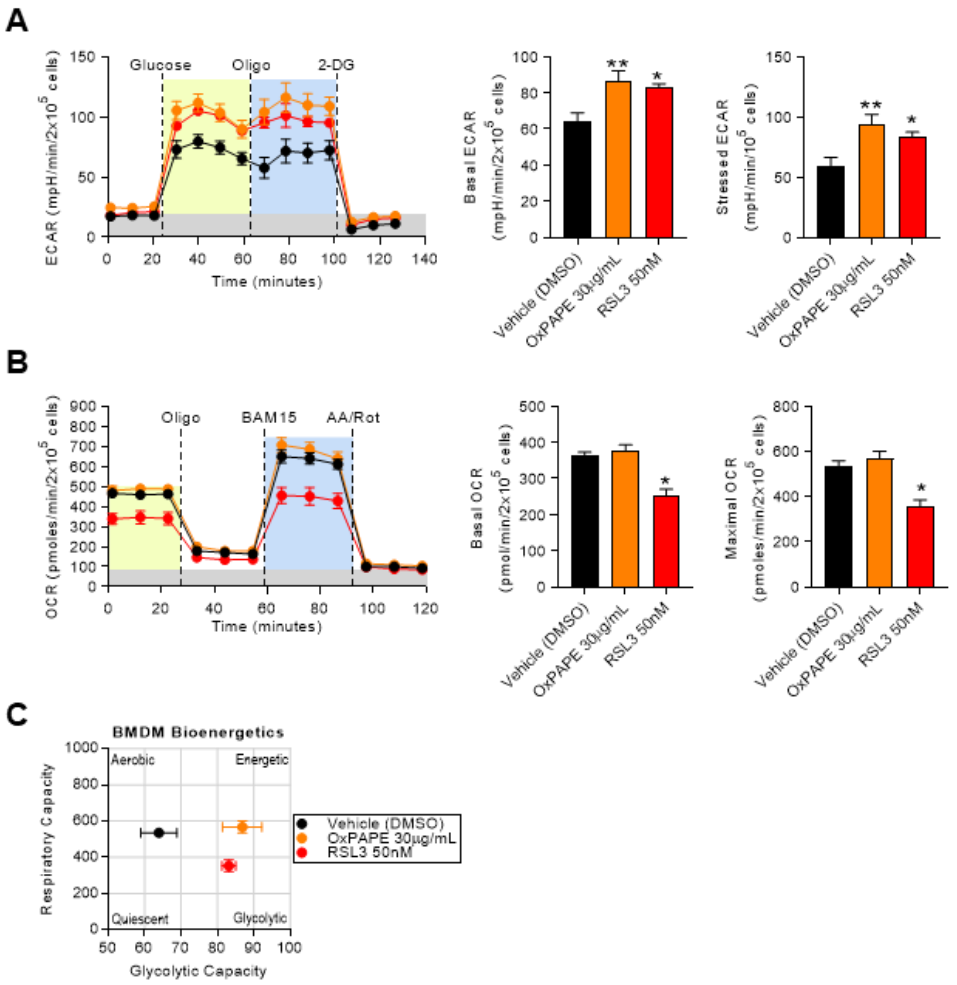

Figure 5-5: Macrophages sensing OxPE shift their metabolism to aerobic glycolysis

Figure 5-5 Legend

A. Glycolytic stress test (GST) of BMDMs treated with vehicle (RPMI media), 30µg/mL OxPAPE, or 50nM RSL3 for 4 hours (n = 4). The extracellular acidification rate (ECAR) was measured after injection of 20mM glucose, 1µM oligomycin, and 80mM 2-DG addition to produce the basal (red), stressed (teal), and background (gray) ECAR, respectively. Basal and stressed ECAR were calculated by subtracting the mean ECAR of the post-glucose (basal) or post-Oligomycin (stressed) measurements from the mean ECAR of the post-2-DG measurements.
B. Mitochondrial stress test (MST) of BMDMs treated with vehicle (RPMI media), 30µg/mL OxPAPE, or 50nM RSL3 for 4 hours (n = 4). The oxygen consumption rate (OCR) was measured initially (basal; red), and after injection of 1µM oligomycin, 2µM of the uncoupler BAM15 (maximal; teal), and 10µM antimycin A & 1µM rotenone (AA/Rot; gray; non-mitochondrial). Basal and maximal OCR were calculated by subtracting the mean OCR of the first three (basal) or post-BAM15 (maximal) measurements from the mean OCR of the post-AA/Rot measurements.
C. Bioenergetics plot relates the cells' respiratory capacity (based on maximal OCR, y-axis) to the glycolytic capacity (based on stressed ECAR, x-axis).

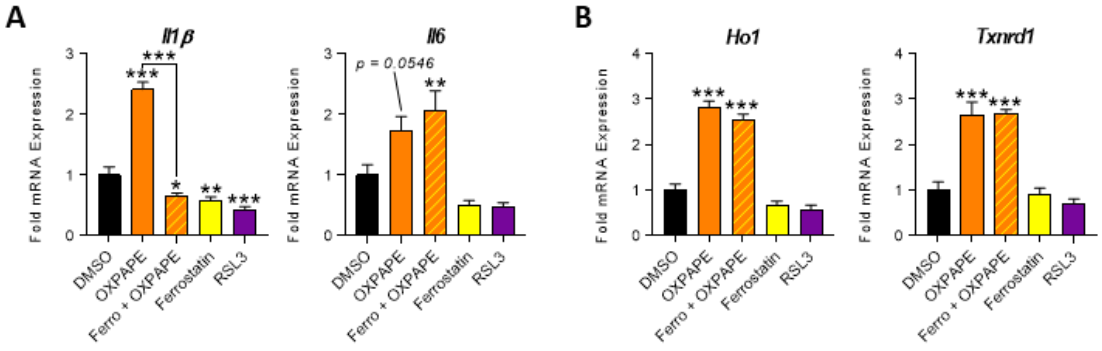

Figure 5-6: Ferrostatin inhibits OxPAPE-induced *Il1β* gene expression

Figure 5-6 Legend

A. mRNA expression of pro-inflammatory genes by qPCR measured in BMDMs treated with vehicle (DMSO), 30µg/mL OxPAPE, 1µM Ferrostatin, OxPAPE & Ferrostatin, or 50nM RSL3 for 4 hours. (n = 4)
B. mRNA expression of antioxidant genes by qPCR measured in BMDMs treated with vehicle (DMSO), 30µg/mL OxPAPE, 1µM Ferrostatin, OxPAPE & Ferrostatin, or 50nM RSL3 for 4 hours. (n = 4)

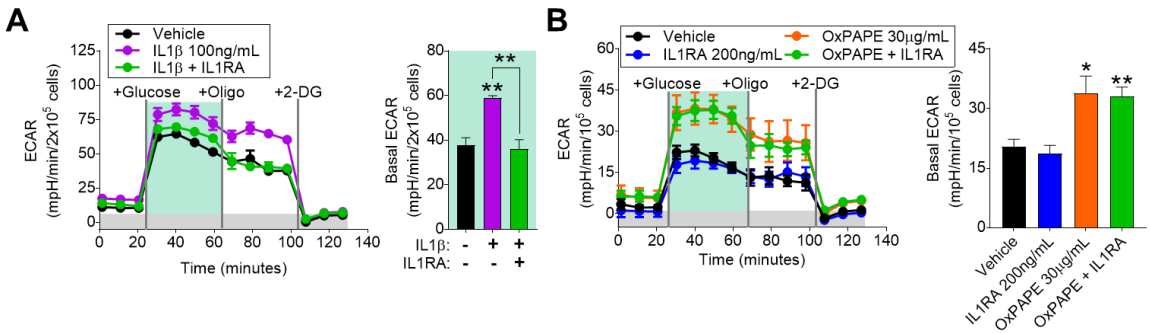

Figure 5-7: OxPAPE-induced aerobic glycolysis is independent of IL1β production

Figure 5-7 Legend

A. Glycolytic stress test (GST) of BMDMs treated with vehicle (RPMI media), 100ng/mL recombinant murine IL1β, or IL1β & IL1-receptor antagonist (IL1RA; 200ng/mL) for 18 hours (n = 4)
B. Glycolytic stress test (GST) of BMDMs treated with vehicle (RPMI media), 200ng/mL IL1RA, 30μg/mL OxPAPE, or IL1RA & OxPAPE for 18 hours (n = 4)

Disclaimer

The work described in this chapter was performed by myself in conjunction with the following team members: Clint Upchurch, Paxton Voigt, Dory DeWeese, and Gael Bories

6 CHAPTER 6: SUMMARY, CONCLUSIONS, DISCUSSION, AND FUTURE DIRECTIONS

The work presented here addresses open questions in the fields of immunometabolism and lipid oxidation. We answer these questions in the context of diet-induced obesity and adipose tissue inflammation. This work provides evidence supporting a new paradigm regarding adipose tissue macrophage transcriptional and metabolic polarization during obesity, detailed below. Furthermore, it shows the presence of oxidized phospholipids (OxPLs) in both lean and obese adipose tissue and describes a mechanism by which OxPLs modulate macrophage metabolism. First, we summarize the key data supporting these points.

6.1 SUMMARY AND CONCLUSIONS

How do OxPLs change macrophage metabolism? To answer this question, we performed extracellular flux analysis, metabolomics, and gene expression analysis on cultured primary murine macrophages (BMDMs) and a murine macrophage cell line (RAW264.7 cells) exposed to OxPAPC. Acute treatment (2-6 hours) with OxPAPC inhibited aerobic glycolysis and mitochondrial respiration in macrophages, implying that OxPLs suppress macrophage bioenergetics. Although OxPAPC inhibited these metabolic pathways, it simultaneously increased glucose uptake. Metabolomics revealed an accumulation of succinate in OxPAPC-treated macrophages, like LTA-treated macrophages. Succinate activates Hif1α to upregulate expression of glycolytic enzymes, including the glucose transporter Glut1, allowing macrophages to pull in more fuel. Metabolomics also revealed an accumulation of glutathione (GSH) precursors in OxPAPC-treated macrophages. Concurrently, OxPAPC acutely decreased the intracellular levels of reducing agent glutathione (GSH) and reductive cofactor NADPH, supporting the idea that the constituents of OxPAPC are not just *oxidized*, but are themselves *oxidative*. Chronic exposure (16-24 hours) to OxPAPC, restored GSH levels to the starting level.

Furthermore, the restoration of GSH levels coincided with an increase in aerobic glycolysis, implying lowered GSH levels instruct the cell to divert glucose towards antioxidant synthesis. 2-deoxyglucose, an inhibitor of hexokinase, inhibited the treatment time-dependent restoration of GSH levels, implying that GSH synthesis requires functional glucose metabolism. OxPAPC requires TLR2 (but not Nrf2)-dependent ceramide accumulation to inhibit macrophage mitochondrial function. Furthermore, knockout or inhibition of Syk lowered intracellular ceramide levels, and consequently, restored OxPAPC-inhibited mitochondrial function in macrophages.

What are the structural components of OxPLs responsible for biological activity?

OxPAPC, OxPAPE, and OxAA all induced gene expression of antioxidant enzymes, pro-inflammatory cytokines, and key enzymes of the pentose phosphate pathway. This provides evidence that the oxidized fatty acid moiety, not the phospholipid head group, is the key structural component required for biological activity. Although OxPLs induced a low level of inflammatory genes, they strongly inhibited inflammatory gene expression induced by TLR2-agonist LTA, supporting the idea that OxPLs are strong inhibitors of classic pro-inflammatory agents. TLR2 and Syk are necessary for OxPL-induced inflammatory gene expression but not antioxidant gene expression. OxPAPC enriched for components containing a truncated oxidized fatty acid (truncated OxPAPC) specifically induced antioxidant gene expression and inhibited mitochondrial function in macrophages. However, OxPAPC enriched for components containing a full-length oxidized fatty acid (full-length OxPAPC) upregulated pro-inflammatory gene expression while concurrently promoting aerobic glycolysis in macrophages. This indicates that truncated OxPLs transcriptionally and metabolically polarize macrophages to Mox, a macrophage phenotype supporting redox homeostasis. Additionally, this implies that full-length OxPLs polarize macrophages to an M1-like pro-inflammatory macrophage.

What is the metabolic profile of ATMs? Based on the currently accepted paradigm of ATM phenotypic polarization, we expected ATMs from lean mice to have an M2-like aerobic metabolism and ATMs from obese mice to have an M1-like glycolytic metabolism. Surprisingly, ATMs purified from lean mice have inhibited mitochondrial function and aerobic glycolysis (quiescent metabolism) as determined by extracellular flux analysis, like BMDMs treated with truncated OxPAPC. Conversely, ATMs from obese mice have boosted mitochondrial function and aerobic glycolysis (energetic metabolism), similar to BMDMs treated with full-length OxPAPC. This implies that ATMs from lean mice are metabolically similar to Mox macrophages, while ATMs from obese mice are best described as having a mixed M1 and M2 metabolism. Considering how drastically different the results were from the expectation, we questioned the paradigm alleging an M2 to M1 switch during obesity.

What is the phenotypic polarization of resident ATMs and macrophages infiltrating during obesity? We designed an antibody panel for flow cytometry to identify ATMs ($CD45^+F4/80^+CD11b^+$), resident ATMs ($CX3CR1^-$), infiltrating macrophages ($CX3CR1^+$), M1 ($CD11c^+$), M2 ($CD206^+$), and Mox ($HO1^+TXNRD1^+$). A single population ($F4/80^{lo}CX3CR1^-HO1^+TXNRD1^+$) predominantly describes resident ATMs, isolated from chow-fed lean mice. Meanwhile, three populations ($F4/80^{hi}CX3CR1^+CD11c^+$), ($F4/80^{hi}CX3CR1^+CD206^+$), and ($F4/80^{hi}CX3CR1^+CD11c^+CD206^+$) described infiltrating macrophages found in adipose tissue of high-fat diet fed mice. This demonstrates that resident ATMs are predominantly Mox. Furthermore, during obesity, the resident ATMs are outnumbered by M1, M2, and hybrid M1/M2 macrophages. Taken together with our earlier findings, we hypothesized that OxPLs are present in adipose tissue and they change during obesity.

What species of OxPLs are present in adipose tissue of lean and obese mice? We isolated the stromal vascular fraction (SVF) from the gonadal fat pads of chow-fed lean and high-fat diet

fed obese mice. Next, we used liquid chromatography-mass spectrometry to analyze OxPL composition. Adipose SVF from obese mice had a greater proportion of full-length OxPAPC and OxPAPE species than the than adipose SVF from lean mice. This implies that obesity changes the OxPL composition of adipose tissue to contain predominantly pro-inflammatory full-length OxPLs. The phospholipid composition warrants further investigation due to the limitations of the current approach. First, we were only able to measure 22 OxPC and 12 OxPE species, and second, we did not have synthetic standards for each of those species. We can address the first limitation by using a mass spectrometer configured for data-independent acquisition.

6.2 DISCUSSION

6.2.1 Is oxidation so bad?

Long before the developed world considered obesity as a problem, oxidative tissue damage was (and still is) regarded as one of the most difficult health problems to successfully address. Oxidative stress has been implicated in the pathogenesis nearly every disease, from aging (267), cancer (268), neurological disorders including Alzheimer's (269) and Parkinson's (270), behavioral disorders such as anxiety (271) and depression (272), bacterial (273) and viral infections (274), autoimmune disorders such as systemic lupus erythematosus (275) and rheumatoid arthritis (276), cardiovascular diseases including atherosclerosis (66, 277, 278) and hypertension (279), to muscular dystrophy (280) and erectile dysfunction (281). Countless advertisements, especially over the last twenty years, prey on this paradigm of biology to sell antioxidant supplements and therapies. The idea of oxidative stress as a detriment has been largely popularized by Harman's free radical theory of aging (282), a short editorial cited over 8,000 times to date. Clinical trials featuring antioxidant therapies have had, at best, mixed results (283), and at worst, shown increased mortality (284). Most studies begin with the assumption that oxidative stress, and by association, oxidation in general, is highly detrimental to an organism, to

be avoided at all costs. A landmark study by Furukawa et al. in 2004 showed that multiple tissues experience oxidative stress during obesity, as detected by accumulation of lipid peroxidation products (155). An overlooked finding from that study showed something even more astounding, which is that adipose tissue from healthy mice already had a high concentration of products resulting from lipid peroxidation, especially compared to other tissues. This observation, which has been recapitulated in other studies, supports our findings that there are OxPLs present in lean, healthy, adipose tissue. The presence of OxPLs in healthy tissue implies that, at least some, OxPLs play a homeostatic role. Given that we found truncated OxPLs suppress macrophage metabolism and produce antioxidant enzymes, we speculate that OxPLs in healthy tissue help promote redox homeostatsis through macrophage metabolic polarization.

6.2.2 The hormetic response of macrophages to oxidative stress

Our work focused on measuring and describing the effects of OxPLs, but it would be a mistake to assume they all act in the same manner. Numerous previous works have shown that mixtures of and individual OxPL have pro-inflammatory, antioxidant, anti-inflammatory, and phagocytic effects. The perspective of many literature reviews seemed to imply that all OxPLs (and products of oxidative stress) were detrimental. This perspective began to change when Bochkov and Leitinger showed that OxPLs can be used to inhibit LPS-induced sepsis (110). This work was further explored by Bochkov, who began to describe the effects of certain OxPLs as ‘hormetic’ (149). The term hormesis refers to a biphasic dose-response of a compound in which a low-dose promotes a beneficial effect while a high dose promotes a detrimental effect (285). In the case of OxPLs, this refers to the production of antioxidant compounds and enzymes, which was explored in Chapter 3. A difficulty we faced early on with this project regarded the multi-phasic metabolic response by macrophages to OxPAPC. One of the first series of experiments we performed tested the effects of a series of concentrations of a single preparation of OxPAPC on macrophage respiratory capacity (data not shown). The result was very difficult to interpret, as

OxPAPC had an inhibitory effect at the lower concentrations (10-20μg/mL), a boosting effect at higher concentrations (30μg/mL), and finally, no apparent response at the highest concentrations (50-100μg/mL). This metabolic response was highly different from the gene expression response, which followed a linear, expected response. A hypothesis to explain this phenomenon is that different oxidized lipids within our mixture exceed their response threshold at different active concentrations. Thus, increasing the overall concentration of the mixture may allow new lipids to reach bioactivity, which may act counter to the lipids perpetuating the initial response. We plan on testing this hypothesis in the near future by performing combination treatments between different OxPL species at various relative doses. An alternative explanation is that as the concentration of an individual lipid increases, it may act on an increasing number of intracellular and extracellular receptors. We also plan on testing this hypothesis by treating with increased concentrations of individual OxPLs and using RNA-Seq to assess the transcriptional regulation of various pathways simultaneously. Many more experiments are required to fully understand this phenomenon.

Macrophages are highly flexible cells, found in every tissue, and responsible for an incredible list of duties. We posit that macrophages are a reactionary cell, changing their internal machinery and function based on the local environment they perceive. In Chapter 4, we showed that macrophage metabolism and phenotypic polarization varied dramatically by different classes of OxPL, which we described as truncated or full-length according to their structure. This highly simplistic approach, using mixtures of OxPLs that were enriched for either truncated or full-length species, supports the notions that macrophages change their function in accordance with the environment they sense and that different OxPLs have drastically different biological activities.

6.2.3 Oxidized lipids are a nuanced system for cellular communication

Dr. Valerian Kagan (University of Pittsburgh) put forth a radical new perspective regarding oxidized lipids. He suggested that oxidized lipids represent a language, of sorts, that organisms use on the cellular and molecular level. Products of lipid oxidation existed long before DNA encoded complex signaling proteins and peptides. As we covered in Chapter 1, even the most basic of organisms on earth uses lipids, namely phospholipids, to separate its metabolic processes from the environment. The unsaturated fatty acids on phospholipids can be oxidized, but the kinetics of oxidation vary by the individual species of fatty acid and the head group of the phospholipid. An arachidonic acid (AA; 20:4)-containing phospholipid, such as PAPC is ~80% oxidized by ambient oxygen in 7-8 days. In contrast, a linoleic acid (LA; 18:2)-containing phospholipid, such as PLPC is ~60% oxidized in 35-40 days. PAPE, the equivalent of PAPC but with a phosphatidylethanolamine head group, is ~80% oxidized in 3-4 days. It is possible that within a cell, these lipids are sensors for external (PC) and internal (PE) oxidation. The heterogenous distribution of phospholipids in the plasma membrane, and within cellular compartments would allow for a wide variety of signaling lipids to form under various redox states. For example, should the environment external to the cell become highly oxidant, OxPC species would form, due to the prevalence of PC species in the outer leaflet of the plasma membrane. Should there be a source of oxidation from within the cell, then OxPE and OxPS species would preferably form, due to the abundance of PE and PS on the inner leaflet of the plasma membrane. Should the mitochondria produce excess reactive oxygen species, then oxidized cardiolipin (OxCL) would preferably form. We propose that compartmentalized sources of redox imbalance produce cellular signals, in the form of lipid oxidation products, that allow for autocrine and paracrine signaling. For example, a macrophage detecting OxPC on another cell may infer that there is a pro-oxidant extracellular environment in the vicinity, and thus commit resources to its antioxidant arsenal in lieu of its phagocytic potential. A macrophage detecting

OxPE or OxPS might infer that a cell has recently undergone apoptosis, and is now marked for engulfment. In this scenario the macrophage would instead shift their metabolism towards aerobic glycolysis, to support inflammation and phagocytosis. Using a similar line of thinking, one can argue that truncated OxPL are signs of extended or protracted oxidative stress, thus requiring an upregulation of antioxidant defense. Full-length OxPL may represent a more controlled (e.g. lipoxygenase-derived), acute, oxidation event, warranting instead an inflammatory and phagocytic response. Much work remains to be done to elucidate the actions of individual OxPL species, and it very well may be that the assignments of groups and classes (i.e. full-length and truncated) may be too simplistic to represent the nuanced actions of OxPL. Does an oxidized fatty acid have the same functions as their analogous OxPL? Does the presence of an un-oxidized fatty acid esterified to a phospholipid affect the availability of the oxidized moiety to be recognized by receptors or reducing agents? Much work has to be done to address these open questions.

6.2.4 Metabolism determines cellular function

In the last 5 years, the O'Neill and Pearce groups have shown that macrophage polarization can influence their metabolism and *vice versa*. Macrophages polarized with a pro-inflammatory stimulus, such as LPS, have strongly inhibited oxidative phosphorylation, with a compensatory boost in aerobic glycolysis (175). On the other hand, macrophages polarized with an anti-inflammatory stimulus, such as IL4, have strongly boosted oxidative phosphorylation (176). These landmark studies revealed a range of metabolic reprogramming that can arise from simple receptor-mediated stimuli. These studies further hinted to the fact that changes in the metabolism were necessary for the respective pro- or anti-inflammatory polarization. In the same initial study, O'Neill's group showed that LPS-induced IL1β expression was dependent on glycolysis by using 2-deoxyglucose (2-DG; inhibitor of hexokinase). In this study, we have shown that macrophage glucose metabolism was necessary for both OxPAPC-induced (Mox) antioxidant and pro-inflammatory gene expression, as well as glutathione synthesis (Chapter 3).

We find that the adipose tissue macrophage polarization during obesity shifts from Mox in healthy tissue to an M1/M2 mixture in obese tissue (Chapter 4). We predict that the Mox macrophages, compared to the M1 and M2, are more capable of handling oxidative stress, though we have not outright tested this hypothesis.

Another limitation of this study is that we have not investigated what the carbon source for glutathione is in OxPL-treated macrophages. We hypothesize that in glucose is used directly for glutathione synthesis (preferentially to glutamine). Other studies have shown the possibility of glucose contributing directly to glutathione synthesis (286). This experiment would be a rather straightforward mass spectrometry-based approach, using heavy-carbon labeled glucose and glutamine. The implications of proving this hypothesis would be far-reaching, considering that inhibiting glucose metabolism is an up and coming therapy for inflammatory diseases and cancer (287–289). For example, many tumors have significantly increased antioxidant defenses. Identifying the metabolic pathways by which cancerous cells upregulate to produce glutathione would open the door for novel therapeutics (47, 48, 290, 291). Indeed, recent studies show that inhibiting aerobic glycolysis in tumors is not enough, mitochondrial function must also be suppressed for effectively stopping tumor development (292–294). All things considered, cellular metabolism, especially of macrophages, is a ripe target for future therapies, though much more needs to be understood regarding the various interplay and compensations of metabolic pathways.

6.3 FUTURE DIRECTIONS

In the future, we hope to synthesize individual full-length OxPC species. With these on hand, we can treat cells and deconvolute the unique biological functions of the full-length species. This is of paramount importance because some full-length OxPLs, such as PECPC (containing an epoxycyclopentenone group) strongly induce Nrf2-dependent antioxidant gene expression through direct binding with Keap1 (31, 148, 200). Additionally, we would be able to make out

mass spectrometry method more quantitative, by generating meaningful standard curves using these synthetic compounds. We also hope to improve our solid phase extraction technique to not only get greater recovery of enriched full-length and truncated OxPL, but to allow for separation between subclasses (e.g. HETE/HPETE separate from Isoprostane).

A priority will be discerning the primary receptors and co-receptors for various OxPL. Establishing a metabolic tracing assay (using ^{13}C glucose) to show whether glucose is funneled through α-ketoglutarate to synthesize glutathione would address that hypothesis conclusively. Finally, establishing an unbiased lipidomic approach to quantify all phospholipid oxidation products in adipose, liver, and other tissues of interest would allow us to focus on which lipids have the greatest changes between the physiological state and the pathological state. This would, hopefully, point in a more focused direction for identifying targets for novel therapeutics to combat redox imbalance.

7 PUBLICATIONS

Below is a compilation of the publications on which I have been included as an author. The publications are divided by those directly resulting from my dissertation work (1st section) and those resulting from my collaboration with others (2nd section).

7.1 PUBLICATIONS RESULTING FROM THIS WORK

1. **Serbulea V**, Leitinger N. Modulation of Toll-Like Receptor Signaling by Oxidized Phospholipids, in Spickett, C. M. & Forman H. J., eds., ***Lipid Oxidation in Health and Disease***. CRC Press, Mar 2015, p. 215-230.
2. **Serbulea V**, DeWeese D, Leitinger N. The effect of oxidized phospholipids on phenotypic polarization and function of macrophages. ***Free Radic Biol Med***. 2017 Feb 21. pii: S0891-5849(17)30107-7. doi: 10.1016/j.freeradbiomed.2017.02.035.
3. Jakobs P*, **Serbulea V***, Leitinger N, Eckers A, Haendeler J. Nuclear Factor (Erythroid-Derived 2)-Like 2 and Thioredoxin-1 in Atherosclerosis and Ischemia/Reperfusion Injury in the Heart. ***Antioxid Redox Signal***. 2017 Apr 20;26(12):630-644. doi: 10.1089/ars.2016.6795.***indicates equal contributions**
4. **Serbulea V**, Upchurch CM, Ahern KW, Bories G, Voigt PE, Deweese DE, Meher AK, Harris TE, Leitinger N. Macrophages sensing oxidized DAMPs reprogram their metabolism to support redox homeostasis and inflammation through a TLR2-Syk-ceramide dependent mechanism. ***Molecular Metabolism***. 2017 Nov 7. doi: 10.1016/j.molmet.2017.11.002
5. **Serbulea V**, Upchurch CM, Schappe MS, Voigt PE, Deweese DE, Desai BN, Meher AK, Leitinger N. Macrophage phenotype and bioenergetics are controlled by oxidized phospholipids identified in lean and obese adipose tissue. **Under review at *PNAS***

7.2 ADDITIONAL PUBLICATIONS

1. Schaheen B, Downs EA, **Serbulea V**, Almenara CC, Spinosa M, Su G, Zhao Y, Srikakulapu P, Butts C, McNamara CA, Leitinger N, Upchurch GR Jr, Meher AK, Ailawadi G. B-Cell Depletion Promotes Aortic Infiltration of Immunosuppressive Cells and Is Protective of Experimental Aortic Aneurysm. ***Arterioscler Thromb Vasc Biol***. 2016 Nov;36(11):2191-2202.
2. Wilkins LR, Brautigan DL, Wu H, Yarmohammadi H, Kubicka E, **Serbulea V**, Leitinger N, Liu W, Haaga JR. Cinnamic Acid Derivatives Enhance the Efficacy of Transarterial Embolization in a Rat Model of Hepatocellular Carcinoma. ***Cardiovasc Intervent Radiol***. 2017 Mar;40(3):430-437. doi: 10.1007/s00270-016-1515-y.

3. Dyballa-Rukes N, Jakobs P, Eckers A, Ale-Agha N, **Serbulea V**, Aufenvenne K, Zschauer TC, Rabanter LL, Jakob S, von Ameln F, Eckermann O, Leitinger N, Goy C, Altschmied J, Haendeler J. The Anti-Apoptotic Properties of APEX1 in the Endothelium Require the First 20 Amino Acids and Converge on Thioredoxin-1. ***Antioxid Redox Signal***. 2017 Apr 20;26(12):616-629. doi: 10.1089/ars.2016.6799. **Featured on journal cover**
4. Olmez I, Brenneman B, Xiao A, **Serbulea V**, Zhang Y, Lee J, Nakano I, Godlewski J, Bronisz A, Abounader R, Leitinger N, Purow B. Combined CDK4/6 and mTOR inhibition is synergistic against glioblastoma via multiple mechanisms. ***Clin Cancer Res***. 2017 Aug 16. doi: 10.1158/1078-0432
5. Kerur N, Fukuda S, Banerjee D, Kim Y, Fu D, Apicella I, Varshney A, Yasuma R, Fowler BJ, Baghdasaryan E, Marion KM, Huang X, Yasuma T, Hirano Y, **Serbulea V**, Ambati M, Ambati VL, Kajiwara Y, Ambati K, Hirahara S, Bastos-Carvalho A, Ogura Y, Terasaki H, Oshika T, Kim KB, Hinton DR, Leitinger N, Cambier JC, Buxbaum JD, Kenney MC, Jazwinski SM, Nagai H, West AP, Fitzgerald KA, Sadda SR, Gelfand BD, Ambati J. cGAS drives non-canonical NLRP3 inflammasome in age-related macular degeneration. ***Nature Medicine***. 2018 Jan 01. doi: 10.1038/nm.4450
6. Meher AK, Spinosa M, Davis J, Pope N, Laubach VE, Su G, **Serbulea V**, Leitinger N, Ailawadi G, Upchurch GR Jr. A novel role of IL-1β in NETosis and Abdominal Aortic Aneurysms. **Accepted at *Arterioscler Thromb Vasc Biol***
7. Kruger N, Biwer LA, Good ME, DeLalio LJ, Murphy S, **Serbulea V**, Best AK, Leitinger N, Sonkusare SK, Godecke A, Ruther U, Isakson BE. Loss of endothelial Fto antagonizes obesity-induced metabolic and vascular alterations. **Under review at *Cell Reports***
8. Morioka S, Perry JSA, Raymond MH, **Serbulea V**, Onengut-Gumuscu S, Leitinger N, Rathmell JC, Ravichandran KS. Dynamic expression and function of solute carrier (SLC) proteins during phagocytosis of apoptotic cells. **Under review at *Nature***

8 REFERENCES

1. Halliwell BB, Gutteridge JM (1985) *Free Radicals in Biology and Medicine* (Oxford University Press, New York).

2. Lennard-Jones J (1929) The electronic structure of some diatomic molecules. *Trans Faraday Soc* 25(668):668–686.

3. GW. W (1937) The valence-bond treatment of the oxygen molecule. *Trans Faraday Soc* 33:1499–1502.

4. Jacobs EE, Rao Sanadi D (1960) Phosphorylation coupled to electron transport mediated by high potential electron carriers. *Biochim Biophys Acta* 38:12–34.

5. Turrens JF, Boveris A (1980) Generation of superoxide anion by the NADH dehydrogenase of bovine heart mitochondria. *Biochem J* 191(2):421–427.

6. Bedard K, Krause K-H (2007) The NOX Family of ROS-Generating NADPH Oxidases: Physiology and Pathophysiology. *Physiol Rev* 87(1):245–313.

7. Thomas DD, et al. (2015) Signaling and stress: The redox landscape in NOS2 biology. *Free Radic Biol Med* 87(301):204–225.

8. Kolberg M, Strand KR, Graff P, Andersson KK (2004) Structure, function, and mechanism of ribonucleotide reductases. *Biochim Biophys Acta - Proteins Proteomics* 1699(1–2):1–34.

9. Zheng GQ, Fu Y, He C (2014) Nucleic Acid Oxidation in DNA Damage Repair and Epigenetics. *Chem Rev* 114(8):4602–4620.

10. Cooke MS (2003) Oxidative DNA damage: mechanisms, mutation, and disease. *FASEB J* 17(10):1195–1214.

11. Haider L, et al. (2011) Oxidative damage in multiple sclerosis lesions. *Brain* 134(7):1914–1924.

12. Uchida K, Stadtman ER (1992) Modification of histidine residues in proteins by reaction with 4-hydroxynonenal. *Proc Natl Acad Sci U S A* 89(10):4544–8.

13. Uchida K (2003) Histidine and lysine as targets of oxidative modification. *Amino Acids* 25(3–4):249–257.

14. Zimmermann K, et al. (2015) Activated AMPK boosts the Nrf2/HO-1 signaling axis - A role for the unfolded protein response. *Free Radic Biol Med* 88(Part B):417–426.

15. Morrow JD, Awad JA, Boss HJ, Blair IA, Roberts LJ (1992) Non-cyclooxygenase-derived prostanoids (F2-isoprostanes) are formed in situ on phospholipids. *Proc Natl Acad Sci U S A* 89(22):10721–5.

16. Rothstein M, Miller LL (1952) The metabolism of glutaric acid-1, 5-C14. I. In normal and phlorhizinized rats. *J Biol Chem* 199(1):199–205.

17. Yamaji-Hasegawa A, Tsujimoto M (2006) Lipid Dynamics and Pathobiology in Membrane Lipid Rafts Asymmetric Distribution of Phospholipids in Biomembranes. *Biol Pharm Bull* 29(August):1547–1553.

18. Virtanen J a, Cheng KH, Somerharju P (1998) Phospholipid composition of the mammalian red cell membrane can be rationalized by a superlattice model. *Proc Natl Acad Sci U S A* 95(April):4964–4969.

19. Greenberg M, Li X, Gugiu B, Gu X (2008) The lipid whisker model of the structure of oxidized cell membranes. *J Biol Chem* 283(4):2385–96.

20. Podrez E a, et al. (2002) Identification of a novel family of oxidized phospholipids that serve as ligands for the macrophage scavenger receptor CD36. *J Biol Chem* 277(41):38503–16.

21. Podrez E a, et al. (2002) A novel family of atherogenic oxidized phospholipids promotes macrophage foam cell formation via the scavenger receptor CD36 and is enriched in atherosclerotic lesions. *J Biol Chem* 277(41):38517–23.

22. Greenberg ME, et al. (2006) Oxidized phosphatidylserine-CD36 interactions play an essential role in macrophage-dependent phagocytosis of apoptotic cells. *J Exp Med* 203(12):2613–25.

23. Hörkkö S, et al. (1999) Monoclonal autoantibodies specific for oxidized phospholipids or oxidized phospholipid-protein adducts inhibit macrophage uptake of oxidized low-density lipoproteins. *J Clin Invest* 103(1):117–128.

24. Clark SR, et al. (2011) Esterified eicosanoids are acutely generated by 5-lipoxygenase in primary human neutrophils and in human and murine infection. *Blood* 117(6):2033–2043.

25. Arai M, Imai H, Metori a, Nakagawa Y (1997) Preferential esterification of endogenously formed 5-hydroxyeicosatetraenoic acid to phospholipids in activated polymorphonuclear leukocytes. *Eur J Biochem* 244(2):513–9.

26. Stenson WF, Parker CW (1979) Metabolism of arachidonic acid in ionophore-stimulated neutrophils. *J Clin Invest* 64(November):1457–1465.

27. Afonyushkin T, et al. (2010) Oxidized phospholipids regulate expression of ATF4 and VEGF in endothelial cells via NRF2-dependent mechanism: Novel point of convergence

between electrophilic and unfolded protein stress pathways. *Arterioscler Thromb Vasc Biol* 30(5):1007–1013.

28. Watson a D, et al. (1997) Structural identification by mass spectrometry of oxidized phospholipids in minimally oxidized low density lipoprotein that induce monocyte/endothelial interactions and evidence for their presence in vivo. *J Biol Chem* 272(21):13597–607.

29. Watson a D, et al. (1999) Structural identification of a novel pro-inflammatory epoxyisoprostane phospholipid in mildly oxidized low density lipoprotein. *J Biol Chem* 274(35):24787–98.

30. Zanoni I, et al. (2016) An endogenous caspase-11 ligand elicits interleukin-1 release from living dendritic cells. *Science (80-)* 352(6290):1–9.

31. Bretscher P, et al. (2015) Phospholipid oxidation generates potent anti-inflammatory lipid mediators that mimic structurally related pro-resolving eicosanoids by activating Nrf 2. *EMBO Mol Med* 7(5):1–16.

32. Egger J, Bretscher P, Freigang S, Kopf M, Carreira EM (2013) Synthesis of epoxyisoprostanes: Effects in reducing secretion of pro-inflammatory cytokines IL-6 and IL-12. *Angew Chemie - Int Ed* 52(20):5382–5385.

33. Salomon RG, et al. (2000) Isolevuglandin-protein adducts in humans: Products of free radical- induced lipid oxidation through the isoprostane pathway. *Biochim Biophys Acta - Mol Cell Biol Lipids* 1485(2–3):225–235.

34. Salomon RG, et al. (1999) Protein Adducts of Iso [4] levuglandin E 2 , a Product of the Isoprostane Pathway , in Oxidized Low Density Lipoprotein *. 274(29):20271–20280.

35. Subbanagounder G, Leitinger N, Shih PT, Faull KF, Berliner J a. (1999) Evidence that phospholipid oxidation products and/or platelet-activating factor play an important role in early atherogenesis : in vitro and In vivo inhibition by WEB 2086. *Circ Res* 85(4):311–8.

36. Leitinger N, Tyner T (1999) Structurally similar oxidized phospholipids differentially regulate endothelial binding of monocytes and neutrophils. *Proc Natl Acad Sci* 96(21):12010–5.

37. Itabe H, et al. (1996) Oxidized Phosphatidylcholines That Modify Proteins. 271(52):33208–33217.

38. Mattila J-P, Sabatini K, Kinnunen PKJ (2008) Interaction of cytochrome c with 1-palmitoyl-2-azelaoyl-sn-glycero-3-phosphocholine: evidence for acyl chain reversal. *Langmuir* 24(8):4157–4160.

39. Sabatini K, Mattila J-P, Megli FM, Kinnunen PKJ (2006) Characterization of two

oxidatively modified phospholipids in mixed monolayers with DPPC. *Biophys J* 90(12):4488–99.

40. Kobayashi A, et al. (2006) Oxidative and Electrophilic Stresses Activate Nrf2 through Inhibition of Ubiquitination Activity of Keap1 Oxidative and Electrophilic Stresses Activate Nrf2 through Inhibition of Ubiquitination Activity of Keap1 †. doi:10.1128/MCB.26.1.221.

41. Tkachev VO, Menshchikova EB, Zenkov NK (2011) Mechanism of the Nrf2/Keap1/ARE signaling system. *Biochemistry (Mosc)* 76(4):407–422.

42. Yamamoto T, et al. (2008) Physiological significance of reactive cysteine residues of Keap1 in determining Nrf2 activity. *Mol Cell Biol* 28(8):2758–70.

43. Lu SC, Shelly C. Lu MD (2014) Glutathione Synthesis. *Biochim Biophys Acta* 1830(5):3143–3153.

44. Montero D, Tachibana C, Rahr Winther J, Appenzeller-Herzog C (2013) Intracellular glutathione pools are heterogeneously concentrated. *Redox Biol* 1(1):508–513.

45. Kosower EM, Kosower NS (1969) Lest I Forget Thee, Glutathione ... *Nature* 224(5215):117–120.

46. Speciale A, et al. (2011) Cellular adaptive response to glutathione depletion modulates endothelial dysfunction triggered by TNF-α. *Toxicol Lett* 207(3):291–7.

47. Estrela JM, Ortega A, Obrador E (2006) *Glutathione in cancer biology and therapy* doi:10.1080/10408360500523878.

48. Traverso N, et al. (2013) Role of Glutathione in Cancer Progression and Chemoresisstance. *Oxid Med Cell Longev* 2013. doi:10.1155/2013/972913.

49. Lillig CH, Berndt C, Holmgren A (2008) Glutaredoxin systems. *Biochim Biophys Acta - Gen Subj* 1780(11):1304–1317.

50. Holmgren A (1979) Glutathione-dependent Synthesis of Deoxyribonucleotides. *J Biol Chem* 2(10):3664–3671.

51. Holmgren A (2000) Antioxidant Function of Thioredoxin and Glutaredoxin Systems. *Antioxid Redox Signal* 2(4):811–820.

52. Berry MJ, Banu L, Harney JW, Larsen PR (1993) Functional characterization of the eukaryotic SECIS elements which direct selenocysteine insertion at UGA codons. *EMBO J* 12(8):3315–22.

53. Xie Y, et al. (2016) Ferroptosis: process and function. *Cell Death Differ* 23(3):369–379.

54. Seiler A, et al. (2008) Glutathione Peroxidase 4 Senses and Translates Oxidative Stress into 12/15-Lipoxygenase Dependent- and AIF-Mediated Cell Death. *Cell Metab* 8(3):237–248.

55. Arroyo A, et al. (2002) NADPH oxidase-dependent oxidation and externalization of phosphatidylserine during apoptosis in Me2SO-differentiated HL-60 cells. Role in phagocytic clearance. *J Biol Chem* 277(51):49965–75.

56. Chang M-K, et al. (2004) Apoptotic cells with oxidation-specific epitopes are immunogenic and proinflammatory. *J Exp Med* 200(11):1359–70.

57. Huber J, et al. (2002) Oxidized membrane vesicles and blebs from apoptotic cells contain biologically active oxidized phospholipids that induce monocyte-endothelial interactions. *Arterioscler Thromb Vasc Biol* 22(January):101–107.

58. Rothe T, et al. (2015) 12/15-lipoxygenase-mediated enzymatic lipid oxidation regulates DC maturation and function. *J Clin Invest* 125(5):1944–1954.

59. Uderhardt S, et al. (2012) 12/15-Lipoxygenase Orchestrates the Clearance of Apoptotic Cells and Maintains Immunologic Tolerance. *Immunity* 36(5):834–46.

60. Huber J, et al. (2002) Oxidized cholesteryl linoleates stimulate endothelial cells to bind monocytes via the extracellular signal-regulated kinase 1/2 pathway. *Arterioscler Thromb Vasc Biol* 22(4):581–586.

61. Choi SH, et al. (2013) Polyoxygenated cholesterol ester hydroperoxide activates TLR4 and SYK dependent signaling in macrophages. *PLoS One* 8(12):1–10.

62. Choi S-HS, et al. (2009) Lipoprotein accumulation in macrophages via toll-like receptor-4-dependent fluid phase uptake. *Circ Res* 104(12):1355–63.

63. Miller Y, Choi S (2012) The SYK side of TLR4: signalling mechanisms in response to LPS and minimally oxidized LDL. *Br J Pharmacol* 167(5):990–999.

64. Bae YS, et al. (2009) Macrophages generate reactive oxygen species in response to minimally oxidized low-density lipoprotein: toll-like receptor 4- and spleen tyrosine kinase-dependent activation of NADPH oxidase 2. *Circ Res* 104(2):210–8.

65. Subbanagounder G, et al. (2000) Determinants of bioactivity of oxidized phospholipids: Specific oxidized fatty acyl groups at the sn-2 position. *Arterioscler Thromb Vasc Biol* 20(10):2248–2254.

66. Berliner JA, Leitinger N, Tsimikas S, J. A. Berliner, N. Leitinger and ST (2009) The role

of oxidized phospholipids in atherosclerosis. *J Lipid Res* 50:S207–S212.

67. Van Der Valk FM, et al. (2016) Oxidized phospholipids on Lipoprotein(a) elicit arterial wall inflammation and an inflammatory monocyte response in humans. *Circulation* 134(8):611–624.

68. Tsiantoulas D, et al. (2015) Circulating microparticles carry oxidation-specific epitopes and are recognized by natural IgM antibodies. *J Lipid Res* 56(2):440–448.

69. Oskolkova O V., et al. (2008) Atf4-dependent transcription is a key mechanism in VEGF up-regulation by oxidized phospholipids: Critical role of oxidized sn-2 residues in activation of unfolded protein response. *Blood* 112(2):330–339.

70. Romanoski CE, et al. (2011) Network for activation of human endothelial cells by oxidized phospholipids: A critical role of heme oxygenase 1. *Circ Res* 109(5). doi:10.1161/CIRCRESAHA.111.241869.

71. Nonas S, et al. (2006) Oxidized phospholipids reduce vascular leak and inflammation in rat model of acute lung injury. *Am J Respir Crit Care Med* 173(10):1130–1138.

72. Huber J, et al. (2006) Specific monocyte adhesion to endothelial cells induced by oxidized phospholipids involves activation of cPLA2 and lipoxygenase. *J Lipid Res* 47(5):1054–1062.

73. Bochkov VN, et al. (2006) Oxidized phospholipids stimulate angiogenesis via autocrine mechanisms, implicating a novel role for lipid oxidation in the evolution of atherosclerotic lesions. *Circ Res* 99(8):900–908.

74. Isakson BE, Kronke G, Kadl A, Leitinger N, Duling BR (2006) Oxidized phospholipids alter vascular connexin expression, phosphorylation, and heterocellular communication. *Arterioscler Thromb Vasc Biol* 26(10):2216–2221.

75. Cherepanova OA, et al. (2009) Oxidized phospholipids induce type VIII collagen expression and vascular smooth muscle cell migration. *Circ Res* 104(5):609–618.

76. Pidkovka NA, et al. (2007) Oxidized phospholipids induce phenotypic switching of vascular smooth muscle cells in vivo and in vitro. *Circ Res* 101(8):792–801.

77. Shankman LS, et al. (2015) KLF4-dependent phenotypic modulation of smooth muscle cells has a key role in atherosclerotic plaque pathogenesis. *Nat Med* 21(6):628–637.

78. Blüml S, et al. (2005) Oxidized phospholipids negatively regulate dendritic cell maturation induced by TLRs and CD40. *J Immunol* 175(1):501–8.

79. Seyerl M, et al. (2008) Oxidized phospholipids induce anergy in human peripheral blood

T cells. *Eur J Immunol* 38(3):778–787.

80. Blüml S, et al. (2009) Epigenetic regulation of dendritic cell differentiation and function by oxidized phospholipids. *Blood* 114(27):5481–9.

81. Boutaud O, Brame CJ, Salomon RG, Roberts LJ, Oates JA (1999) Characterization of the lysyl adducts formed from prostaglandin H2 via the levuglandin pathway. *Biochemistry* 38(29):9389–9396.

82. Hoppe G, Subbanagounder G, O'Neil J, Salomon RG, Hoff HF (1997) Macrophage recognition of LDL modified by levuglandin E2, an oxidation product of arachidonic acid. *Biochim Biophys Acta - Lipids Lipid Metab* 1344(1):1–5.

83. Salomon RG, et al. (1997) Levuglandin E2-protein adducts in human plasma and vasculature. *Chem Res Toxicol* 10(5):536–545.

84. Salomon RG, Bi W (2015) Isolevuglandin Adducts in Disease. *Antioxid Redox Signal* 22(18):1703–1718.

85. Guo L, Chen Z, Amarnath V, Davies SS (2012) Identification of novel bioactive aldehyde-modified phosphatidylethanolamines formed by lipid peroxidation. *Free Radic Biol Med* 53(6):1226–1238.

86. Guo L, Davies SS (2013) Bioactive aldehyde-modified phosphatidylethanolamines. *Biochimie* 95(1):74–78.

87. Guo L, et al. (2015) Isolevuglandin-Type Lipid Aldehydes Induce the Inflammatory Response of Macrophages by Modifying Phosphatidylethanolamines and Activating the Receptor for Advanced Glycation Endproducts. *Antioxid Redox Signal* 22(18):1633–1645.

88. Sullivan CB, Matafonova E, Roberts LJ, Amarnath V, Davies SS (2010) Isoketals form cytotoxic phosphatidylethanolamine adducts in cells. *J Lipid Res* 51(5):999–1009.

89. Kirabo A, et al. (2014) DC isoketal-modified proteins activate T cells and promote hypertension. *J Clin Invest* 124(10):4642–4656.

90. Chen Z, et al. (2014) Incorporation of Therapeutically Modified Bacteria into Gut Microbiota inhibits obesity. *J Clin Invest* 124(8):3391–3406.

91. Biswas S, et al. (2016) Novel phosphatidylethanolamine derivatives accumulate in circulation in hyperlipidemic ApoE-/- mice and activate platelets via TLR2. *Blood* 127(21):2618–2629.

92. West XZ, et al. (2010) Oxidative stress induces angiogenesis by activating TLR2 with novel endogenous ligands. *Nature* 467(7318):972–6.

93. Hollyfield JG, et al. (2008) Oxidative damage–induced inflammation initiates age-related macular degeneration. *Nat Med* 14(2):194–198.

94. Binder CJ, Papac-milicevic N, Witztum JL (2016) Innate sensing of oxidation-specific epitopes in health and disease. *Nat Rev Immunol* 16(8):485–497.

95. Henriksen EJ, Diamond-Stanic MK, Marchionne EM (2011) Oxidative stress and the etiology of insulin resistance and type 2 diabetes. *Free Radic Biol Med* 51(5):993–999.

96. Walton KA, et al. (2003) Receptors involved in the oxidized 1-palmitoyl-2-arachidonoyl-sn-glycero-3-phosphorylcholine-mediated synthesis of interleukin-8: A role for toll-like receptor 4 and a glycosylphosphatidylinositol-anchored protein. *J Biol Chem* 278(32):29661–29666.

97. Jyrkkänen HK, et al. (2008) Nrf2 regulates antioxidant gene expression evoked by oxidized phospholipids in endothelial cells and murine arteries in vivo. *Circ Res* 103(1). doi:10.1161/CIRCRESAHA.108.176883.

98. Kadl A, et al. (2011) Oxidized phospholipid-induced inflammation is mediated by Toll-like receptor 2. *Free Radic Biol Med* 51(10):1903–9.

99. Erridge C, Kennedy S, Spickett CMC, Webb DJDDJ (2008) Oxidized phospholipid inhibition of toll-like receptor (TLR) signaling is restricted to TLR2 and TLR4: roles for CD14, LPS-binding protein, and MD2 as targets for specificity of inhibition. *J Biol …* 283(36):24748–59.

100. Erridge C, Kennedy S, Spickett CM, Webb DJ (2008) Oxidized phospholipid inhibition of Toll-Like Receptor (TLR) signaling is restricted to TLR2 and TLR4: Roles for CD14, LPS-binding protein, aErridge, C., Kennedy, S., Spickett, C. M., & Webb, D. J. (2008). Oxidized phospholipid inhibition of Toll-Like Rec. *J Biol Chem* 283(36):24748–24759.

101. Oskolkova OVOO V, et al. (2010) Oxidized Phospholipids Are More Potent Antagonists of Lipopolysaccharide than Inducers of Inflammation. *J Immunol* 185(12):7706–7712.

102. Von Schlieffen E, et al. (2009) Multi-hit inhibition of circulating and cell-associated components of the toll-like receptor 4 pathway by oxidized phospholipids. *Arterioscler Thromb Vasc Biol* 29(3):356–362.

103. Walton K, Gugiu B, Thomas M (2006) A role for neutral sphingomyelinase activation in the inhibition of LPS action by phospholipid oxidation products. *J Lipid Res* 47(9):1967–74.

104. Stemmer U, et al. (2012) Uptake and protein targeting of fluorescent oxidized phospholipids in cultured RAW 264.7 macrophages. *Biochim Biophys Acta - Mol Cell Biol Lipids* 1821(4):706–718.

105. Gugiu BG, et al. (2008) Protein targets of oxidized phospholipids in endothelial cells. *J Lipid Res* 49(3):510–520.

106. Springstead JR, et al. (2012) Evidence for the importance of OxPAPC interaction with cysteines in regulating endothelial cell function. *J Lipid Res* 53(7):1304–1315.

107. Miller YI, et al. (2012) Oxidation-specific epitopes are danger associated molecular patterns recognized by pattern recognition receptors of innate immunity. *Circ Res* 108(2):235–248.

108. Stewart CR, et al. (2010) CD36 ligands promote sterile inflammation through assembly of a Toll-like receptor 4 and 6 heterodimer. *Nat Immunol* 11(2):155–61.

109. Bochkov VN, et al. (2010) Generation and biological activities of oxidized phospholipids. *Antioxid Redox Signal* 12(8):1009–59.

110. Bochkov V, et al. (2002) Protective role of phospholipid oxidation products in endotoxin-induced tissue damage. *Nature* 4(June):77–81.

111. Walton KA, et al. (2003) Specific phospholipid oxidation products inhibit ligand activation of toll-like receptors 4 and 2. *Arterioscler Thromb Vasc Biol* 23(7):1197–1203.

112. Riedemann N, Ward P (2002) Oxidized lipid protects against sepsis. *Nat Med* 8(10):1084–5.

113. Shaw PX, et al. (2000) Natural antibodies with the T15 idiotype may act in atherosclerosis, apoptotic clearance, and protective immunity. *J Clin Invest* 105(12):1731–40.

114. Tsimikas S, et al. (2003) Temporal increases in plasma markers of oxidized low-density lipoprotein strongly reflect the presence of acute coronary syndromes. *J Am Coll Cardiol* 41(3):360–370.

115. Alves JD, Ames PRJ (2003) Atherosclerosis, oxidative stress and auto-antibodies in systemic lupus erythematosus and primary antiphospholipid syndrome. *Immunobiology* 207(1):23–8.

116. Friedman P, Hörkkö S, Steinberg D, Witztum JL, Dennis EA (2002) Correlation of antiphospholipid antibody recognition with the structure of synthetic oxidized phospholipids. Importance of Schiff base formation and aldol condensation. *J Biol Chem* 277(9):7010–7020.

117. Chang MK, et al. (1999) Monoclonal antibodies against oxidized low-density lipoprotein bind to apoptotic cells and inhibit their phagocytosis by elicited macrophages: evidence that oxidation-specific epitopes mediate macrophage recognition. *Proc Natl Acad Sci U S A* 96(11):6353–8.

118. Su GL, Dorko K, Strom SC, N"ussler AK, Wang SC (1999) {CD14} expression and production by human hepatocytes. *J Hepatol* 31(3):435442.

119. Pan Z, Zhou L, Hetherington CJ, Zhang DE (2000) Hepatocytes contribute to soluble CD14 production, and CD14 expression is differentially regulated in hepatocytes and monocytes. *J Biol Chem* 275(46):36430–36435.

120. Miller YI, et al. (2003) Minimally modified LDL binds to CD14, induces macrophage spreading via TLR4/MD-2, and inhibits phagocytosis of apoptotic cells. *J Biol Chem* 278(3):1561–8.

121. Kim MJ, et al. (2013) Suppression of Toll-like receptor 4 activation by endogenous oxidized phosphatidylcholine, KOdiA-PC by inhibiting LPS binding to MD2. *Inflamm Res* 62(6):571–580.

122. Ohto U, Fukase K, Miyake K, Shimizu T (2012) Structural basis of species-specific endotoxin sensing by innate immune receptor TLR4/MD-2. *Proc Natl Acad Sci* 109(19):7421–7426.

123. Wang Y, et al. (2016) TLR4/MD-2 activation by a synthetic agonist with no similarity to LPS. *Proc Natl Acad Sci* 113(7):E884–E893.

124. Handberg A, et al. (2010) Soluble CD36 (sCD36) clusters with markers of insulin resistance, and high sCD36 is associated with increased type 2 diabetes risk. *J Clin Endocrinol Metab* 95(4):1939–1945.

125. Jimenez-Dalmaroni MJ, et al. (2009) Soluble CD36 ectodomain binds negatively charged diacylglycerol ligands and acts as a co-receptor for TLR2. *PLoS One* 4(10). doi:10.1371/journal.pone.0007411.

126. Dramane G, et al. (2012) STIM1 regulates calcium signaling in taste bud cells and preference for fat in mice. *J Clin Invest* 122(6):2267–2282.

127. Corrine M. Spickett HJF ed. (2015) *Lipid Oxidation in Health and Disease* (CRC Pres, Boca Raton).

128. Davies SS, Guo L (2014) Lipid peroxidation generates biologically active phospholipids including oxidatively N-modified phospholipids. *Chem Phys Lipids* 181:1–33.

129. Farhat K, Riekenberg S (2008) Heterodimerization of TLR2 with TLR1 or TLR6 expands the ligand spectrum but does not lead to differential signaling. *J Leukoc Biol* 83(3):692–701.

130. Jin MS, et al. (2007) Crystal Structure of the TLR1-TLR2 Heterodimer Induced by Binding of a Tri-Acylated Lipopeptide. *Cell* 130(6):1071–1082.

131. Carneiro AB, et al. (2013) Lysophosphatidylcholine Triggers TLR2- and TLR4-Mediated Signaling Pathways but Counteracts LPS-Induced NO Synthesis in Peritoneal Macrophages by Inhibiting NF-??B Translocation and MAPK/ERK Phosphorylation. *PLoS One* 8(9):1–9.

132. Makide K, et al. (2014) Novel lysophosphoplipid receptors: their structure and function. *J Lipid Res* 55(10):1986–95.

133. Salomon RG (2012) Structural Identification and Cardiovascular Activities of Oxidized Phospholipids. *Circ Res* 111(7):930–946.

134. Mullick A, Tobias P, Curtiss L (2005) Modulation of atherosclerosis in mice by Toll-like receptor 2. *J Clin Immunol* 115(11):3149–3156.

135. Leemans JC, et al. (2005) Renal-associated TLR2 mediates ischemia/reperfusion injury in the kidney. *J Clin Invest* 115(10):2894–2903.

136. Ehses J a., et al. (2010) Toll-like receptor 2-deficient mice are protected from insulin resistance and beta cell dysfunction induced by a high-fat diet. *Diabetologia* 53(8):1795–1806.

137. Mogensen TH (2009) Pathogen recognition and inflammatory signaling in innate immune defenses. *Clin Microbiol Rev* 22(2):240–273.

138. Imai Y, et al. (2008) Identification of Oxidative Stress and Toll-like Receptor 4 Signaling as a Key Pathway of Acute Lung Injury. *Cell* 133(2):235–249.

139. Erridge C, Webb D, Spickett C (2007) Toll-like receptor 4 signalling is neither sufficient nor required for oxidised phospholipid mediated induction of interleukin-8 expression. *Atherosclerosis* 193(1):77–85.

140. Panigrahi S, et al. (2013) Engagement of platelet toll-like receptor 9 by novel endogenous ligands promotes platelet hyperreactivity and thrombosis. *Circ Res* 112(1):103–112.

141. Podrez EA, et al. (2007) Platelet CD36 links hyperlipidemia, oxidant stress and a prothrombotic phenotype. *Nat Med* 13(9):1086–1095.

142. Surh Y-J, Kundu JK, Na H-K (2008) Nrf2 as a master redox switch in turning on the cellular signaling involved in the induction of cytoprotective genes by some chemopreventive phytochemicals. *Planta Med* 74(13):1526–39.

143. Kobayashi M, et al. (2002) Identification of the interactive interface and phylogenic conservation of the Nrf2-Keap1 system. *Genes Cells* 7(8):807–20.

144. Ishii T, et al. (2000) Transcription factor Nrf2 coordinately regulates a group of oxidative

stress-inducible genes in macrophages. *J Biol Chem* 275(21):16023–16029.

145. Furman C, et al. (2004) Thioredoxin reductase 1 is upregulated in atherosclerotic plaques: Specific induction of the promoter in human macrophages by oxidized low-density lipoproteins. *Free Radic Biol Med* 37(1):71–85.

146. Kadl A, et al. (2010) Identification of a novel macrophage phenotype that develops in response to atherogenic phospholipids via Nrf2. *Circ Res* 107(6):737–746.

147. Harada N, et al. (2012) Nrf2 in bone marrow-derived cells positively contributes to the advanced stage of atherosclerotic plaque formation. *Free Radic Biol Med* 53(12):2256–2262.

148. Friedli O, Freigang S (2017) Cyclopentenone-containing oxidized phospholipids and their isoprostanes as pro-resolving mediators of inflammation. *Biochim Biophys Acta - Mol Cell Biol Lipids* 1862(4):382–392.

149. Mauerhofer C, Philippova M, Oskolkova O V., Bochkov VN (2016) Hormetic and anti-inflammatory properties of oxidized phospholipids. *Mol Aspects Med* 49(July):78–90.

150. Bloom DA, Jaiswal AK (2003) Phosphorylation of Nrf2 at Ser40 by Protein Kinase C in Response to Antioxidants Leads to the Release of Nrf2 from INrf2, but Is Not Required for Nrf2 Stabilization/Accumulation in the Nucleus and Transcriptional Activation of Antioxidant Response Element. *J Biol Chem* 278(45):44675–44682.

151. Huang HC, Nguyen T, Pickett CB (2002) Phosphorylation of Nrf2 at Ser-40 by protein kinase C regulates antioxidant response element-mediated transcription. *J Biol Chem* 277(45):42769–42774.

152. Yeon SH, Yang G, Lee HE, Lee JY (2016) Oxidized phosphatidylcholine induces the activation of NLRP3 inflammasome in macrophages. *J Leukoc Biol* 100(October):1–11.

153. Chu LH, et al. (2018) The oxidized phospholipid oxPAPC protects from septic shock by targeting the non-canonical inflammasome in macrophages. *Nat Commun* 9(1):996.

154. Ogden CLL, Carroll MDD, Kit BKK, Flegal KMM (2014) Prevalence of childhood and adult obesity in the United States, 2011-2012. *Jama* 311(8):806–814.

155. Furukawa S, et al. (2004) Increased oxidative stress in obesity and its impact on metabolic syndrome. *J Clin Invest* 114(12):1752–1761.

156. Findeisen HM, et al. (2011) Oxidative stress accumulates in adipose tissue during aging and inhibits adipogenesis. *PLoS One* 6(4):e18532.

157. Evans JL, Maddux BA, Olson KR (2005) The Molecular Basis for Oxidative Stress-

Induced Insulin Resistance. *Antioxid Redox Signal* 7(55):1040–1052.

158. Den Hartigh LJ, et al. (2017) Adipocyte-Specific Deficiency of NADPH Oxidase 4 Delays the Onset of Insulin Resistance and Attenuates Adipose Tissue Inflammation in Obesity. *Arterioscler Thromb Vasc Biol* 37(3):466–475.

159. Kusminski CM, Scherer PE (2012) Mitochondrial dysfunction in white adipose tissue. *Trends Endocrinol Metab* 23(9):435–43.

160. Vernochet C, Mourier A, Bezy O, Macotela Y (2012) Adipose-specific deletion of TFAM increases mitochondrial oxidation and protects mice against obesity and insulin resistance. *Cell Metab* 16(6):765–76.

161. Shi X, et al. (2008) Paradoxical effect of mitochondrial respiratory chain impairment on insulin signaling and glucose transport in adipose cells. *J Biol Chem* 283(45):30658–67.

162. Lumeng CN, Bodzin JL, Saltiel AR (2007) Obesity induces a phenotipic switch in adipose tissue macrophage polarization. *J Clin Invest* 117(1):175–184.

163. Patsouris D, et al. (2008) Ablation of CD11c-Positive Cells Normalizes Insulin Sensitivity in Obese Insulin Resistant Animals. *Cell Metab* 8(4):301–309.

164. Wentworth JM, Naselli G, Brown WA, Doyle L (2010) Pro-inflammatory CD11c+ CD206+ adipose tissue macrophages are associated with insulin resistance in human obesity. *Diabetes* 59(July):1648–1656.

165. Li P, et al. (2010) Functional heterogeneity of CD11c-positive adipose tissue macrophages in diet-induced obese mice. *J Biol Chem* 285(20):15333–15345.

166. Jager J, Grémeaux T, Cormont M, Le Marchand-Brustel Y, Tanti J-FF (2007) Interleukin-1β-induced insulin resistance in adipocytes through down-regulation of insulin receptor substrate-1 expression. *Endocrinology* 148(1):241–251.

167. Olefsky JM, Glass CK (2010) *Macrophages, inflammation, and insulin resistance.* doi:10.1146/annurev-physiol-021909-135846.

168. de Luca C, Olefsky JM (2008) Inflammation and insulin resistance. *FEBS Lett* 582(1):97–105.

169. Heilbronn LK, Campbell L V (2008) Adipose tissue macrophages, low grade inflammation and insulin resistance in human obesity. *Curr Pharm Des* 14(12):1225–1230.

170. Suganami T, Ogawa Y (2010) Adipose tissue macrophages: their role in adipose tissue remodeling. *J Leukoc Biol* 88(1):33–9.

171. Bourlier V, Bouloumie A (2009) Role of macrophage tissue infiltration in obesity and insulin resistance. *Diabetes Metab* 35(4):251–60.

172. Stienstra R, Netea-Maier RT, Riksen NP, Joosten LAB, Netea MG (2017) Specific and Complex Reprogramming of Cellular Metabolism in Myeloid Cells during Innate Immune Responses. *Cell Metab* 26(1):142–156.

173. Cheng S-C, et al. (2016) Broad defects in the energy metabolism of leukocytes underlie immunoparalysis in sepsis. *Nat Immunol* (January). doi:10.1038/ni.3398.

174. Norata GDD, et al. (2015) The Cellular and Molecular Basis of Translational Immunometabolism. *Immunity* 43(3):421–434.

175. Tannahill GM, et al. (2013) Succinate is an inflammatory signal that induces IL-1β through HIF-1α. *Nature* 496(7444):238–242.

176. Huang SC, et al. (2014) Cell-intrinsic lysosomal lipolysis is essential for alternative activation of macrophages. *Nat Immunol* 15(August):1–12.

177. Jha AK, et al. (2015) Network Integration of Parallel Metabolic and Transcriptional Data Reveals Metabolic Modules that Regulate Macrophage Polarization. *Immunity* 42(3):419–430.

178. Davies LC, Jenkins SJ, Allen JE, Taylor PR (2013) Tissue-resident macrophages. *Nat Immunol* 14(10):986–995.

179. Perdiguero EG, et al. (2014) Tissue-resident macrophages originate from yolk-sac-derived erythro-myeloid progenitors. *Nature* 518(7540):547–551.

180. Bain CC, et al. (2014) Constant replenishment from circulating monocytes maintains the macrophage pool in the intestine of adult mice. *Nat Immunol* 15(10):929–37.

181. Kratz M, et al. (2014) Metabolic dysfunction drives a mechanistically distinct proinflammatory phenotype in adipose tissue macrophages. *Cell Metab* 20(4):614–625.

182. Serbulea V, et al. (2017) Macrophages sensing oxidized DAMPs reprogram their metabolism to support redox homeostasis and inflammation through a TLR2-Syk-ceramide dependent mechanism. *Mol Metab*:1–12.

183. Serbulea V, DeWeese D, Leitinger N (2017) The effect of oxidized phospholipids on phenotypic polarization and function of macrophages. *Free Radic Biol Med* 111(December 2016):156–168.

184. Milne GL, Yin H, Hardy KD, Davies SS, Roberts LJ (2011) Isoprostane generation and function. *Chem Rev* 111(10):5973–96.

185. Thomas CP, et al. (2010) Phospholipid-esterified eicosanoids are generated in agonist-activated human platelets and enhance tissue factor-dependent thrombin generation. *J Biol Chem* 285(10):6891–6903.

186. Subbanagounder G, et al. (2002) Epoxyisoprostane and epoxycyclopentenone phospholipids regulate monocyte chemotactic protein-1 and interleukin-8 synthesis. Formation of these oxidized phospholipids in response to interleukin-1β. *J Biol Chem* 277(9):7271–7281.

187. Lu J, et al. (2017) Identification of a Novel Series of Anti-inflammatory and Anti-oxidative Phospholipid Oxidation Products Containing Cyclopentenone Moiety in vitro and in vivo: Implication in Atherosclerosis. *J Biol Chem* 292(Ldl):5378–5391.

188. Pégorier S, Stengel D, Durand H, Croset M, Ninio E (2006) Oxidized phospholipid: POVPC binds to platelet-activating-factor receptor on human macrophages. Implications in atherosclerosis. *Atherosclerosis* 188(2):433–43.

189. Loidl A, Sevcsik E, Riesenhuber G, Deigner H-P, Hermetter A (2003) Oxidized phospholipids in minimally modified low density lipoprotein induce apoptotic signaling via activation of acid sphingomyelinase in arterial smooth muscle cells. *J Biol Chem* 278(35):32921–8.

190. Kenwood BM, et al. (2014) Identification of a novel mitochondrial uncoupler that does not depolarize the plasma membrane. *Mol Metab* 3(2):114–23.

191. Kim H, Salem N (1990) Separation of lipid classes by solid phase extraction. *J Lipid Res* 31(3):2285–2289.

192. Adamson SE, et al. (2016) Disabled homolog 2 controls macrophage phenotypic polarization and adipose tissue inflammation. 126(19):1–12.

193. Okabe Y, Medzhitov R (2015) Tissue biology perspective on macrophages. *Nat Immunol* 17(1):9–17.

194. Kamstrup PR, Hung M-Y, Witztum JL, Tsimikas S, Nordestgaard BG (2017) Oxidized Phospholipids and Risk of Calcific Aortic Valve Disease. *Arterioscler Thromb Vasc Biol*:ATVBAHA.116.308761.

195. Capoulade R, et al. (2015) Oxidized phospholipids, lipoprotein(a), and progression of calcific aortic valve stenosis. *J Am Coll Cardiol* 66(11):1236–1246.

196. Tsimikas S, Witztum JL (2008) The role of oxidized phospholipids in mediating lipoprotein(a) atherogenicity. *Curr Opin Lipidol* 19(4):369–377.

197. Berliner J a, Leitinger N, Tsimikas S (2009) The role of oxidized phospholipids in atherosclerosis. *J Lipid Res* 50 Suppl:S207-12.

198. Leitinger N, Watson AD, Faull KF, Fogelman AM, Berliner JA (1997) Monocyte binding to endothelial cells induced by oxidized phospholipids present in minimally oxidized low density lipoprotein is inhibited by a platelet activating factor receptor antagonist. *Adv Exp Med Biol* 433:379–382.

199. Miller YI, Shyy JY-J (2016) Context-Dependent Role of Oxidized Lipids and Lipoproteins in Inflammation. *Trends Endocrinol Metab* xx:1–10.

200. Egger J, Bretscher P, Freigang S, Kopf M, Carreira EM (2014) Discovery of a Highly Potent Anti-inflammatory Epoxyisoprostane- Derived Lactone. 2–5.

201. Mcadoo SP, Tam FWK (2009) Fostamatinib Disodium. *Drug Data Rep* 31(2):173.

202. Dennehy KM, et al. (2008) Syk kinase is required for collaborative cytokine production induced through Dectin-1 and Toll-like receptors. *Eur J Immunol* 38(2):500–506.

203. Fälker K, Klarström-Engström K, Bengtsson T, Lindahl TL, Grenegård M (2014) The toll-like receptor 2/1 (TLR2/1) complex initiates human platelet activation via the src/Syk/LAT/PLCγ2 signalling cascade. *Cell Signal* 26(2):279–86.

204. Slack EC, et al. (2007) Syk-dependent ERK activation regulates IL-2 and IL-10 production by DC stimulated with zymosan. *Eur J Immunol* 37(6):1600–1612.

205. van Bergenhenegouwen J, et al. (2013) TLR2 & Co: a critical analysis of the complex interactions between TLR2 and coreceptors. *J Leukoc Biol* 94(5):885–902.

206. Lin Y-LY-CY-CY-LY-CY-LY-C, et al. (2013) The tyrosine kinase Syk differentially regulates Toll-like receptor signaling downstream of the adaptor molecules TRAF6 and TRAF3. *Sci Signal* 6(289):ra71.

207. Hilgendorf I, et al. (2011) The oral spleen tyrosine kinase inhibitor fostamatinib attenuates inflammation and atherogenesis in low-density lipoprotein receptor-deficient mice. *Arterioscler Thromb Vasc Biol* 31(9):1991–9.

208. Van den Bossche J, et al. (2016) Mitochondrial Dysfunction Prevents Repolarization of Inflammatory Macrophages. *Cell Rep* 17(3):684–696.

209. Darley-Usmar VM, Severn A, O'Leary VJ, Rogers M (1991) Treatment of macrophages with oxidized low-density lipoprotein increases their intracellular glutathione content. *Biochem J* 278 (Pt 2:429–34.

210. Hayes JD, Dinkova-Kostova AT (2014) The Nrf2 regulatory network provides an interface between redox and intermediary metabolism. *Trends Biochem Sci* 39(4):199–218.

211. Holmström KM, et al. (2013) Nrf2 impacts cellular bioenergetics by controlling substrate availability for mitochondrial respiration. *Biol Open* 2(8):761–70.

212. Cheng X, Siow RCMR, Mann GEG (2011) Impaired Redox signaling and antioxidant gene expression in endothelial cells in diabetes: a role for mitochondria and the nuclear factor-E2-related factor 2-Kelch-like ECH-associated protein 1 defense pathway. *Antioxid Redox Signal* 14(3):469–487.

213. Calkins M, Johnson D (2009) The Nrf2/ARE pathway as a potential therapeutic target in neurodegenerative disease. *Antioxidants redox Signal redox Signal* 11(3). doi:10.1089/ars.2008.2242.

214. Mitsuishi Y, et al. (2012) Nrf2 Redirects Glucose and Glutamine into Anabolic Pathways in Metabolic Reprogramming. *Cancer Cell* 22(1):66–79.

215. Freemerman AJ, et al. (2014) Metabolic reprogramming of macrophages: Glucose transporter 1 (GLUT1)-mediated glucose metabolism drives a proinflammatory phenotype. *J Biol Chem* 289(11):7884–7896.

216. Sun Y (1990) Free radicals, antioxidant enzymes, and carcinogenesis. *Free Radic Biol Med* 8(6):583–599.

217. Peng M, et al. (2016) Aerobic glycolysis promotes T helper 1 cell differentiation through an epigenetic mechanism. *Science (80-)* 354(6311):481–484.

218. Everts B, et al. (2012) Commitment to glycolysis sustains survival of nitric oxide-producing inflammatory dendritic cells. *Blood*. doi:10.1182/blood-2012-03-419747.

219. Polotsky VYVVYVVY, et al. (2010) Intermittent and sustained hypoxia induce a similar gene expression profile in human aortic endothelial cells. *Physiol Genomics* 41(3):306–14.

220. Huang SCC, et al. (2016) Metabolic Reprogramming Mediated by the mTORC2-IRF4 Signaling Axis Is Essential for Macrophage Alternative Activation. *Immunity* 45(4):817–830.

221. Ellinger JJ, Lewis IA, Markley JL (2011) Role of aminotransferases in glutamate metabolism of human erythrocytes. *J Biomol NMR* 49(3–4):221–229.

222. Melo DR, Mirandola SR, Assunção NA, Castilho RF (2012) Methylmalonate impairs mitochondrial respiration supported by NADH-linked substrates: Involvement of mitochondrial glutamate metabolism. *J Neurosci Res* 90(6):1190–1199.

223. Sentelle R, et al. (2012) Ceramide targets autophagosomes to mitochondria and induces lethal mitophagy. *Nat Chem Biol* 8(10):831–838.

224. Halasiddappa LM, Koefeler H, Futerman AH, Hermetter A (2013) Oxidized Phospholipids Induce Ceramide Accumulation in RAW 264.7 Macrophages: Role of Ceramide Synthases. *PLoS One* 8(7):e70002.

225. MacKenzie ED, et al. (2007) Cell-Permeating -Ketoglutarate Derivatives Alleviate Pseudohypoxia in Succinate Dehydrogenase-Deficient Cells. *Mol Cell Biol* 27(9):3282–3289.

226. Gorres KL, Raines RT (2010) *Prolyl 4-Hydroxylase* doi:10.3109/10409231003627991.Prolyl.

227. Weinblatt ME, et al. (2014) Effects of fostamatinib, an oral spleen tyrosine kinase inhibitor, in rheumatoid arthritis patients with an inadequate response to methotrexate: Results from a phase iii, multicenter, randomized, double-blind, placebo-controlled, parallel-group study. *Arthritis Rheumatol* 66(12):3255–3264.

228. Rolf MG, et al. (2015) In vitro pharmacological profiling of R406 identifies molecular targets underlying the clinical effects of fostamatinib. 3:1–12.

229. O'Neill LAJ, et al. (2015) Immunometabolism governs dendritic cell and macrophage function. *J Exp Med* 213(1):jem.20151570.

230. Zanoni I, Tan Y, Di Gioia M, Springstead JR, Kagan JC (2017) By Capturing Inflammatory Lipids Released from Dying Cells, the Receptor CD14 Induces Inflammasome-Dependent Phagocyte Hyperactivation. *Immunity* 47(4):697–709.e3.

231. Kagan VE, et al. (2016) Oxidized arachidonic and adrenic PEs navigate cells to ferroptosis. *Nat Chem Biol* 13(january):81–90.

232. Wenzel SE, et al. (2017) PEBP1 Wardens Ferroptosis by Enabling Lipoxygenase Generation of Lipid Death Signals. *Cell* 171(3):628–641.e26.

233. Friedmann Angeli JP, et al. (2014) Inactivation of the ferroptosis regulator Gpx4 triggers acute renal failure in mice. *Nat Cell Biol* 3(August):1–9.

234. Doll S, et al. (2016) ACSL4 dictates ferroptosis sensitivity by shaping cellular lipid composition. *Nat Chem Biol* 13(1):91–98.

235. Meliton AY, et al. (2015) Oxidized phospholipids protect against lung injury and endothelial barrier dysfunction caused by heat-inactivated Staphylococcus aureus. *Am J Physiol - Lung Cell Mol Physiol* 308(6):L550–L562.

236. Furnkranz a, Leitinger N (2004) Regulation of inflammatory responses by oxidized phospholipids: structure-function relationships. *Curr Pharm Des* 10(8):915–21.

237. Lumeng CN, Delproposto JB, Westcott DJ, Saltiel AR (2008) Phenotypic switching of adipose tissue macrophages with obesity is generated by spatiotemporal differences in macrophage subtypes. *Diabetes* 57(12):3239–3246.

238. Chacko BK, et al. (2013) Methods for defining distinct bioenergetic profiles in platelets, lymphocytes, monocytes, and neutrophils, and the oxidative burst from human blood. *Lab Invest* 93(6):690–700.

239. Dranka BPB, Hill BBG, Darley-Usmar VVM (2010) Mitochondrial reserve capacity in endothelial cells: The impact of nitric oxide and reactive oxygen species. *Free Radic Biol Med* 48(7):905–14.

240. Gutierrez DA, et al. (2011) Aberrant accumulation of undifferentiated myeloid cells in the adipose tissue of CCR2-deficient mice delays improvements in insulin sensitivity. *Diabetes* 60(11):2820–2829.

241. Bassaganya-Riera J, Misyak S, Guri AJ, Hontecillas R (2009) PPARg is highly expressed in F4/80hi adipose tissue macrophages and dampens adipose-tissue inflammation. *Cell Immunol* 258(2):138–146.

242. Madsen DH, et al. (2013) M2-like macrophages are responsible for collagen degradation through a mannose receptor-mediated pathway. *J Cell Biol*. doi:10.1083/jcb.201301081.

243. Zeyda M, et al. (2010) Newly identified adipose tissue macrophage populations in obesity with distinct chemokine and chemokine receptor expression. *Int J Obes (Lond)* 34(12):1684–1694.

244. Spickett CM, Reis A, Pitt AR (2011) Identification of oxidized phospholipids by electrospray ionization mass spectrometry and LC-MS using a QQLIT instrument. *Free Radic Biol Med* 51(12):2133–2149.

245. O'Donnell VB (2011) Mass spectrometry analysis of oxidized phosphatidylcholine and phosphatidylethanolamine. *Biochim Biophys Acta - Mol Cell Biol Lipids* 1811(11):818–826.

246. Kerur N, et al. (2017) cGAS drives noncanonical-inflammasome activation in age-related macular degeneration. *Nat Med* (November). doi:10.1038/nm.4450.

247. Gruber F, Bicker W, Oskolkova O V., Tschachler E, Bochkov VN (2012) A simplified procedure for semi-targeted lipidomic analysis of oxidized phosphatidylcholines induced by UVA irradiation. *J Lipid Res* 53(6):1232–1242.

248. Choi J, et al. (2011) Lysophosphatidylcholine is generated by spontaneous deacylation of oxidized phospholipids. *Chem Res Toxicol* 24(1):111–118.

249. Ferré N, et al. (2001) Effects of high-fat, low-cholesterol diets on hepatic peroxidation and

antioxidants in apolipoprotein E-deficient mice. *Mol Cell Biochem* 218(1–2):165–169.

250. Aroor AR, DeMarco VG (2014) Oxidative stress and obesity: The chicken or the egg? *Diabetes* 63(7):2216–2218.

251. Kadl A, Bochkov VN, Huber J, Leitinger N (2004) Apoptotic cells as sources for biologically active oxidized phospholipids. *Antioxid Redox Signal* 6(2):311–20.

252. Napoli C, et al. (2006) Physical training and metabolic supplementation reduce spontaneous atherosclerotic plaque rupture and prolong survival in hypercholesterolemic mice. *Proc Natl Acad Sci U S A* 103(27):10479–10484.

253. Kiechl S, et al. (2007) Oxidized phospholipids, lipoprotein(a), lipoprotein-associated phospholipase A2 Activity, and 10-year cardiovascular outcomes: Prospective results from the bruneck study. *Arterioscler Thromb Vasc Biol* 27(8):1788–1795.

254. Viney NJ, et al. (2016) Antisense oligonucleotides targeting apolipoprotein(a) in people with raised lipoprotein(a): two randomised, double-blind, placebo-controlled, dose-ranging trials. *Lancet* 388(10057):2239–2253.

255. Tsimikas S, et al. (2015) Antisense therapy targeting apolipoprotein(a): a randomised, double-blind, placebo-controlled phase 1 study. *Lancet* 386(10002):1472–1483.

256. Tsimikas S, et al. (2005) Oxidized Phospholipids, Lp(a) Lipoprotein, and Coronary Artery Disease. *N Engl J Med* 353(1):46–57.

257. Chou M-Y, et al. (2008) Oxidation-specific epitopes are important targets of innate immunity. *J Intern Med* 263(5):479–88.

258. Spickett CM, Pitt AR (2015) Oxidative Lipidomics Coming of Age: Advances in Analysis of Oxidized Phospholipids in Physiology and Pathology. *Antioxid Redox Signal* 22(18):1646–1666.

259. Gonçalves I, et al. (2012) Evidence supporting a key role of Lp-PLA2-generated lysophosphatidylcholine in human atherosclerotic plaque inflammation. *Arterioscler Thromb Vasc Biol* 32(6):1505–1512.

260. Abe A, Hiraoka M, Ohguro H, Tesmer JJ, Shayman JA (2016) Preferential hydrolysis of truncated oxidized glycerophospholipids by lysosomal phospholipase A2. *J Lipid Res* 58:339–349.

261. Orr JS, et al. (2014) Obesity alters adipose tissue macrophage iron content and tissue iron distribution. *Diabetes* 63(2):421–432.

262. Jain SK (1985) In vivo externalization of phosphatidylserine and

phosphatidylethanolamine in the membrane bilayer and hypercoagulability by the lipid peroxidation of erythrocytes in rats. *J Clin Invest* 76(1):281–286.

263. Zieseniss S, Zahler S, Müller I, Hermetter A, Engelmann B (2001) Modified Phosphatidylethanolamine as the Active Component of Oxidized Low Density Lipoprotein Promoting Platelet Prothrombinase Activity. *J Biol Chem* 276(23):19828–19835.

264. Poyton MF, Sendecki AM, Cong X, Cremer PS (2016) Cu2+ Binds to Phosphatidylethanolamine and Increases Oxidation in Lipid Membranes. *J Am Chem Soc* 138(5):1584–1590.

265. Knapp S, et al. (2007) Oxidized phospholipids inhibit phagocytosis and impair outcome in gram-negative sepsis in vivo. *J Immunol* 178(2):993–1001.

266. Lee I-T, et al. (2008) Lipoteichoic Acid Induces HO-1 Expression via the TLR2/MyD88/c-Src/NADPH Oxidase Pathway and Nrf2 in Human Tracheal Smooth Muscle Cells. *J Immunol* 181(7):5098–5110.

267. Berlett BS, Stadtman ER (1997) Protein Oxidation in Aging, Disease, and Oxidative Stress. *J Biol Chem* 272(33):20313–20316.

268. Reuter S, Gupta SC, Chaturvedi MM, Aggarwal BB (2010) Oxidative stress, inflammation, and cancer: How are they linked? *Free Radic Biol Med* 49(11):1603–1616.

269. Perry G, Cash AD, Smith M a. (2002) Alzheimer Disease and Oxidative Stress. *J Biomed Biotechnol* 2(3):120–123.

270. Hwang O (2013) Role of Oxidative Stress in Parkinson's Disease. *Exp Neurobiol* 22(1):11.

271. Bouayed J, Rammal H, Soulimani R (2009) Oxidative stress and anxiety. *Oxid Med Cell Longev* 2(2):63–67.

272. Michel TM, Pülschen D, Thome J (2012) The Role of Oxidative Stress in Depressive Disorders. *Curr Pharm Des* 18:5890–5899.

273. Ding S-Z, et al. (2007) Helicobacter pylori infection induces oxidative stress and programmed cell death in human gastric epithelial cells. *Infect Immun* 75(8):4030–9.

274. Schwarz KB (1996) Oxidative stress during viral infection: a review. *Free Radic Biol Med* 21(5):641–649.

275. Perl A (2013) Oxidative stress in the pathology and treatment of systemic lupus erythematosus. *Nat Rev Rheumatol* 9(11):674–686.

276. Wruck CJ, et al. (2011) Role of oxidative stress in rheumatoid arthritis: Insights from the Nrf2-knockout mice. *Ann Rheum Dis* 70(5):844–850.

277. Collins AR, et al. (2009) Age-accelerated atherosclerosis correlates with failure to upregulate antioxidant genes. *Circ Res* 104(6):42–54.

278. Mayr M, Sidibe A, Zampetaki A (2008) The Paradox of Hypoxic and Oxidative Stress in Atherosclerosis**Editorials published in the Journal of the American College of Cardiology reflect the views of the authors and do not necessarily represent the views of JACC or the American College of Cardio. *J Am Coll Cardiol* 51(13):1266–1267.

279. Dhalla NS, Temsah RM, Netticadan T (2000) Role of oxidative stress in cardiovascular diseases. *J Hypertens* 18(6):655–73.

280. Murphy ME, Kehrer JP (1989) Oxidative stress and muscular dystrophy. *Chem Biol Interact* 69:101–173.

281. Azadzoi KM, Schulman RN, Aviram M, Siroky MB (2005) Oxidative stress in arteriogenic erectile dysfunction: Prophylactic role of antioxidants. *J Urol* 174(1):386–393.

282. Harman D (1956) Aging: a theory based on free radical and radiation chemistry. *J Gerontol* 11(3):298–300.

283. Steinhubl SR (2008) Why Have Antioxidants Failed in Clinical Trials? *Am J Cardiol* 101(10 SUPPL.). doi:10.1016/j.amjcard.2008.02.003.

284. Miller ERI, Pastor-barriuso R, Dalal D, Riemersma R a (2005) Review Meta-Analysis : High-Dosage Vitamin E Supplementation May Increase all Cause Mortality. *Ann Intern Med* 142:37–46.

285. Mattson MP (2008) Hormesis defined. *Ageing Res Rev* 7(1):1–7.

286. Whillier S, Garcia B, Chapman BE, Kuchel PW, Raftos JE (2011) Glutamine and a-ketoglutarate as glutamate sources for glutathione synthesis in human erythrocytes. *FEBS J* 278(17):3152–3163.

287. Ganapathy-Kanniappan S, Geschwind J-FH (2013) Tumor glycolysis as a target for cancer therapy: progress and prospects. *Mol Cancer* 12(1):152.

288. Shirai T, et al. (2016) The glycolytic enzyme PKM2 bridges metabolic and inflammatory dysfunction in coronary artery disease. *J Exp Med* 213(3):337–354.

289. Pelicano H, Martin DS, Xu R-H, Huang P (2006) Glycolysis inhibition for anticancer treatment. *Oncogene* 25(34):4633–4646.

290. Andringa KK, et al. (2006) Inhibition of glutamate cysteine ligase activity sensitizes human breast cancer cells to the toxicity of 2-deoxy-D-glucose. *Cancer Res* 66(3):1605–1610.

291. Ortega AL, Mena S, Estrela JM (2011) Glutathione in cancer cell death. *Cancers (Basel)* 3(1):1285–1310.

292. Cheong J-H, et al. (2011) Dual Inhibition of Tumor Energy Pathway by 2-Deoxyglucose and Metformin Is Effective against a Broad Spectrum of Preclinical Cancer Models. *Mol Cancer Ther* 10(12):2350–2362.

293. Wheaton WW, et al. (2014) Metformin inhibits mitochondrial complex I of cancer cells to reduce tumorigenesis. *Elife* 2014(3):1–18.

294. Lee M, Yoon J-H (2015) Metabolic interplay between glycolysis and mitochondrial oxidation: The reverse Warburg effect and its therapeutic implication. *World J Biol Chem* 6(3):148.